DISCOVERY OF NOVEL INHIBITORS OF CELLULAR EFFLUX BY HIGH-CONTENT SCREENING WITH A FLUORESCENT MIMIC OF TAXOL

By

Tomas J. Smith

Submitted to the graduate degree program in Medicinal Chemistry and the Graduate Faculty of the University of Kansas in partial fulfillment of the requirements for the degree of Master of Science.

_____

Chairperson Dr. Blake R. Peterson

_____

Dr. Mark Farrell

_____

Dr. Jeffrey Krise

Date Defended: July 17, 2019

The Dissertation Committee for Tomas J. Smith

certifies that this is the approved version of the final thesis:

DISCOVERY OF NOVEL INHIBITORS OF CELLULAR EFFLUX BY HIGH-CONTENT SCREENING WITH A FLUORESCENT MIMIC OF TAXOL

_____

Chairperson Dr. Blake R. Peterson

Date Approved: July 17, 2019

ABSTRACT

Fluorescence-based assays play key roles in drug discovery and development. These assays are widely used due to the widespread availability of fluorescent probes and highly sensitive detection platforms. This method is a mainstay of high-throughput drug screening (HTS) campaigns, where simple and inexpensive assays are preferred for scalability and repeatability. This approach can identify novel chemotypes that may lead to new methods to treat disease. To develop a new phenotypic assay for drug discovery, we investigated a fluorescent mimic of the anticancer drug Taxol, termed Pacific Blue-Gly-taxol (PBGT). This molecular probe binds cellular microtubules and is a highly sensitive substrate of the cellular efflux transporter P-glycoprotein (P-gp). When HeLa cervical carcinoma cells are cotreated with PBGT (1 μM) and the P-gp inhibitor verapamil (25 μM), cellular fluorescence increases by ~ 10-fold as analyzed by confocal microscopy or flow cytometry. Because of the simplicity and sensitivity of this assay of P-gp activity, we envisioned that it could be optimized in a 96-well plate format to provide a useful method to investigate cellular efflux mediated by this protein transporter. To provide a proof of concept, 1584 diverse compounds obtained from the National Cancer Institute (NCI) were screened using automated pipetting and flow cytometry. The primary screen yielded more than 23 hit compounds with equivalent or of higher activity than verapamil (25 μM). Among these hits, we identified diarylureas that do not appear to associate directly with P-gp but rather disrupt the typical rod-like structure of mitochondria. These compounds may inhibit P-gp indirectly by affecting mitochondria or via a target that additionally affects this organelle. These results demonstrate that PBGT is a highly sensitive probe for discovery of inhibitors of P-gp and may allow identification of alternative mechanisms of inhibition of this major drug transporter.

ACKNOWLEDGMENTS

First, I would like to thank my advisor Dr. Blake Peterson for his mentorship during my time at KU. His guidance and support have been essential to my success, and I am forever grateful for his mentorship. I would also like to thank the members of my committee, Dr. Mark Farrell and Dr. Jeffrey Krise, for their careful critique of my work. I'd like to thank the entire Department of Medicinal Chemistry for their support, both academically and professionally. It's been an honor to be a part of a department with such a rich history and one that boasts such esteemed scientists.

I would also like to thank all of the members of the Peterson group. I am very grateful to have such a supportive group, as each individual has been critical in my development as a scientist. I'd like to give a special thanks to former members Dr. Zhe Gao, Dr. Molly Lee, and Dr. Bailin Lei for their work on fluorescent toxoids which laid out the framework for my project.

Finally, I'd like to give thanks to my friends and family for their support in my academic and professional pursuits. To Dana, Casey, Tyler, Pat, and my parents, you've been a continuous source of encouragement on this journey. From my boxing days, I know that having a "good corner" is not only essential for success in the ring but also in life. My successes are not my own, but a product of the many people who motivate and inspire me. No matter how large or small, each one of your contributions and outside perspectives is much appreciated.

TABLE OF CONTENTS

LIST OF FIGURES

Chapter 1

Fluorescent Probes in Drug Discovery

Despite recent advances in medical science, humans continue to suffer from a wide variety of diseases. Although treatments for many diseases have drastically improved in the past century, a large unmet medical need remains for incurable or otherwise ongoing chronic conditions. In 2019, the US Center for Disease Control estimated that 6 out of 10 adults suffer from a chronic illness, and treatment of these illnesses is a leading driver of the 3.3 trillion dollars needed annually for healthcare in the USA.[1] In addition, patient non-adherence, which is often due to undesirable side effects of prescription medication, has been linked to negative healthcare outcomes, higher rates of hospitalization, and increased overall healthcare costs.[2-3]

To bridge this gap between patients who suffer from treatment-resistant diseases and therapies with more positive outcomes, pharmaceutical companies have invested copious amounts of time and money on drug discovery. In recent years, many innovative new medicines stem from advances in the field of chemical biology, a research area focused on using methods of chemistry to interrogate biological function. Often, studies in chemical biology lead to an enhanced understanding of the underlying mechanisms of disease and push the boundaries of how scientists can manipulate native biological function. These efforts have afforded new biological targets for drugs, new methods to validate these targets, and novel ways to engage previously undruggable targets.[4-6]

1.1. Fluorescence-based assay development

Numerous methods have been developed for interrogating the function of biomolecules. In the field of chemical biology, fluorescence-based approaches are particularly widely used because of the high sensitivity of this method, its ease of use, and the diversity of available fluorescent probes.[7] Fluorescent probes can be designed to localize in specific tissues, cells, or subcellular regions of biological samples or whole organisms. This localization can be an important tool for bioimaging applications.[8] In addition, because intracellular compartments and organelles can maintain specific signaling molecules, metabolites, and ions, some fluorescent probes can be used as biosensors that react with endogenous or exogenous molecules to create or release a fluorescent molecule that can be detected. Biosensors that localize to specific organelles can be particularly useful for understanding the subcellular dynamics and abundance of analytes.[9] Although other important applications of fluorescent probes can be found outside of chemical biology, this thesis is primarily focused on studies of specific types of bioimaging agents and biosensors.

1.1.1 Introduction to fluorescence spectroscopy

Since its first observation by Fredrick Herschel in 1845, and its subsequent rationalization in 1852 by G.G. Stokes, the photophysical property of fluorescence has provided an important tool to qualitatively and quantitatively analyze a wide variety of biological phenomena.[10-12] Fluorescence, a distinct form of photoluminescence, is the emission of light from a substance that has absorbed light or electromagnetic radiation at a shorter wavelength.[13] This process is governed by three main steps as detailed in

Figure 1.1. The first step in the process, excitation, occurs when a photon from a source of light or electromagnetic radiation is absorbed by a fluorescent compound or material termed a fluorophore. This causes electrons of the fluorophore to transition from the ground state (S_0) to an excited state. Next, the fluorophore undergoes vibrational relaxation, where the fluorophore relaxes to the lowest energy level of the excited state (S_1). Last, the fluorophore emits a red-shifted photon as it returns its ground state (S_0) by the process of emission.[14]

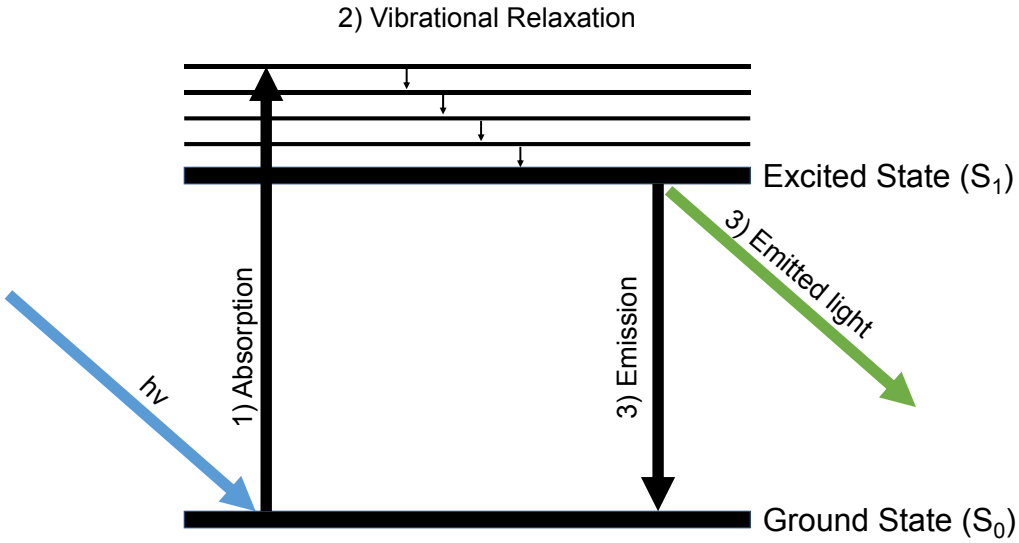

FIGURE 1.1. A Jablonski diagram illustrating the three-step process of fluorescence. A photon is absorbed by a fluorophore that subsequently emits a photon of a longer wavelength.

Fluorophores can be characterized by their excitation and emission spectra. The wavelengths of the maximum peaks in these spectra are denoted as the excitation and emission maxima. The difference between these wavelengths is termed the Stokes shift.[15] When choosing a fluorophore for a fluorescence-based assay, it is important to consider this value. When fluorophores possess only a small difference between their

excitation and emission maxima (small Stokes shift), the sensitivity of fluorescence-based assays can be limited because of the difficulty in separating the light used to excite the fluorophore from its fluorescence emission.[16]

In bioassays involving more than one fluorophore, fluorophores generally need to be spectrally orthogonal, ideally with emission and excitation bands that are non-overlapping and relatively narrow. However, in some instances it is desired for the emission of one fluorophore to overlap with the excitation band of another fluorophore. If the fluorophores are in sufficiently close proximity, this can produce a donor-acceptor interaction between the emission of the shorter wavelength fluorophore and the excitation of the longer wavelength fluorophore. This phenomenon is the basis of Förster Resonance Energy (FRET) and has been extensively used to interrogate biological processes.[17-20] However, in this thesis, the experiments described will focus on simpler measurements of biological activity that rely on fluorescence intensity.

1.1.2 Common fluorescent small molecules

Many compounds, both natural and synthetic, are intrinsically fluorescent.[21-22] Most fluorescent small molecules contain multiple conjugated pi bonds and are frequently polycyclic aromatic compounds. These highly extended conjugated systems can greatly decrease the energy difference between the S_0 and S_1 states of the fluorophore. In turn, this decreases the energy of light needed to excite the fluorophore, meaning that a longer wavelength of light can be used for excitation. Examples of some small molecule fluorophores organized relative to their absorption and excitation maxima (λ_{max}) are shown in Figure 1.2.

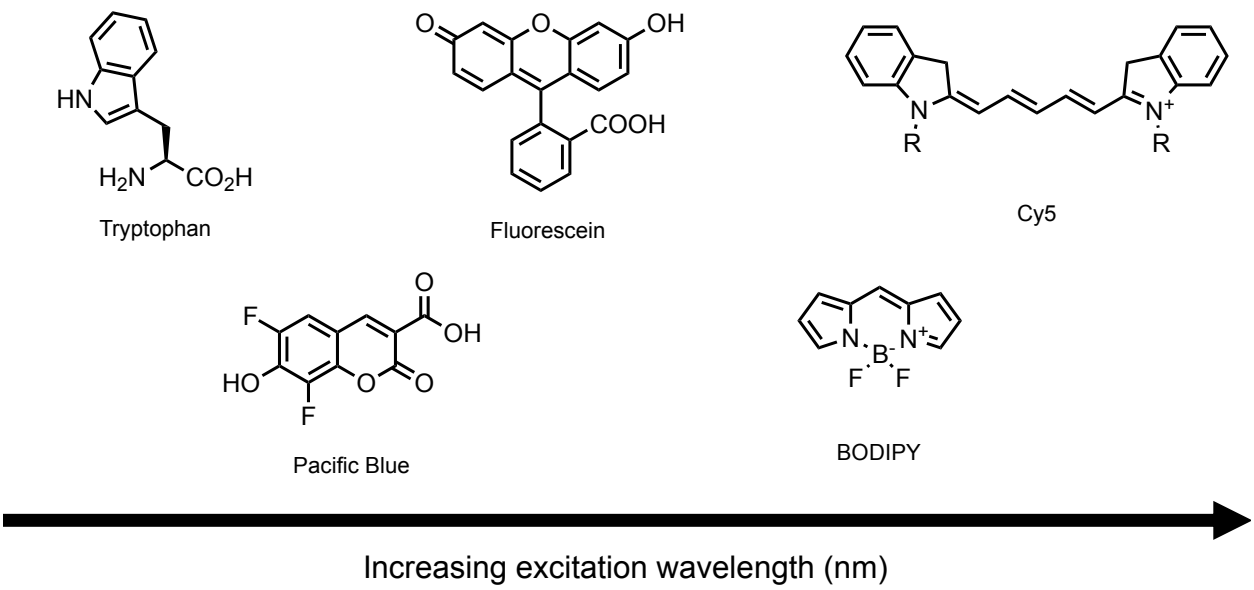

Figure 1.2. Examples of fluorescent small molecules organized by excitation wavelength. From left to right, the fluorophores tryptophan, Pacific Blue, Fluorescein, BODIPY, and Cy5 are shown. The core structures of fluorescein, BODIPY, and Cy5 have been extensively modified to further tune spectral properties and generate numerous other fluorophores for fluorescence-based assay development.

Although molecular structure plays a large role in the spectroscopic properties of small molecules, other factors can influence absorption/excitation and emission spectra. For some fluorophores, environmental factors such as pH, solvent, and the molecular environment, such as whether or not the fluorophore is bound to a specific protein, have profound effects on fluorescence properties.[23] Consequently, when new fluorophores are designed or discovered, their spectral properties are generally assessed in a variety of different conditions such as varying pH in aqueous buffers and in different solvents.[24-27]

Additionally, because the spectral properties of a fluorophore can change in a protein-bound vs unbound state, assays have been developed to detect these differences. One of the most common protein binding assays relies on fluorescence polarization,

which measures the fluorescence of a fluorophore upon excitation with plane-polarized light. In this assay, a small fluorophore that is unbound would theoretically be in rapid motion and upon excitation with plane polarized light will emit light in multiple different directions compared with the excitation plane. However, a fluorophore bound to a much larger molecule such as a target protein, would have less free motion, causing the emission of polarized light. This increase in fluorescence polarization provides a method to measure the affinity of small molecules to proteins through direct interactions or competition assays. This method has played a critical role in protein biochemistry and has been extensively used multiple subfields such as immunoassays. [28-29] In addition, fluorescence polarization is frequently used in high-throughput screening to find small molecule binders for a variety of different proteins. [30-33]

1.1.3 Fluorescent proteins

Another method used to develop fluorescence-based assays involves intrinsically fluorescent proteins and related fluorescent fusion proteins. Fusion proteins are designer protein products that can be prepared by recombinant DNA technology. This molecular biology approach can combine DNA fragments from different species, reinsert the recombinant DNA back into a host organism, and express proteins of interest fused to intrinsically fluorescent proteins for analysis.[34] Fluorescent proteins are often used for studies of subcellular localization of other fused proteins and to confirm gene expression by generation of fluorescent cells.[37] Fusion proteins have also been crucial for the development of multiple biologic drugs including Fc-fusion proteins.[35-36]

Green fluorescent protein (GFP) is one of the most widely investigated intrinsically fluorescent proteins. Initially isolated from *Aequorea Victoria* in 1962 by Shimomura et al.,[38] more than three decades passed before GFP was widely employed by scientists outside of the marine biology community.[39] In 1994, it was first reported that GFP could be used as a marker for gene expression experiments.[40] These findings became recognized as a major scientific breakthrough, and fluorescent proteins have since been widely utilized as tools for studies of cellular and developmental biology. Much time and effort has been spent in both improving and expanding the palette of fluorescent proteins.[41] This work has led to the creation of dozens of fluorescent proteins with distinct spectral properties that can be used to develop fluorescence-based biological assays.

1.2 Qualitative and quantitative analysis of cellular fluorescence

Sensitive and reliable methods have been developed to use fluorescence to analyze cellular properties and intracellular dynamics. Qualitative methods can readily detect cellular events and the subcellular localization of fluorophores in real time. In addition, quantitative methods can be used to measure the abundance and dynamics of endogenous and exogenous biomolecules. Whereas there are many ways to analyze these properties, flow cytometry and fluorescence microscopy are two of the most widely used methods for qualitative and quantitative evaluation of cellular fluorescence.[42-44]

1.2.1 Flow cytometry

Flow cytometry is a powerful tool for high-content fluorescence-based analysis of cells and other suspended particles. A flow cytometer can measure multiple physical

properties by flowing suspended cells past a monochromatic light source (generally a laser). In turn, light is emitted from individual cells and collected via a series of emission filters.[45] The scattering of this light can be related to the size and shape of the cell. The intensity of light that is emitted from cells and isolated by the filters is reported in arbitrary fluorescence units. A diagram of this process is shown in Figure 1.3.

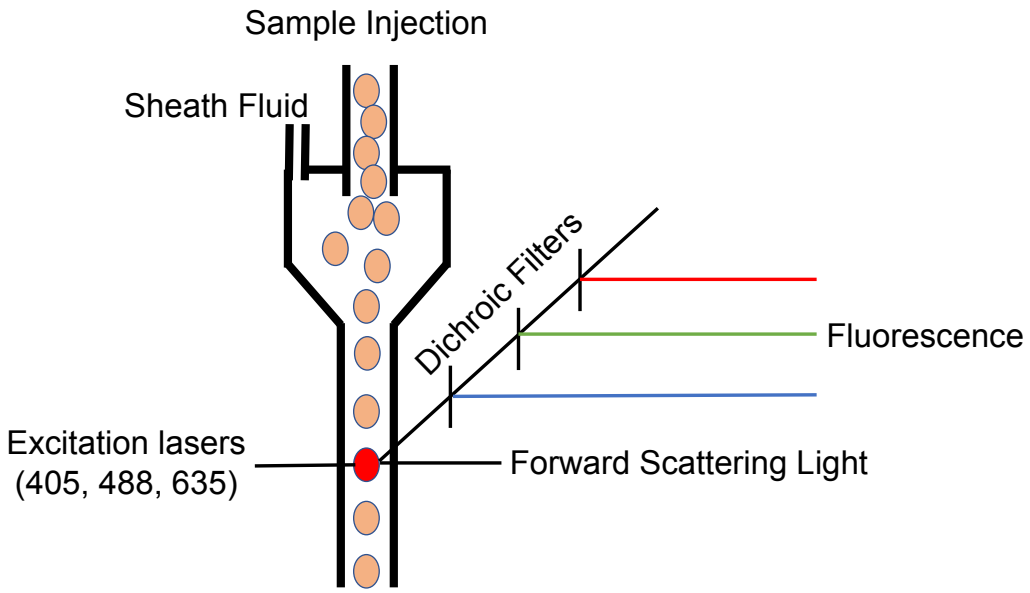

Figure 1.3. Principles of flow cytometry. A sample of cells in suspension is injected into the instrument. The concentrated cells are diluted with sheath fluid and subsequently flow single-file past a light source. The scattering of this light and the emission of longer wavelength light by the cell can be assessed by the instrument.

Flow cytometry is used in multiple subfields in biology. In particular, this method has played an important role in clinical microbiology and oncology where it is used to detect various microbial infections and cancers.[46-49] Additionally, because this process is relatively fast and allows for a multiparametric analysis of each cell, it has also become an attractive method for high-throughput/high-content phenotypic drug screening

campaigns.[50] For example, high-throughput flow cytometry has become a core discovery technology within the major pharmaceutical company AstraZeneca.[51]

Even though flow cytometry is a fantastic tool to quantify cellular fluorescence, there are also disadvantages to this method. An increase in fluorescence intensity obtained from this method will only indicate that the cell is becoming brighter, not precisely why the sample is increasing in brightness. In drug screens, cellular fluorescence and morphology can provide a reasonable phenotype to assay against, but additional studies of subcellular localization are often needed to provide important information about the mechanism of changes in fluorescence.

1.2.2 Confocal laser scanning microscopy

Another high-content fluorescence-based method relies on confocal laser-scanning microscopy and related confocal microscopy techniques. This imaging method can be used to investigate biological processes within living cells and the impact of xenobiotics on cellular fluorescence. Other types of fluorescence microscopes are often used for imaging, but confocal microscopes can uniquely acquire thin (micron-thick) optical slices to create high resolution images.[52] This process removes out of focus light that reduces the clarity of fluorescent images generated with traditional wide-field microscopes. Whereas wide-field (e.g. epifluorescence) microscopes are often more sensitive than confocal microscopes, the thin optical slices of a confocal microscope can be used to create 3D reconstructions of samples and are generally better suited for quantitative microscopy applications.[53]

Due to the high resolution of confocal images, this method is widely used to investigate the cellular mechanism of action of small molecules. Cellular organelles, proteins, and nucleic acids can be labeled with fluorescent dyes and imaged in high definition using confocal microscopy.[54-56] Fluorescent analogues of compounds can be synthesized and tested to observe their subcellular localization, suggesting potential mechanisms of action.[57-58] Studies of the subcellular localization of fluorescent fusion proteins can also provide useful mechanistic information. Furthermore, biomolecular interactions in cells can also be assessed by co-localization or FRET-based assays using orthogonally fluorescent fusion proteins, two orthogonally fluorescent small molecules, or both a fluorescent fusion protein and an orthogonally fluorescent small molecule.[59-60]

1.3. High-throughput and high-content screening methods

An important application of fluorescence-based assays for drug discovery involves high-throughput screening (HTS). HTS employs large chemical libraries for rapid screening against biological targets of interest to identify chemical modulators.[61] Compounds found to be the most active are termed “hits” and are moved forward in the discovery process. Their activity can then be improved in a hit-to-lead campaign. During preclinical drug development, the pharmacokinetic/pharmacodynamic properties of the best lead compounds are optimized before compounds are advanced to clinical trials.[62] However, in the past two decades, the difficulty in identifying high-quality hits via HTS has been suggested to be a contributor to the slowing productivity of the pharmaceutical industry.[63-64] However, a paper from Macarron et al, published in *Nature Reviews Drug Discovery* in 2011, aimed to dismiss these accusations and illustrate the benefits of HTS

for drug discovery.[65] Although not all screens directly put a compound on the market, HTS campaigns have proven successful in other areas such as providing chemical probes that can later be used in basic research to influence drug discovery in different ways.[66] In addition, these screens have been particularly successful at identifying novel chemotypes active against particular biological targets.[67-69]

Fluorescence-based HTS approaches have been widely used due to the potential for high sensitivity and versatility. For HTS campaigns, fluorescence intensity, fluorescence polarization, FRET, and fluorescence correlation spectroscopy (FCS) assays have been widely used,[70] Compared to fluorescence intensity, FCS is a more complex technique that relies on analysis of fluctuations in fluorescence intensity over time. In a closed system, Brownian motion of fluorescent molecules causes fluctuations in the fluorescence intensity. Events such as chemical reactions or other biomolecular interactions can disrupt these baseline fluctuations and can be detected by a device such as a high resolution confocal microscope.[71-72] FCS experiments generally interrogate mesoscopic systems and only require concentrations of fluorescent molecules in the nanomolar range.[73] Due to the high costs of a large HTS campaign, a method which requires such small amounts of material such as FCS would be ideal. However, FCS has its limitations. Although effective in vitro, limitations associated with studies of living cells have hindered use in drug discovery, but recent efforts have been directed at further development of this method for this application.[74-75]

HTS assays that rely on measurements of fluorescence intensity on multiwell plates are common due to their simplicity.[76] Modern plate readers can analyze absorbance and fluorescence using a variety of different plate formats, typically using 96, 384, or 1526

wells/plate. Additionally, because the screening process can be completed for an entire assay plate in minutes or less, this sample format is generally desirable for large HTS campaigns where hundreds of thousands of compounds are assayed. A plate reader works by shining a light source, either from a lamp, laser, or light emitting diode, on each individual assay well. Filters or monochrometers can collect light emitted corresponding by the fluorophore used in the assay.[77] However, plate reading can generate false positive data resulting from intrinsically fluorescent library compounds.

Even though false positives are present in most screens, there are methods which can lower their occurrence and make their detection simpler. An exemplary method is that of high-content screening (HCS), which obtains detailed information regarding cell morphology and multi-color fluorescence in each individual assay. Each assay investigates more than one parameter and not a single read-out like a plate reader, so false positives and false negatives can be more easily ruled out.[78] HCS was first reported in 1996 as a method to ease downstream bottlenecks in the drug discovery process such as target validation and lead optimization.[79] Since the initial discovery of HCS, there have been many advances in data mining of cellular populations,[80] automated microscopy,[81] and systems biology.[82] These advances have allowed HCS to become a widely used tool for phenotypic drug discovery.[83]

Although HCS has been widely successful, this method is not without its limitations. As an increasing number of parameters are used to analyze cells and screening libraries become larger, the data generated from each screen increases substantially. To counter this complexity, much effort has recently been focused on the incorporation of deep learning techniques within HCS.[84-85] One such technology, intelligent image-activated cell

sorting, has been developed by Nitta et al in 2018.[86] In this method, a technology was developed to autonomously sort microalgal and blood cells by subcellular protein localization and cell-cell interactions. Whereas this technology was piloted using only two cell types, it is expected to be translative to other cell types and perhaps larger cell spheroids, tissues, and small organisms. Moreover, this technology serves as a prime example of the incorporation machine learning in HCS. Such discoveries reduce the need for human-mediated data mining, and could be particularly useful in the development of large HCS screens where vast amounts of data are generated.

HSC has also been incorporated into other scientific disciplines such as translational and precision medicine.[87] For traditional biomedical applications, HCS analyzes cell phenotypes in the presence of libraries of small molecules. In contrast, HCS for precision medicine utilizes patient-derived cell lines and small molecules as possible therapeutics. This approach could lead to a deeper understanding of the sensitivity profile of a particular cell line and lead to better patient outcomes. An example of this strategy was recently published by Yu et al.[88] In this study, 83 FDA approved chemotherapeutics were screened against seven cell lines derived from patients with glioblastoma (cultured as both monolayers and 3D neutrospheres). This method identified several non-standard chemotherapeutics that were efficacious in vitro against primary and recurrent glioblastomas. This assay could be useful in identifying new therapies to treat patient-specific cancers.

In a different study conducted by Prins et al, a high-content assay was developed for precision medicine discovery in cystic fibrosis (CF).[89] CF involves mutations in a gene that encodes a particular ion channel, the cystic fibrosis transmembrane conductance

regulator (CFTR). This new high-content assay focused on assessing CFTR's function and the membrane density of its variants by utilizing multicolored halide-activated CFTR proteins. As a proof of concept, the known CFTR potentiator VX-770 was screened against 62 CFTR variants. Data from this screen showed that this compound was not efficacious in CFTR variants bearing mutations at a particular ATP-binding site. Moreover, this high-content assay could be useful to screen compounds against patient specific CFTR mutations. Both of these two examples illustrate that HCS could also be an important tool in the development of precision medicines of the future.

One platform often utilized for HCS is high-content flow cytometry. This method allows for a large population of cells within an assay well to be analyzed. Since flow cytometry is a high-content technique, much more information can be obtained per assay well than possible with a traditional plate reader. For example, since the morphology of each cell is evaluated by light scattering, cytotoxicity of library compounds can be assessed in the primary screen.[90] This approach saves time and money by avoiding some of the need for downstream cytotoxicity assays on hit compounds. Flow cytometry can readily detect the accumulation of a fluorescent compound or the production of a fluorescent protein within cells.[91-93] These types of high-content assays could be potentially useful for studies of drug resistance related to cellular efflux. We describe in Chapter 2 a fluorescent efflux substrate that can be used in a phenotypic screen to discover novel chemotypes that inhibit cellular efflux of small molecules involving the multidrug efflux protein P-glycoprotein.

1.4 Conclusions

Fluorescence-based assays have played a crucial role in the understanding of biological processes and in the development of new medicines. Due to their sensitivity, ease of use, and diversity of possible probes, they have been a mainstay for chemical biologists who seek to investigate and manipulate biological function. To keep up with the needs of biomedical scientists, the toolbox of fluorescent probes and palette of fluorescent proteins has been consistently expanding. In addition, methods which these tools can be analyzed are becoming increasingly sensitive and optimized for high throughput and high-content screening. The continued development of these types of probes and methodologies will allow for a deeper investigation into a wide variety of biological processes. These findings contribute to our understanding of the etiology of human disease and provide new approaches for the discovery and development of therapeutics.

1.5 References

1. Chronic Disease In America. www.cdc.gov. CDC's National Center for Chronic Disease Prevention and Health Promotion. **2017.** www.cdc.gov/chronicdisease/pdf/infographics/chronic-disease-H.pdf

2. Neiman, A.B.; Ruppar, T.; Ho, M.; Garber, L.; Weidle, P.J.; et al., CDC grand rounds: improving medication adherence for chronic disease management - innovations and opportunities. *Morbidity and Mortality Weekly Report.* **2012,** 66(45).

3. Dimatteo, M.R., Variations in patients' adherence to medicial recommendations: a quatitative review of 50 years. *Med Care.* **2004,** 42, 200-209.

4. Castaldi, P.M.; Zuhl, A.; Ricchuito, P.; Hendricks, A.D., Chapter Ten - Chemical biology in drug discovery. *Annul. Rep. Med. Chem.* **2017,** 50, 335-370.

5. Altmann, K.H.; Buchner, J.; Kessler, H.; Diederich, F.; Krautler, B.; et al, The state of the art of chemical biology. *ChemBioChem.* **2008,** 10, 16-29.

6. Zhu, Y.; Xiao, T.; Lei, S.; Zhou, F.; Wang, M.W., Application of chemical biology in target indentification and drug discovery. *Arch. Pharmical. Res*. **2015,** 38, 1642-1650.

7. Yao, J.; Yang, M.; Duan, Y., Chemistry, biology, and medicine of fluorescent nanomaterials and related systems: new insights into biosensing, bioimaging, genomics, diagnostics, and therapy. *Chem. Rev.* **2014,** 114, 6130-6178.

8. Leblond, F.; Davis, S.C.; Valdes, P.A.; Pogue, B.W., Pre-clinical whole-body fluorescence imaging: review of instruments, methods and applications. *J. Photochem. Photobiol. B;* **2010,** 98, 77-94.

9. Okumoto, S.; Jones, A.; Frommer, W.B., Quantitative imaging with fluorescent biosensor. *Annul. Rev. Plant Biol.* **2012,** 63, 663-706.

10. Herschel, J.F.W., On a case of superficial colour presented by a homogenous liquid internally colourless. **1845,** 135, 143-145.

11. Stokes, G.G., On the change of refrangibility of light. **1852,** 142, 463-562

12. Renz, M., Fluorescence microscopy - a historical and technical perspective. *J. of Quan. Cell Sci.* **2013,** 83, 767-779.

13. Valeur, B.; Berberan-Santos, M.N., A breif history of fluorescence and phosphorescence before the emergence of quantum theory. *J. Chem. Edu.* **2012,** 88, 731-738.

14. Powell, A.L., The fundamentals of fluorescence. J. Chem. Educ. **1947,** 423-428.

15. Lavis, L.D.; Raines, R.T., Bright ideas for chemical biology. *ACS Chemical Biology.* **2008,** 3, 142-155.

16. Pysical properties that define fluorecence. www.thermofisher.com. ThermoFisher Scientific. www.thermofisher.com/us/en/home/life-science/cell-analysis/cell-analysis-learning-center/molecular-probes-school-of-fluorescence/imaging-basics/fundamentals-of-fluorescence-microscopy/physical-properties-that-define-fluorescence.html

17. Piston, D.W.; Kremers, G.J., Fluorescent protein FRET: the good, the bad, and the ugly. *Trends Biochem. Sci.* **2007,** 32, 407-414.

18. Bajar, B.T.; Wang, E.S.; Zhang, S.; Lin, M.Z.; Chu, J., A guide to fluorescent protein FRET pairs. *Sensors.* **2018,** 16, 1488.

19. Padilla-Parra, S.; Tramier, M., FRET microscopy in the living cell: different approaches, strengths, and weaknesses. *Probing Molecular Dynamics and Interactions.* **2012,** 34, 369-376.

20. Lerner, E.; Cordes, T.; Ingargiola, A.; Alhadid, Y.; Chung, S.; et al., Toward dynamic structural biology: two decades of single molecule forster resonance energy transfer. *Science. **2018,*** 359, 1-12.

21. Duval, R.; Duplais, C., Fluorescent natural products as probes and tracers in biology. *Nat. Prod. Rep.* **2017,** 34, 125-222.

22. Martynoz, V.I.; Pakhomov, A.A.; Popova, N.V.; Deyev, I.E.; Petrenko, A.G., Synthetic fluorescence for visualizing biomolecules in living systems. *ActaNaturae.* **2016,** 8, 33-46.

23. Lakowics, J.R., Principles of fluorescence spectroscopy. *Springer.* **2006,** 205-235.

24. Fink, D.W.; Koehler, W.R., pH Effects on fluorescence of umbelliferone. *Anal. Chem.* **1970,** 42, 990-993.

25. Nag, A.; Goswami, D., Solvent effect on two-photon absorption and fluorescence of rhodamine dyes. *J. photochem. photobiol. A.* **2009,** 206, 188-197.

26. Ogunsipe, A.; Maree, D.; Nyokong, T., Solvent effects on the photochemical and fluorescence properties of zinc phthalocyanine derivatives. *J. mol. struc.* **2003,** 650, 131-140.

27. Romero-Ale, E.E.; Olives, A.I.; Martin, A.M.; Castillo, B.D.; Lopex-Alvarado, P.; et al., Environmental effects on the fluorescence behaviour of carbazole derivatization reagents. *J. Biol Chem. Lum.* **2005,** 20, 162-169.

28. Nielsen, K.; Lin, M.; Gall, D.; Jolley, M., FLuorescence polarization immunoassay: detection of antibody to *Brucella abortus*. *Methods.* **2000,** 22, 71-76.

29. Maragos, C., Fluorescence polarization immunoassay of mycotoxins: a review. *Toxins.* **2009,** 1, 196-207.

30. Nasir, M.S.; Jolley, M.E., Fluorescence polarization: an analytical tool for immunoassay and drug discovery. *Comb. Chem. High. Throughput Screen.* **1999,** 2, 177-190.

31. Huang, X.; Aulabaugh, A., Application of fluorescence polarization in HTS assays. *High Throughput Screening.* **2016,** 1439, 115-130.

32. Parker, G.J.; Law, T.L.; Lenoch, F.J.; Bolger, R.E., Development of high throughput sceening assays using fluorescence polarization: nuclear receptor-ligand binding and kinase/phosaphatase assays. *J Biomol Screen.* **2000,** 5, 77-88.

33. Lea, W.A.; Simeonov, A., Fluorescence polarization assays in small molecule screening. *Exp. Opin. Drug Discov.* **2011,** 6, 17-32.

34. Khan, S.; Ullah, M.W.; Siddique, R.; Nabi, G.; Manan, S.; et al., Role of recombinant DNA technology to improve life. *Int J Genomics.* **2016,** 2016, 1-14.

35. Lagasse, D.H.A.; Alexaki, A.; Simhadri, V.L.; Katagiri, N.H.; Jankowski, W.; et al., Recent advances in therapeutic protein drug development. *F1000Res.* **2017,** 6.

36. Czajkowsky, D.M.; Ju, J.; Shao, Z.; Pleass, R.J., Fc-fusion proteins: new developments and future prospectives. *EMBO Mol. Med.* **2012,** 4(10), 1015-1028.

37. Snapp, E., Design and use of fluorescent fusion proteins in cell biology. Curr. Protoc. *Cell Biol.* **2010,** 27(1), 21.4.1-21.4.13.

38. Shimomura, O.; Johnson, F.H.; Saiga, Y., Extraction, purification and properties of Aequorin, a bioluminescent protein from the luminous hydromedusan, Aequorea. *J Cell Comp. Physiol.* **1962,** 59, 223-39.

39. Chudakov, D.M.; Matz, M.V.; Lukyanov, S.; Lukyanov, K.A., Fluorescent proteins and their applications in imaging living cells and tissues. *Physiol. rev..* **2010,** 90, 1103-1163.

40. Chalfie, M.; Tu, Y.; Euskirchen, G.; Ward, W.W.; Prasher, D.C., Green fluorescent protein as a marker for gene expression. *Science.* **1994,** 263(5148), 802-805.

41. Rodriguez, E.A.; Campbell, R.E.; Lin, J.Y.; Shu, X.; Zhang, J.; et al., The growing and glowing toolbox of fluorescent and photoactive proteins. *Trends Biochem. Sci.* **2016,** 42(2), 111-129.

42. Lichtman, J.W.; Conchello, J.A., Fluorescence microscopy. *Nature Methods.* **2005,** 2, 910-919.

43. Sahl, S.J.; Hell, S.W; Jakobs, S., Fluorescence nanscopy in cell biology. *Nat. Rev. Mol. Cell Biol.* **2017,** 18, 685-701.

44. Schmutz, A.; Valente, M.; Cumano, A.; Novault, S., Spectral cytometry has unique properties allowing multicolor analysis of cell suspensions isolated from solid tissues. *PLOS One.* **2016,** 1-15.

45. Brown, M.; Wittwer, C., Flow cytometry: principles and clincial applications in hematology. *Clin. Chem.* **2000,** 46(8), 1221-1229.

46. Alvarez-Barrientos, A.; Arroyo, J.; Canton, R.; Nombela, C.; Sanchez-Perez, M., Applications of flow cytometry to clinical microbiology. *Clin. Microbiol. Rev.* **2000,** 13(2), 167-195.

47. McSharry, J.J., Analysis of virus-infected cells by flow cytometry. *Methods.* **2000,** 21(3), 249-257.

48. Barlogie, B., Flow cytometry as a diagnostic and prognostic tool in cancer medicine. *Tumor Aneuploidy.* **1985,** 107-134.

49. Karo, O.; Wahl, A.; Nicol, S.B.; Brachert, J.; Lambrecht, B.; et al., Bacteria detection by flow cytometry. *Clin. Chem. Lab. Met.* **2008,** 47(7), 947-953.

50. Edwards, B.S.; Opera, T.; Prossnitz, E.R.; Sklar, L.A., Flow cytometry for high-throughput, high-content screening. *Curr. Opin. Chem. Biol.* **2005,** 8(4), 392-398.

51. Ding, M.; Clark, R.; Bardelle, C.; Backmark, A.; Norris, T.; et al., Application of high-throughput flow cytometry in early drug discovery: an AstraZeneca perspective. *SLAS Discovery.* **2018,** 23(7), 719-731.

52. Combs, C.A., Fluorescence microscopy: a concise guide to current imaging methods. *Curr. Protoc. Neurosci.* **2010,** 50(1), 2.1.1-2.1.14.

53. Jonkman, J.; Brown, C.M., Any way you slice it - a comparison of confocal microscopy techniques. *J. Biomol. Tech.* **2015,** 26(2), 54-65.

54. Mitra, K.; Lippincott-Schwartz, J., Analysis of mitochondrial dynamics and functions using imaging approaches. *Curr. Protoc. Cell. Biol.* **2010,** 46(1), 4.25.1-4.25.21.

55. Chen, X.; Wang, T.; Li, P.; Yan, X.; Hou, S.; et al., Lysosomal targeting with stable and sensitive fluorescent probes: applications for lysosome labeling and tracking during apoptosis. *Nature Scientific Reports.* **2015,** 5, 1-10.

56. Arai, S.; Lee, S.C.; Zhai, D.; Suzuki, M.; Chang, Y.T., A molecular fluorescent probe for targeted visualization of temperature at the endoplasmic reticulum. *Nature Scientific Reports.* **2014,** 4, 1-6.

57. Leriche, G.; Chen, A.; Kim, S.; Selkoe, D.J.; Yang, J., Fluorescent analogue of batimastat enables imaging of a α-secretase in living cells. *ACS Chem. Neurosci..* **2015,** 7, 40-45.

58. Kuder, C.H.; Neighbors, J.D.; Hohl, R.J.; Weimer, D.F., Synthesis and biological activity of a fluorescent schweinfurthin analogue. *Bioorg. Med. Chem.* **2009,** 17(13), 4718-4723.

59. Madsen, B.W.; Beglan, C.L.; Spivak, C.E., Fluorescein-labeled naloxone binding to mu opioid receptors on live chinese hamster ovary cells using confocal fluorescent microscopy. *J. Neurosci. Met..* **2000,** 97(2), 123-131.

60. Costes, S.V.; Daelemans, D.D.; Cho, E.H.; Dobbin, Z.; Pavlakis, G.; et al., Automatic and quantitative measurement of protein-protein colocalization in live cells. *Biophysical Journal.* **2004,** 86(6), 3993-4003.

61. Entzeroth, M.; Flotow, H.; Condron, P., Overview of high-throughput screening. *Curr. Prot. Pharmacol.* **2009,** 44(1), 9.4.1-9.4.27.

62. Hughes, J.P.; Rees, S.; Kalindjian, S.B.; Philpott, K.L., Principles of early drug discovery. *Br. J. Pharmacol.* **2011,** 162(6), 1239-1249.

63. Garnier, J.P., Rebuilding the R&D engine in big pharma. *Harvard Business Review.* **2008,** 86, 68-76.

64. Dimitri, N., An assesment of R&D productivity in the pharmaceutical industry. *Trends Pharmacol. Sci.* **2011,** 32(12), 683-685.

65. Macarron, R.; Banks, M.N.; Bojanic, D.; Burns, D.J.; Cirovic, D.A.; et al., Impact of high-throughput screening in biomedical research. *Nat. Rev. Drug Discov.* **2011,** 10, 188-195.

66. Inglese, J.; Johnson, R.L.; Simeonov, A.; Xia, M.; Zheng, W.; et al., High-throughput screening assays for the identification of chemical probes. *Nat. Chem. Biol.* **2007,** 3, 466-479.

67. Johnston, K.L.; Cook, D.A.; Berry, N.G.; Hong, W.D.; Clare, R.H.; et al., Identification and prioritization of novel anti-*Wolbachia* chemotypes from screening 10,000-compound diversity library. *Science Advances.* **2017,** 3, 1-10.

68. Bompiani, K.M.; Caglic, D.; Krutein, M.C.; Benoni, G.; Hrones, M.; et al., High-throughput screening uncovers novel botulinum neurotoxin inhibitor chemotypes. *ACS Comb. Sci.* **2016,** 18(8), 461-474.

69. Clare, R.H; Bardelle, C.; Harper, P.; Hong, W.D.; Borjesson, U.; et al., Industrial scale high-throughput screening delivers multiple fast acting macrofilaricides. *Nat. Commun.* **2019,** 10, 1-8.

70. Rogers, M.V., Light on high-throughput screening: fluorescence-based assay technologies. *Drug Discov. Today.* **1997,** 2(4), 156-160.

71. Tian, Y.; Martinex, M.M.; Pappas, D., Fluorescence correlation spectroscopy: a review of biochemical and microfluitic applications. *Appl. Spectrosc.* **2011,** 65(4), 115-124.

72. Kim, S.A.; Heinze, K.G.; Schwille, P., Fluorescence correlation spectroscopy in living cells. *Nature Methods.* **2007,** 4(11), 963-973.

73. Elsons, E.L., Fluorescence correlation spectroscopy: past, present, future. *Biophys. J.* **2011,** 101(12), 2855-2870.

74. Ries, J.; Schwille, P., Fluorescence correlation spectroscopy. *BioEssays.* **2012,** 34, 361-368.

75. Machan, R.; Wohland, T., Recent applications of fluorescence correlation spectroscopy in live systems. *FEBS Letters.* **2014,** 588(19), 3571-3584.

76. Jones, E.; Michael, S.; Sittampalam, S.G., Basics of assay equipment and instrumentation for high throughput screening. *Assay Guidance Manual.* **2012.**

77. Szymula, K.P.; Magaraci, M.S.; Patterson, M.; Clark, A.; Mannickarouttu, S.G.; et al., An open-source plate reader. *Biochemistry.* **2019,** 58(6), 468-473.

78. Caraus, I.; Alsuwailem, A.A.; Nadon, R.; Makarenkov, V., Detecting and overcoming systemic bias in high-throughput screening technologies:a comprehensive review of practical issues and methodological solutions. *Breif Bioinform.* **2015,** 16(6), 974-986.

79. Giuliano, K.A.; DeBiasio, R.L.; Dunlay, R.T.; Gough, A.; Volosky, J.M., High-content screening:a new approach to easing key bottlenecks in drug discovery process. *J. Biomol. Screen.* **1997,** 2(4), 249-259.

80. Loo, L.H.; Lin, H.J.; Steininger, R.J.; Wang, Y.; Wu, L.F.; et al., An approach for esxtensively profiling the molecular states of cellular subpopulations. *Nat. Methods.* **2009,** 6(10), 759-765.

81. Perlman, Z.E.; Slack, M.D., Feng, Y.; Mitchison, T.J.; Wu, L.F.; et al., Multidimensional drug profiling by automated microscopy. *Science.* **2004,** 306(5699), 1194-1198.

82. Slack, M.D.; Martinez, E.D.; Wu, L.F.; Altschuler, S.J, Characterizing heterogenous cellular responses to perturbations. *Proc. Natl. Acad. Sci.* **2008,** 104(49) 19306-19311.

83. Horman, S.R., Complex high-content phenotypic screening. *IntechOpen.* **2016,** 73-104.

84. Kraus, O.Z.; Hrys, B.T.; Ba, J.; Chong, Y.; Frey, B.J.; et al., Automated analysis of high-content microscopy data with deep learning. *Mol. Syst. Biol.* **2017,** 13(924), 1-15.

85. Sommer, C.; Hoefler, R.; Samwer, M.; Gerlich, D.W., A deep learning and novelty detection framework for rapid phenotyping in high-content screening. *Mol. Biol. Cell.* **2017,** 28(23), 31330-3470.

86. Nitta, N.; Sugimura, T.; Isozaki, A.; Mikami, H.; Hiraki, K.; et al., Intelligent image-activated cell sorting. *Cell.* **2018,** 175(1), 266-276.

87. Linding, R.; Kubicek, S.; Periyasamy, G., New technologies for translational research: applying high-content screening in cancer research and personalized medicine. *Science Webinar Series.* **2015,** 348(6231), 246.

88. Yu, K.K.H.; Taylor, J.T.; Pathmanaban, O.N.; Youshani, A.S.; Beyit, D.; et al., High content screening of patient-derived cell lines highlights the potential of non-standard chemotherapeutic agents for the treatment of glioblastoma. *PLOS One.* **2018,** 13(3), 1-17.

89. Prins, S.; Langron, E.; Hastings, C.; Hill, E.; Stefan, A.C.; et al., High-content assay for precision medicine discovery in cystic fibrosis. *Biorxiv.* **2019,** 1-36.

90. Ruban, G.I.; Berdnik, V.V.; Marinitch, D.V.; Gongcharova, N.V.; Loiko, V.A., Light scattering and morphology of the lymphocyte as applied to flow cytometry for distinguishing healthy and infected individuals. *J. Biomed. Opt.* **2010,** 15(5), 1-9.

91. Illien, F.; Rodrigues, N.; Amoura, M.; Joliot, A.; Pallerla, M.; et al., Quantitative fluorescence spectroscopy and flow cytometry analyses of cell-penetrating peptides and intenralization pathways: optimization, pitfalls, comparison with mass spectrometry quantification. *Nature Scientific Reports.* **2016,** 6.

92. Leonard, L.; Chibane, L.B.; Bouhedda, B.O.; De-graeve, P.; Oulahal, N., Recent advances on multi-parameter flow cytometry to characterize antimicrobial treatments. *Front. Microbiol.* **2016,** 7, 1-16.

93. Sakaguchi, Y.; Maehara, Y.; Inutsuka, S.; Takahashi, I.; Yoshida, M.; et al., Laser flow cytometric studies on the intracellular accumulation of anthracyclines when combined with heat. *Cancer Chemother. Pharmacol.* **1994,** 33(5), 371-377.

Chapter 2

Discovery of novel small molecule inhibitors of efflux involving P-glycoprotein

Cancer is a collection of related diseases. Whereas cancers can start almost anywhere in the human body, their etiology results from dysregulated cell growth.[1] For some cancers, these unregulated cells grow into a mass called a tumor, and malignant cancers can metastasize to a variety of different locations in the body. Eventually, normal biological function can be disrupted, decreasing the overall quality of life of the patient, and potentially leading to death. Cancer therapies have drastically improved in the past century and there are now many options for treatment including small molecule chemotherapeutics, radiation, immunotherapy, and surgery.[2-4] Common classes of small molecule chemotherapeutics include DNA alkylating agents,[5] antifolates,[6] DNA intercalators,[7] tyrosine kinase inhibitors,[8] and tubulin binding agents.[9] Although the mechanisms of which these treatments vary, they result in antiproliferative effects on cancer cells.

While existing therapies have been successful in treating some types of cancer, drug resistance remains a major limitation to the effectiveness to small molecule chemotherapeutics.[10] Although this resistance can result from multiple potential mechanisms, the overexpression of multidrug efflux pumps such as P-glycoprotein (P-gp) often plays a key role. Consequently, cancers that highly express P-gp have been linked to poor prognoses for patients.[11] This ATP-dependent efflux pump decreases the intracellular concentrations of xenobiotics by cycling between outward and inward facing conformations that traverse the cell membrane. Recently, a cryo-EM structure of the human P-gp in its outward facing conformation was reported[12] and compared with a

structure of the inward facing conformation of mouse P-gp, providing key insight into its mechanism of cellular efflux (Figure 2.1).[12]

In addition to its role in cancer biology, P-gp is a target of interest to increase the uptake of compounds with poor bioavailability, due to its expression in enterocytes that line the intestine.[13] Although much effort has been made to inhibit or reduce the expression of this protein using small molecules, there are currently no FDA approved drugs that specifically target this protein. Compounds that have entered clinical trials to evaluate efficacy in inhibiting P-gp have often failed due to lack of potency or toxicity due to the presence of P-gp in healthy tissues such as at the blood brain barier.[14] The development of novel probes of pathways that influence P-gp activity could shed light on potential new approaches for inhibition of drug resistance. Furthermore, using these probes to find new inhibitors in high throughput screening campaigns could lead to the discovery of novel chemotypes or mechanisms that inhibit this major drug transporter.

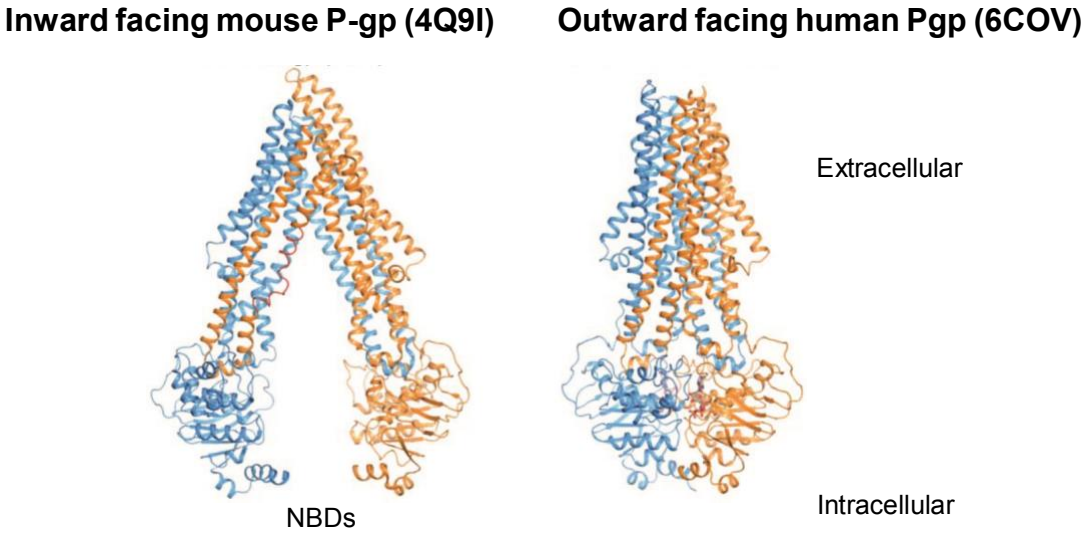

Figure 2.1. Comparison of structures of inward-facing mouse P-gp (left) and outward-facing human P-gp (right) as described by Kim et al.[12] When bound to two ATP molecules, the two nucleotide binding domains (NBDs) dimerize and reorient the drug binding domain into the intracellular space. These structures indicate that ATP binding, rather than hydrolysis, enables substrate release.

2.1 Introduction

Whereas P-gp can transport a broad spectrum of diverse substrates, a notable substrate in the context of cancer biology is the widely used chemotherapeutic drug paclitaxel (Taxol).[15] The Peterson group previously developed novel fluorescent analogues of Taxol that contain the coumarin-derived drug-like fluorophore Pacific Blue.[16] Unlike other widely used fluorescent taxoids, such as commercially available Flutax-2, one of these analogues, Pacific Blue-Gly-Taxol (PBGT, structure shown in Figure 2.2a), was found to maintain substantial cytotoxicity. Additionally, similar to Taxol, PBGT readily binds microtubules in living cancer cells. However, this probe is a highly efficient substrate of P-gp, and inhibition of P-gp by cotreatment with the small molecule verapamil is necessary to observe high levels of fluorescence in most living cell lines. When HeLa cervical carcinoma cells are cotreated with PBGT (1 μM) and verapamil (25 μM), cellular fluorescence increases by ~ 10-fold as analyzed by flow cytometry or confocal microscopy (Figure 2.2).

(A)

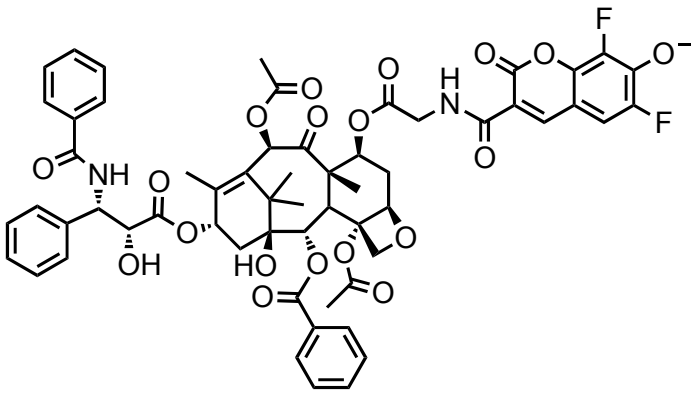

(B) (**C**)

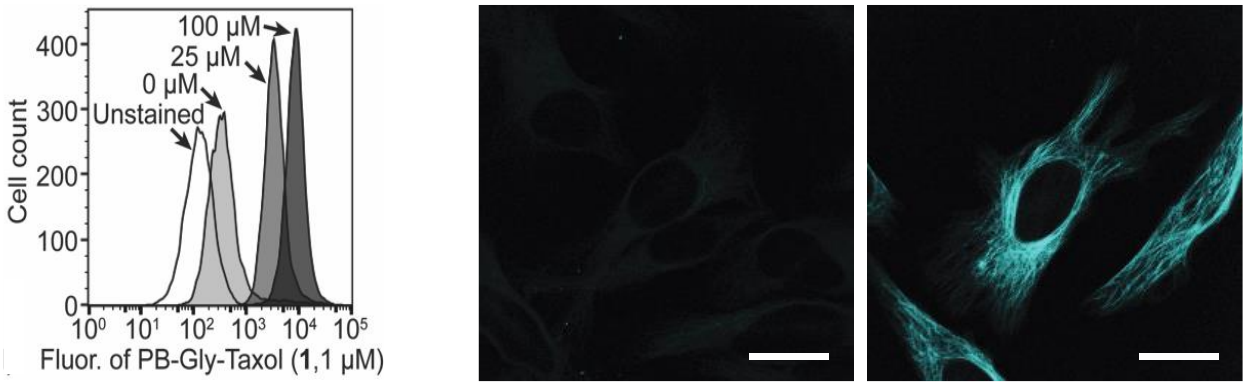

Figure 2.2. (A) The structure of Pacific Blue-Gly-Taxol (PBGT). (B) Previously reported[15] flow cytometry data showing the fluorescence of unstained HeLa cells, HeLa cells dosed with PBGT (1 μM, grey histograms), and HeLa cells additionally co-treated with verapamil (25 and 100 μM). C) Previously reported[16] confocal laser scanning microscopy images of HeLa cells treated with PBGT (1 μM). Cells in the left panel were treated with PBGT alone and cells in the right panel were co-dosed with verapamil (25 μM). Cells were excited at 405 nm and the fluorescence emission was collected from 425-500 nm.[16] Scalebar = 10 microns.

Because of the simplicity and sensitivity of this assay, we envisioned that it could provide a useful method to investigate cellular efflux mediated by P-gp. Small molecules that inhibit P-gp would theoretically cause P-gp expressing cells to accumulate a higher amount of PBGT and increase cellular fluorescence. High-content flow cytometry could also be used to screen against this phenotype while also providing a multi-parameter analysis of each population of cells.

What makes PBGT such a useful probe of P-gp is its ability to detect accumulation in cells that express low levels of P-gp. Other probes, such as rhodamine 123 and calcein-AM, have been used to screen for novel inhibitors of P-gp.[17-19] However, the Peterson laboratory has previously shown that in HeLa cells PBGT is much more sensitive than rhodamine 123 as a probe of P-gp.[16] To further explore its sensitivity, we recently compared this compound with Calcein-AM. This P-gp substrate is a pro-fluorophore ester derived from the green fluorescent fluorophore calcein (Figure 2.3a). It accumulates in cells and its esters are cleaved by esterases. This releases the fluorescent derivative calcein, which is highly charged and can no longer traverse the plasma membrane. In cells that express high levels of P-gp, this process is hindered due to efflux of the cell-permeable pro-fluorophore. Similar to PBGT, inhibition of P-gp increases cellular fluorescence due to the accumulation of calcein-AM and its product fluorophore calcein. To compare these two probes, cells were dosed with calcein-AM (0.25 μM), PBGT (1 μM), and co-dosed with verapamil (25 μM and 100 μM) in Jurkat lymphocytes. The cells were incubated for 1 h at 37 °C and analyzed via flow cytometry. This treatment with PBGT resulted in a 6.2-fold increase in fluorescence between wells in the absence and presence of verapamil (25 μM). In contrast, calcein-AM showed a smaller 1.4-fold increase in fluorescence. In addition, PBGT could detect changes in inhibitor concentrations with greater sensitivity. For calcein-AM, a significant ($p = 0.018$) difference was observed in the fluorescence of cells treated with verapamil at 100 μM and 25 μM, however PBGT measured a more significant ($p = 0.0014$) 1.7-fold increase in fluorescence when the verapamil concentration was increased from 25 μM to 100 μM. This data provides

evidence that PBGT is a much more sensitive probe than Calcein-AM for detection of P-gp in Jurkat lymphocytes (Figure 2.3b).

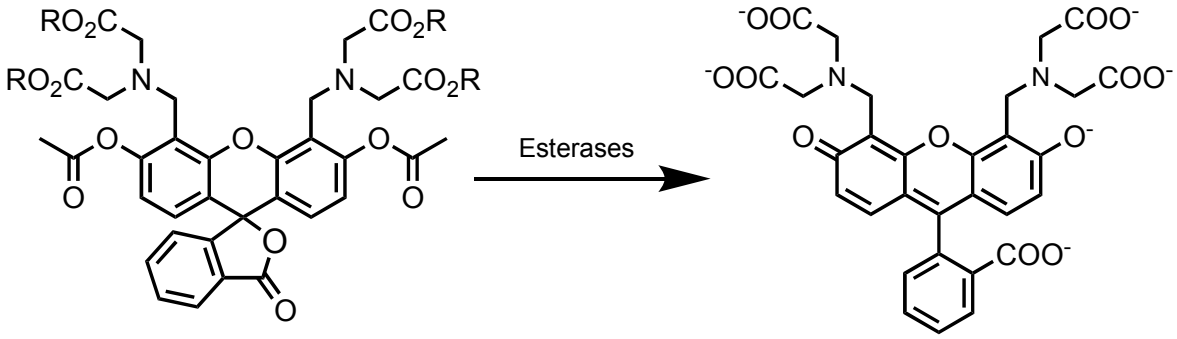

R = $CH_2OCOOCH_3$

Profluorophore Calcein-AM

Fluorophore Calcein
pH = 7

A)

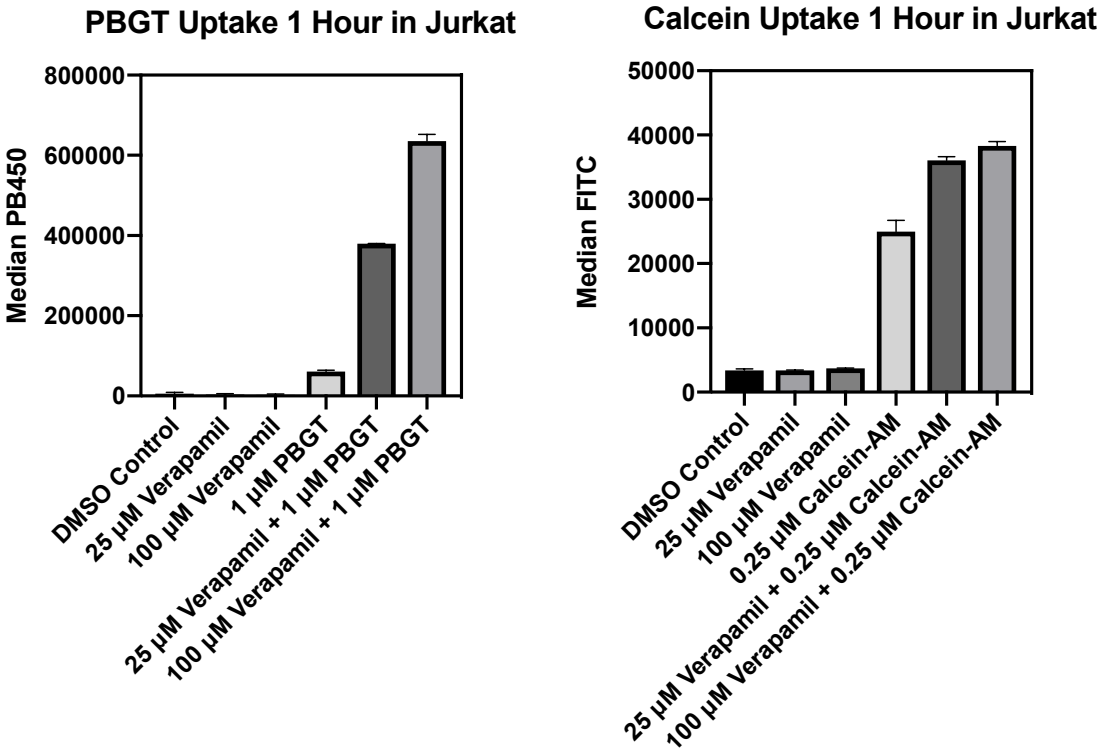

B)

Figure 2.3. (A) Structure of the profluorophore Calcein-AM and the product fluorophore calcein resulting from hydrolysis by esterases. (B) Fluorescence of Jurkat lymphocytes after treatment with PBGT (left) or Calcein-AM (right) and the P-gp inhibitor verapamil.

2.2 Considerations for primary screening by flow cytometry

Because it is such a sensitive probe, we envisioned that PBGT could be used in a phenotypic screening campaign to discover novel inhibitors of P-gp mediated efflux. In particular, we investigated high-content flow cytometry as a screening platform. This approach would allow multiparametric analysis of compound activity including both cellular fluorescence and acute cytotoxicity. To turn this idea into a feasible screen, we still needed to choose a suitable small molecule library, optimize the original assay for 96-well plates, and plan a counter-screen to eliminate the intrinsic fluorescence of some library members. Section 2.2 will focus on methods used to develop a P-gp assay suitable for screening of living cells by flow cytometry on 96-well plates.

2.2.1 Selection of a chemical library

On the surface, high throughput screening can be compared to a game of darts that is played in the dark, where random compounds are screened against a target of interest in hopes of finding some “on-target” hits. In reality, careful selection of an appropriate small molecule library is critical for a successful screen. In terms of how these small molecule libraries are assembled, they generally exclude compounds with reactive moieties that cause systemic toxicity and Pan-assay interference compounds (PAINs) that can lead to false positives.[20-21] Libraries generally include diverse small molecules of varying complexity. More recently, focused libraries have been developed to target specific proteins.[22] These libraries contain families of small molecules that are generally known to be active modulators of a particular protein or protein type such as G-protein coupled receptors, kinases, and voltage-gated ion channels. Selection of a library

generally takes into account the target of interest and the physiochemical properties required in a drug candidate. For instance, if a screen was developed to discover a small molecule modulator of a central nervous system target, screening compounds with poor blood brain barrier penetration would be counterproductive towards the end goal.

The library we chose for this screen was the NCI diversity set VI library. This library is a made up of 1584 diverse small molecules and is derived from a 140000-compound repository. The 1584 compounds in this library are made up of a number of diverse and relatively rigid small molecules and is available arrayed on twenty 96-well plates. Pharmacological liabilities such as electrophiles, polycyclic aromatics, and organometallics have been excluded from this library.[23] Besides its diverse range of compounds, it also contains some known P-gp substrates. While this feature would not aid us in finding novel inhibitors of P-gp, detecting these molecules in our screen could further validate that this phenotypic screening method might identify inhibitors of this major efflux protein.

2.2.2 Choosing a suitable non-adherent cell line

Due to the sheer size of a screening campaign, it is critical to remove or replace non-essential assay steps that are repetitive or error prone. One such non-essential step in the initial cellular studies of PBGT was the trypsinization of adherent HeLa cells required for analysis by flow cytometry. Because we intended to use flow cytometry as a detection platform, the cells need to be in suspension prior to analysis. To simplify the assay, we reasoned that the use of a non-adherent cell line could allow us to forgo this additional step.

To find a non-adherent cell line suitable for detection of P-gp activity, we added PBGT (1 μM) alone and coadministered with the P-gp inhibitor verapamil (25 μM and 100 μM) to the suspension cell lines Ramos, Raji, HL-60, and Jurkat and compared these results with trypsinized HeLa cells. Although Jurkat cells did not exhibit the highest fluorescence intensity, this cell line had the highest fold increase when treated with PBGT (1 μM) compared with a combination of PBGT (1 μM) and verapamil (25 μM). These results indicated that the Jurkat cell line would allow us to readily detect changes in accumulation of PBGT and was selected for the screen.

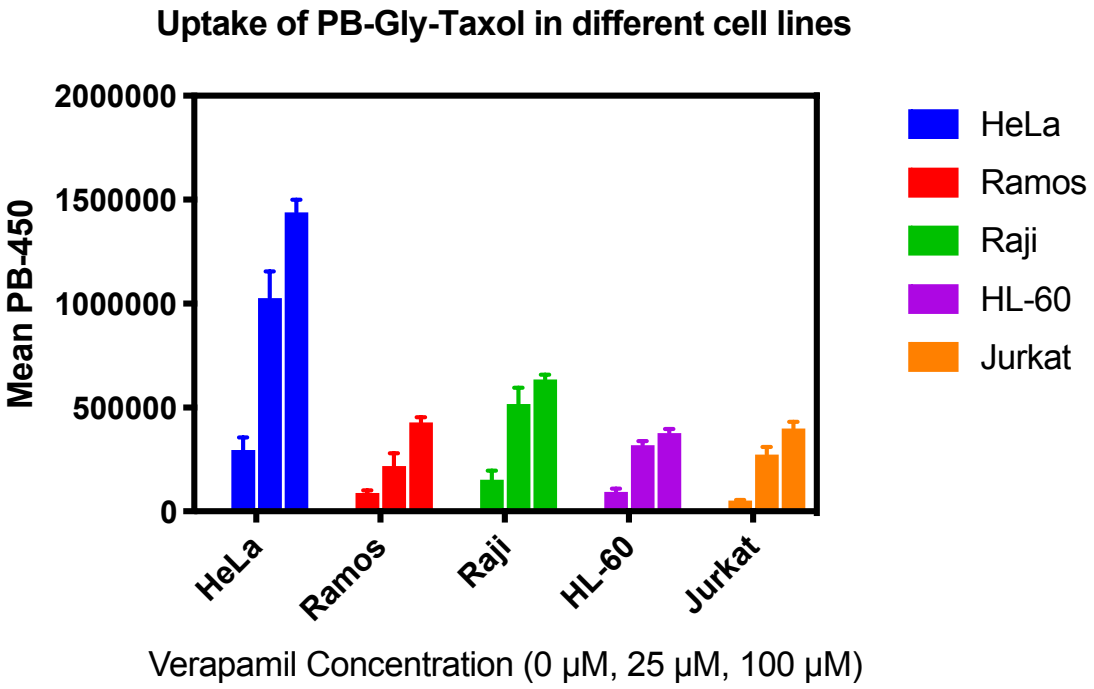

Figure 2.4. Fold increase in different cell lines. Trypsinized HeLa, and the suspension cell lines Ramos, Raji, HL-60, and Jurkat cell lines were treated with PBGT (1 μM) alone and in conjunction with verapamil (25 and 100 μM), incubated for 1 h at 37 °C, and analyzed via flow cytometry. Data provided by Zhe Gao.

2.2.3 Assay automation

To further improve the screening process, we employed an automated Integra pipetting robot. This robot uses a multichannel pipette attached to a robotic arm to allow transfers between different 96 or 384 well plates. We utilized this robot in both the seeding of Jurkat cells and for treatment with library compounds. Because the media of the cells was supplemented with concentrated PBGT prior to seeding in a 96 well plate, the concentration of the probe should be consistent throughout all 96 wells of each plate. Library compounds were transferred using this robot to allow accurate delivery to each well.

2.2.4 Assessment of intrinsic fluorescence

A potential complication associated with this screening approach was the possibility that particular library members might be intrinsically fluorescent and detected with the same emission filter as our probe. To assess this issue, each 96 well plate was treated with library compounds and analyzed via flow cytometry before running the assay plate with PBGT. This allowed subtraction of intrinsic fluorescence from assay fluorescence values to give a more accurate measurement of the fluorescence changes due to cellular uptake of PBGT.

2.2.5 Controls

The last consideration was the positive and negative controls to include on each assay plate. Negative controls consisted of three wells treated with only the DMSO vehicle. These controls are vital because they exemplify data from what should be a

healthy population of cells. The light scattering histogram of these cells can be gated in the flow cytometry software and compared to each assay well to assess any rapid cytotoxic effects. Positive controls consisted of at least three wells for each of two different concentrations of verapamil (25 μM, 100 μM). These wells on each plate were critical for the accurate analysis of all of the library compounds. Cell-based assays are sensitive, and variations can be observed with very slight changes in assay conditions including cell passage number and density (or confluency).[24-25] Having these controls provided a means to compare the effects of library inhibitors in comparison to the known competitive inhibitor verapamil. If the final analysis used only a single fluorescence measurement, these values would be a less accurate assessment of compound activity.

2.3 Analysis of data from screening the NCI Diversity Set-VI library

After the assay was optimized, all 1584 compounds in the NCI diversity set VI were screened and analyzed. We aimed to analyze the data in such a way that each plate can be compared to one another with minimization of false positives. The intrinsic fluorescence intensity of the library compound, evaluated on the same day and same cell passage number, was subtracted from the assay fluorescence intensity. This adjusted fluorescence intensity was then divided by the fluorescence intensity of PBGT (1 μM) to yield the fold increase in fluorescence intensity due to the library compound. This fold increase value was then divided by the fold increase for 25 μM verapamil to give the percent activity compared with 25 μM verapamil. Finally, to account for any rapid cytotoxic effects of the library compound, we multiplied by the percent viability. Rapid cytotoxic

effects resulted in enhanced cellular fluorescence and including this factor reduced the frequency of false positives. This equation is shown in Figure 2.5.

$$\left(\frac{(FA - FI)}{NC} \div PC\right) \times viability = \%\ activity\ of\ 25\ \mu M\ Verapamil$$

Figure 2.5. HTS analysis equation: The above equation was used to analyze fluorescence intensities from the screen. Variables: FA = assay fluorescence, FI = intrinsic fluorescence, NC = mean of negative control (1 μM PBGT wells), PC = fold increase of positive control (25 μM verapamil wells).

After each value for fluorescence intensity was converted into percent activity of 25 μM verapamil, we plotted this data as a histogram for further comparison. This histogram is shown in Figure 2.6. Each plate is represented by a different symbol and on the X-axis is each well of the 96 plate. On the Y-axis is the percent activity of 25 μM verapamil with the cytotoxicity factor included.

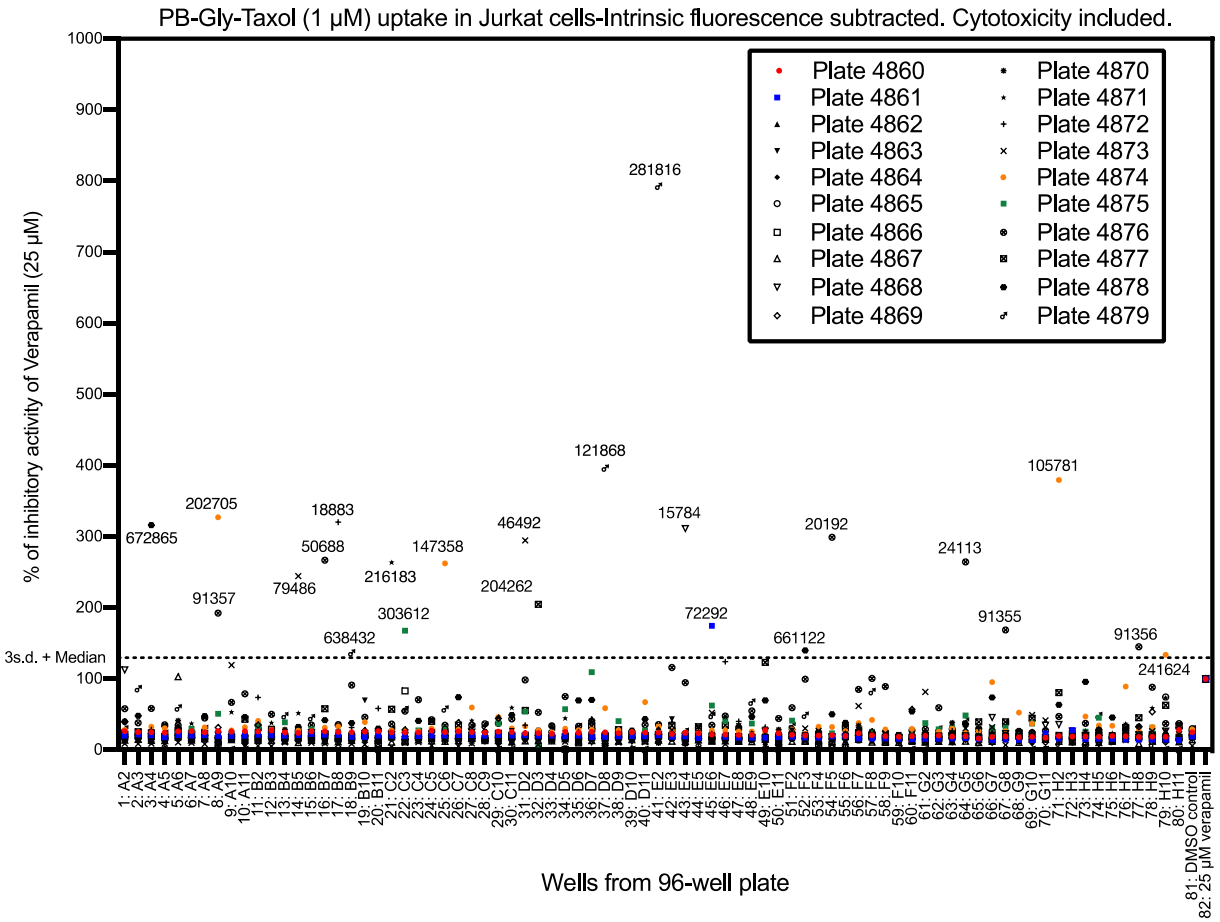

Figure 2.6. Histogram of treated screening data: Primary median fluorescence after screening of the NCI diversity set VI against PBGT in Jurkat lymphocytes. Compound activity is shown based on each well of a 96-well assay plate. Each plate is represented by a different symbol as shown in the key. For each "hit compound", defined as greater than the median + 3 SD, the corresponding NSC number is provided.

The cutoff we chose for "hit" compounds was 3 times the standard deviation of all of the library values plus the median of all of the library values. This cutoff is shown as a dotted line in Figure 2.6. This analysis ensures that our hits are far enough away from the median value and are significantly different than the average library member. This method of analysis provided 23 hit compounds and a hit rate of 1.45%. While most high-throughput screens generally have a hit rate of less than 1%,[26] it is understandable that a screen focusing on efflux related to the notoriously promiscuous P-gp might have a

higher than normal hit rate.[27] A sorted list of these hits based on their % activity of 25 verapamil is shown in Figure 2.7.

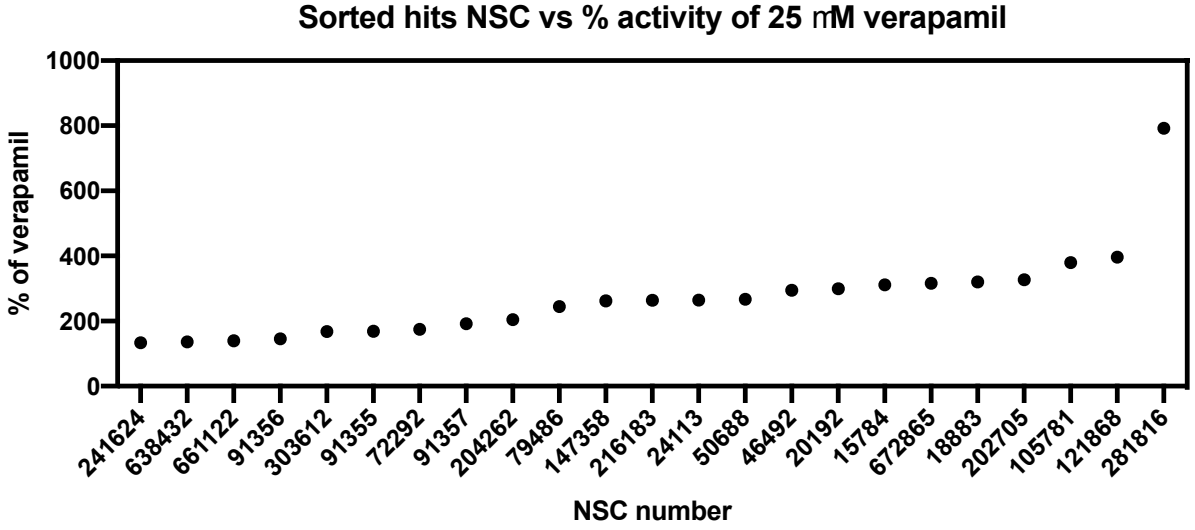

Figure 2.7. Ranked hits: Hit compounds of 3 times the standard deviation of the median library values or greater are shown above. They are ranked based on percent activity compared with 25 μM verapamil.

2.3.1 Families of small molecule hits

Within the 23 hit compounds which came out of this screen, there were several distinct families that displayed high structural similarity to each other. The first family of inhibitors we will outline are the phenothiazines and associated compounds. A complete list of hit molecules containing either a phenothiazine or the ring expanded NSC 281816 is shown in Figure 2.8.

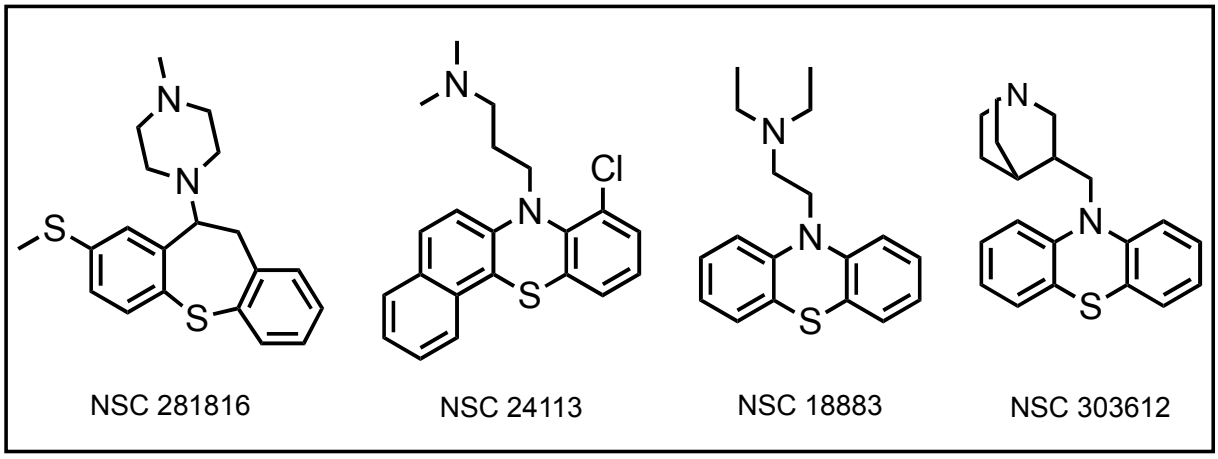

Figure 2.8. Phenothiazines and associated compounds: Structures and NSC numbers of phenothiazine hits and the related compound NSC 281816.

Phenothiazines have been studied for a wide variety of biomedical applications and are considered to be a privileged scaffold in medicinal chemistry.[28] The discovery of this scaffold is not a novel finding because this class of compound has already been well studied for their role in the modulation of multidrug resistence.[29-30] In particular, they have been shown to be antagonists of P-gp mediated efflux and conversely they have been linked to stimulation of multidrug resistance-associated protein 1 (MRP1).[31] While this class of compounds was already known to inhibit P-gp, the fact that such compounds were detected up by our screen further validates that our assay can detect modulators of P-gp mediated efflux.

The next class of hits found to inhibit cellular efflux of PBGT was a family of carbazole-containing compounds. Carbazoles are structurally analogous to the previously discussed phenothiazines, and they can be synthesized from them via a ring contraction to extrude the sulfur atom of the phenothiazine.[32] Carbazole and associated hits are shown in Figure 2.9.

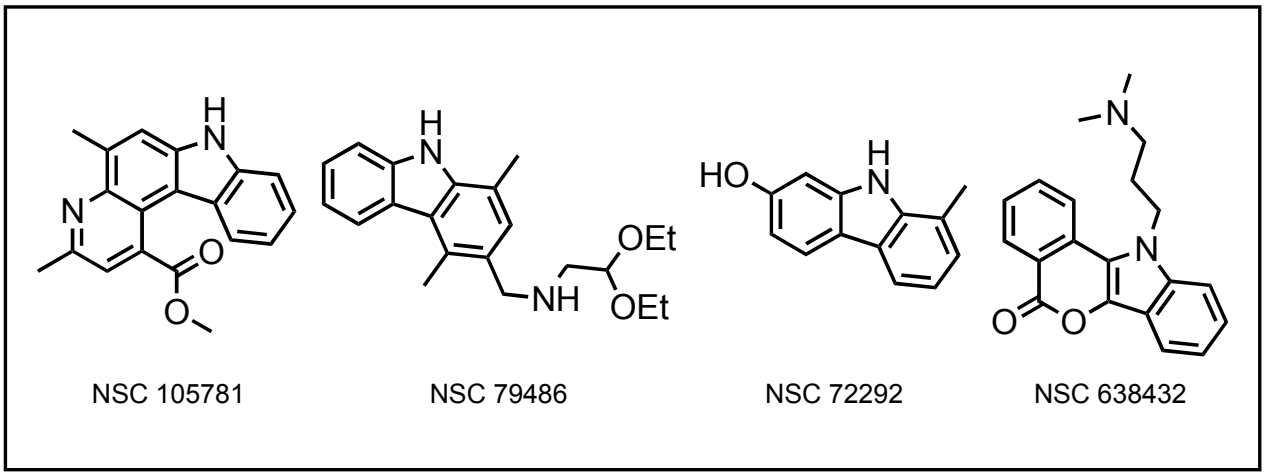

Figure 2.9. Carbazole and associated hits: Structures and NSC numbers of carbazole hits and the related compound NSC 638432.

Since carbazoles have a high structural similarity to the previously discussed phenothiazines, it is reasonable to envision that they could also be inhibitors of P-gp mediated efflux. These compounds have not been extensively studied as modulators of cellular efflux, but some carbazole-containing compounds have been shown to be substrates of P-gp.[33] Similarly, some compounds with in vitro efficacy against Alzheimer's targets have shown decreased in vivo efficacy due to P-gp mediated efflux at the blood brain barrier.[34-35] These findings support that P-gp modulation is detected by our assay, however these compounds were not pursued further due to their lack of novelty.

A major class of compounds identified from the primary screen were diaryl derivatives. These simple compounds generally link two aryl groups together by either a urea, carbamate, or amide bond and is the largest family of compounds identified from the screen. These structures are shown in Figure 2.10.

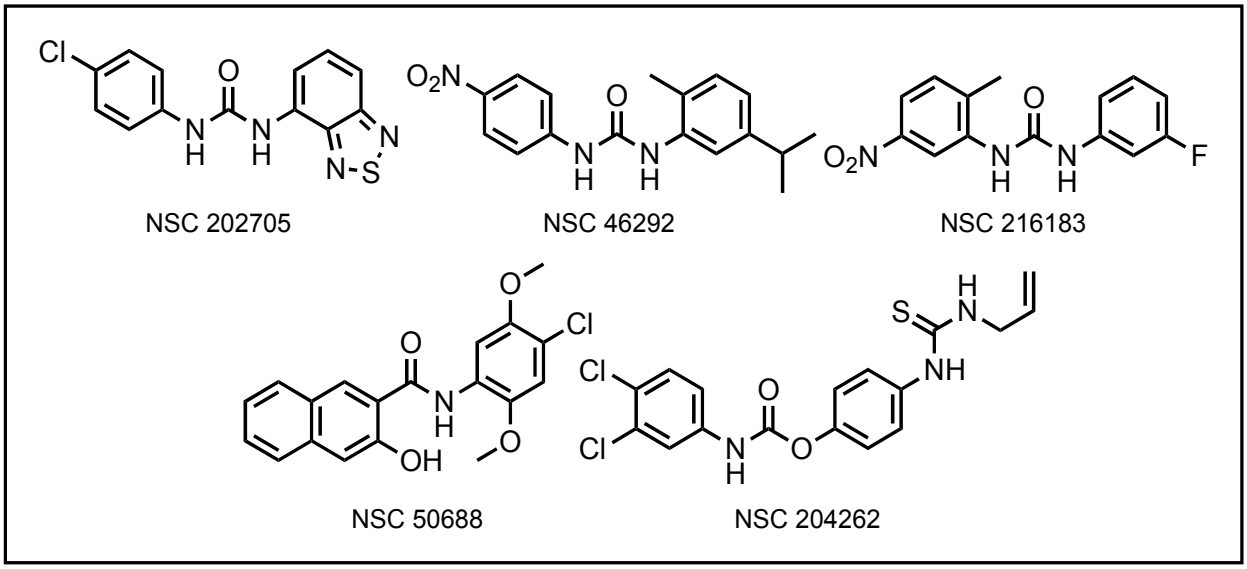

Figure 2.10. Diaryl and associated compounds. Structures and NSC numbers of diaryl ureas, carbamates, and amide-containing hit compounds.

Although these diaryl compounds are relatively simple organic molecules, they have not been previously reported as inhibitors of P-gp-mediated cellular efflux. Furthermore, these diaryl compounds are not known to be substrates for efflux by P-gp. Consequently, we hypothesized that these agents might provide a new chemotype for inhibition of cellular efflux involving P-gp.

2.4 Diarylureas as novel inhibitors of cellular efflux

Due to their novelty as cellular efflux modulators, and unexplored mechanism of inhibition, we further investigated the activity of the diarylureas. In the past, urea has been extensively studied for its role as a destabilizing agent that can disrupt critical hydrogen bonds of proteins.[36-37] Furthermore, diarylureas have become a privileged structure in anticancer agents and exhibit a wide range of antiproliferative activity in cells.[38-40] Experiments to assess the relative potency of these diarylureas at inhibiting cellular efflux

were conducted using flow cytometry. Further experiments to investigate possible mechanisms of inhibition were conducted using confocal laser scanning microscopy.

2.4.1 Hit validation

To confirm the activity and to assess the relative potency of these compounds, as shown in Figure 2.11, we generated a dose response curve with our most active diarylurea hit, NSC 202705. The dose response curve was generated in comparison with verapamil with Jurkat lymphocytes, 1 μM PBGT, and the urea from 100 μM to 100 pM in 1:10 dilutions.

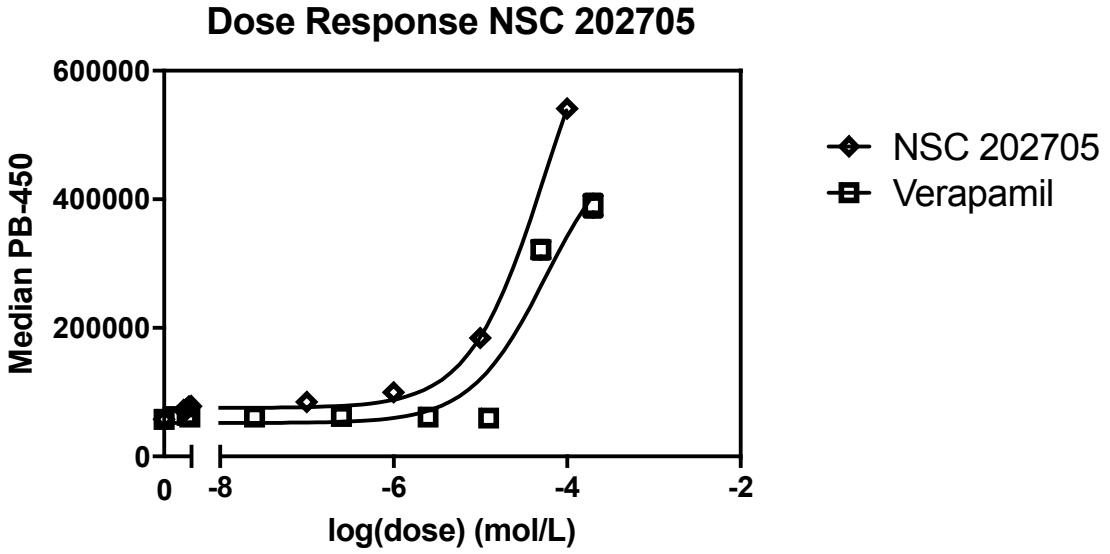

Figure 2.11. Dose response data NSC 202705 in the PBGT/Jurkat efflux assay. Cells were treated with inhibitors at concentrations ranging from 100 μM to 100 pM, incubated for 1 hour at 37 °C, and analyzed by flow cytometry.

From this dose-dependent inhibition data, NSC 202705 initially appeared to be more potent with potentially higher efficacy than verapamil. Based on the best curve fit NSC 202705 had an IC_{50} of 55 μM, whereas verapamil exhibited an IC_{50} of 57 μM. However, we additionally found that this urea was weakly fluorescent at 450 nm, and it

can be observed on the same fluorescence channel as PBGT. This made it difficult to determine its relative potency because it was not possible to distinguish the signal from PBGT from the signal due to the urea. In addition, because intrinsic fluorescence contributes to the observed activity, the IC_{50} for this compound appears to be more potent than its actual value. Because a blue fluorescent urea such as NSC 202705 might be problematic for analysis with PBGT, we designed a potentially orthogonally fluorescent urea for further analysis with PBGT. With the assistance of KU Synthetic Chemical Biology Core, we generated a green fluorescent urea (GF urea, Figure 2.12a), derived from the NBD fluorophore, that is very similar in structure to NSC 202705. We confirmed that this compound, termed the green fluorescent urea (GF-urea), did not spectrally overlap with PBGT, and this compound also inhibited the cellular efflux of PBGT (Figure 2.11b). Additionally, as shown in Figure 2.12c, the IC50 of the GF-urea was measured to be 10 μM, roughly 5-fold greater in potency compared with verapamil.

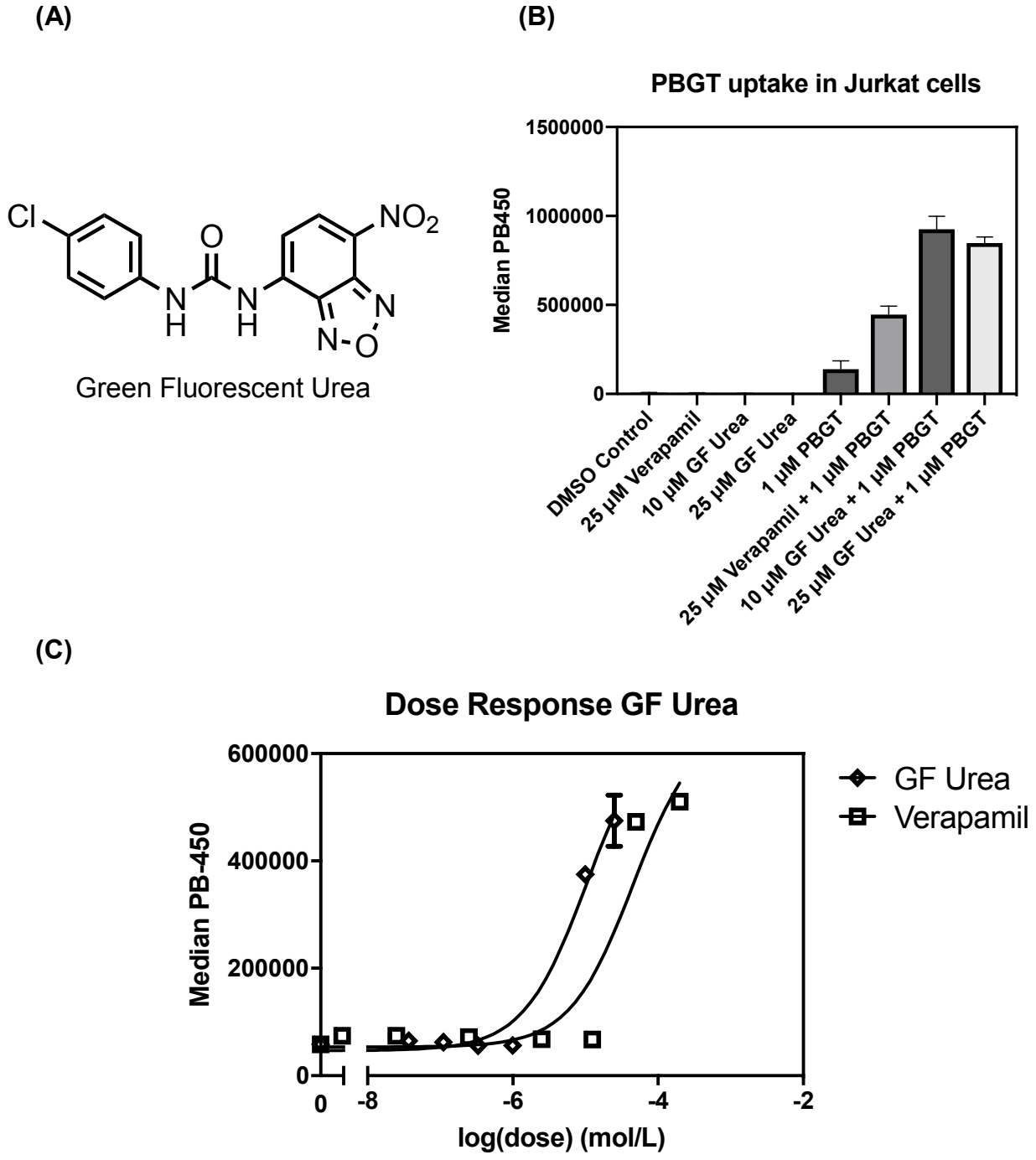

Figure 2.12. (A) The structure of the GF-urea analogue of NSC 202705. (B) Analysis of the GF-urea in the PBGT/Jurkat assay by flow cytometry. (C) Dose response of the GF-urea compared with verapamil.

We hypothesized that this green fluorescent analogue of NSC 202705 could potentially facilitate analysis of possible mechanisms of inhibition for this class of

compounds. In addition, since it is orthogonally fluorescent when compared to PBGT, both of these compounds can be simultaneously analyzed in cells by confocal microscopy. To qualitatively validate that this compound can overcome cellular efflux and promote the accumulation of PBGT, HeLa cells were treated with 25 μM urea and 1 μM PBGT. Confocal micrographs of HeLa cells treated in this way are shown in Figure 2.13.

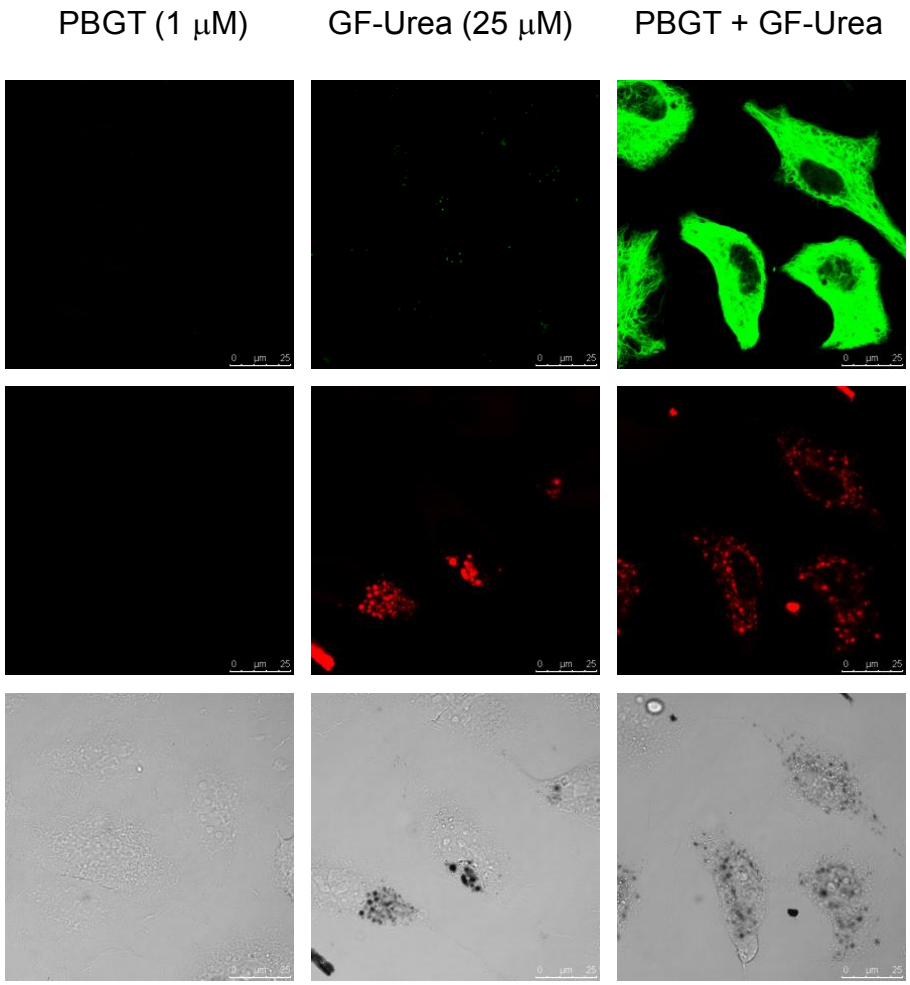

Figure 2.13. Confocal and DIC images of HeLa cells treated with PBGT (1 μM, left), the GF-urea (25 μM, center), and both of these compounds (right). The top row shows excitation at 405 nm with emission from 420-480 nm (blue fluorescent). The middle row shows excitation at 488 nm with emission from 500-600 nm (green fluorescent). The bottom row shows DIC images.

Confocal images of HeLa cells treated with 25 μM green fluorescent urea demonstrated that this compound promotes cellular uptake of PBGT. Another interesting finding from these images was the unique localization of the urea compound. This compound appeared to be either aggregating or localizing in a particular subcellular compartment. We hypothesized that this localization might be related to the cellular accumulation of PBGT, but the involvement of P-gp would require further studies of possible mechanisms of inhibition.

2.4.2 Investigation of mechanisms of inhibition of P-gp by diaryl ureas

As previously discussed in chapter one, fluorescent fusion proteins can provide a valuable method to probe biological interactions. To further investigate possible mechanisms of inhibition of P-gp by diarylurea compounds, we employed the use of pHaMDR-EGFP, a plasmid encoding P-gp fused to enhanced green fluorescent protein. Because this fusion protein is green fluorescent, we could not use the green fluorescent urea as a probe. Instead, we used the original blue fluorescent hit, NSC 202705, to examine colocalization with P-gp, which is normally expressed on the plasma membrane.

For these studies, we transiently transfected PC-3 prostate cancer cells, which do not appear to express P-gp, with pHaMDR-EGFP. Cells were treated with 10 μM NSC 202705 and analyzed by confocal microscopy. Although NSC 202705 exhibited relatively weak fluorescence when examined by flow cytometry methods, it proved to be a bright fluorescent probe when analyzed by confocal microscopy. Because of this, we could assess its accumulation in cells that express green fluorescent P-gp. The images shown in Figure 2.14 revealed that there was not much of a difference in the concentration of the

urea in transfected cells that express P-gp compared with non-transfected cells, indicating that this urea is not likely to be a sensitive substrate of P-gp. We additionally did not notice any changes in the localization of P-gp when transfected cells were treated with NSC 202705 (Figure 2.14).

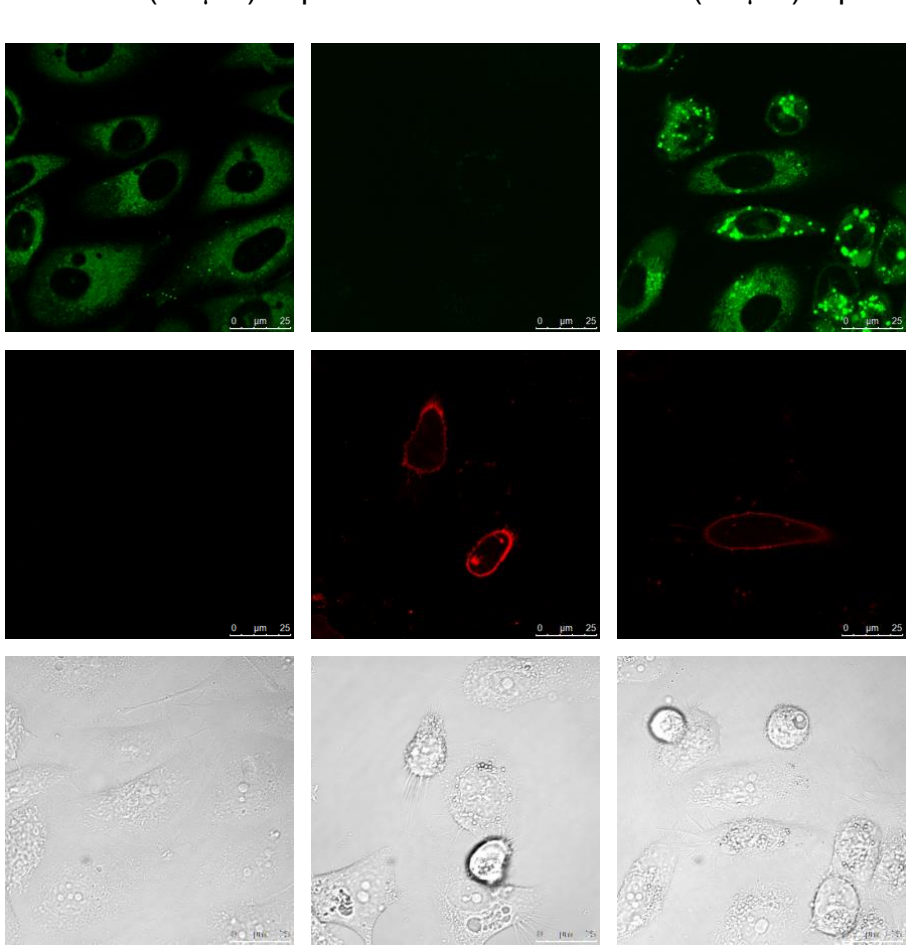

Figure 2.14. Transfection of PC-3 cells with pHaMDR-EGFP in. Confocal laser scanning and DIC microscopy of PC-3 prostate cancer cells transiently transfected with pHaMDR-EGFP and / or treated with 10 μM NSC 202705. The top row shows excitation at 405 nm with emission from 420-470 (blue fluorescent). The middle row shows excitation at 488 nm with emission from 500-600 nm (green fluorescent). The bottom row shows DIC images.

Although NSC 202705 did not appear to affect the localization of P-gp-EGFP, the localization of the compound suggested a possible explanation as to how this compound

might affect the uptake of PBGT. After a literature review, we discovered that the structurally similar diarylsulfonylureas have been shown to localize in mitochondria.[41-42] Furthermore, some quinazolinyl-diarylurea derivatives can decrease the mitochondrial membrane potential and disrupt mitochondria.[43]

To see whether this particular diarylurea affects mitochondria, we treated cells with MitoTracker deep red, a fluorescent probe that specifically stains mitochondria. HeLa cells were treated with 100 nM MitoTracker deep red and 10 μM NSC 202705, incubated for 1 hour at 37 °C, and subsequently imaged with a confocal microscope. As shown in Figure 2.15a, some colocalization (shown in yellow) was observed between these compounds. Additionally, we found that cells treated with only MitoTracker exhibit healthy rod-shaped mitochondria, whereas cells treated with both MitoTracker and the urea exhibit an altered more spherical mitochondrial morphology, indicating potential mitochondrial stress or disruption (Figure 2.15b).

(A)

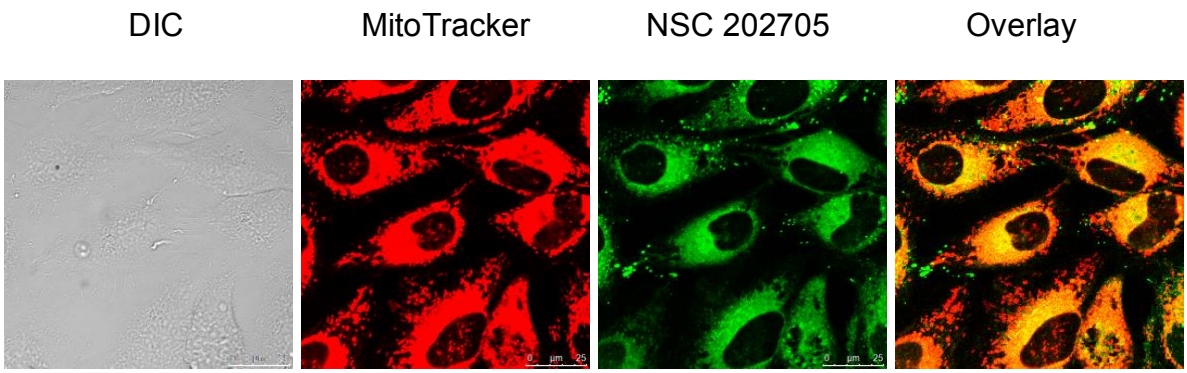

(B)

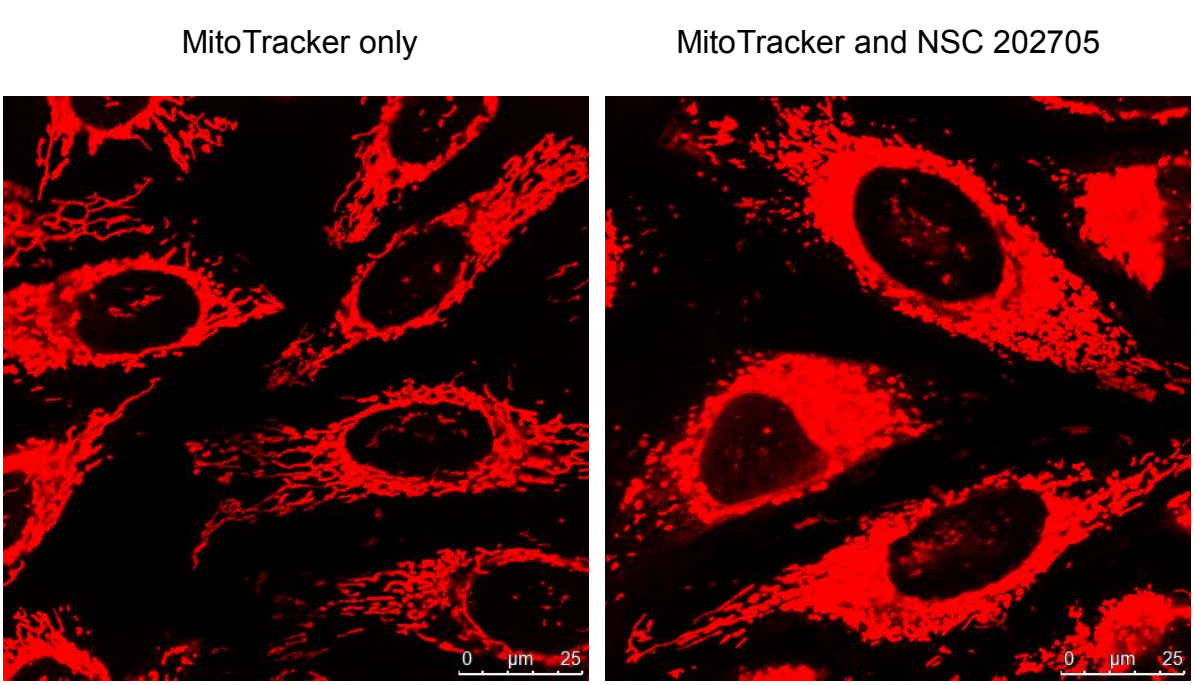

Figure 2.15. Localization in mitochondria and effects of NSC 2020705 on these organelles. (A) Confocal laser scanning and DIC microscopy of HeLa cells co-treated with 10 μM NSC202705 and 100 nM MitoTracker deep red. MitoTracker was excited at 635 nm and the emission collected from 645-700 nm. NSC 202705 was excited at 405 nm and the emission collected from 420-470 nm. B) Confocal laser scanning of HeLa cells treated with only 100 nM MitoTracker (left image) and co-treated with 100 nM MitoTracker and 10 μM NSC202705 (right image).

To further investigate the effects of diarylureas on mitochondria, HeLa cells were treated with mitotracker deep red and the urea compounds NSC 202705, 46492, 216183, and GF urea. Confocal micrographs of these cells are shown in Figure 2.16.

MitoTracker only

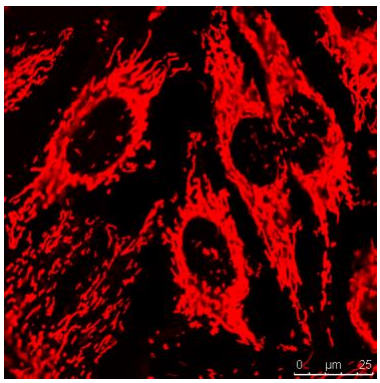

MitoTracker & NSC 46492

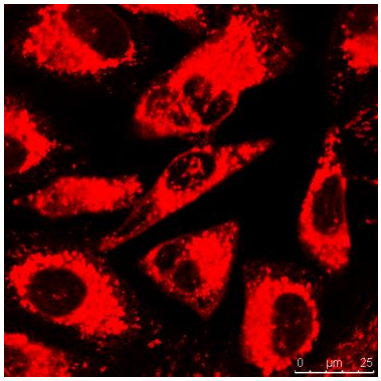

MitoTracker & NSC 216183

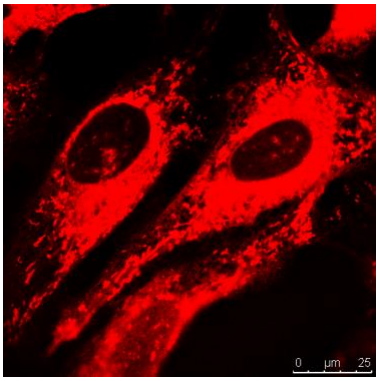

MitoTracker & GF Urea

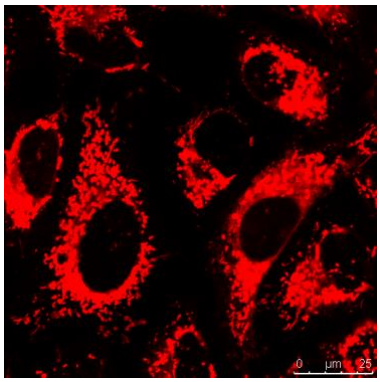

MitoTracker & NSC 202705

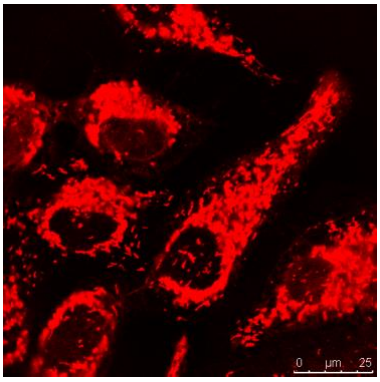

Figure 2.16. Mitochondrial disruption observed upon treatment with all urea hits. Confocal laser scanning micrographs of HeLa cells treated with 100 nM MitoTracker deep red without and with each urea hit from our screen and the GF urea analogue.

For each well co-treated with a diarylurea, the native rod-like morphology of the mitochondria appeared to be lost. The mitochondria become fragmented, a phenotype often observed in the early stages of apoptosis.[44] Treatment with each of these diarylureas can change mitochondrial morphology and potentially disrupt mitochondrial function. Based on other studies that have shown that nanoparticles that disrupt mitochondria can affect P-gp through depletion of ATP,[45] we hypothesized that disruption of mitochondria by the GF-urea could potentially lead to plunging ATP levels within the cell and consequent inhibition of ATP-dependent P-gp-mediated efflux.

To test this hypothesis, we worked with the High Throughput Screening Laboratory at KU to analyze the effect of NSC 202705 on cellular ATP levels in both HeLa and Jurkat cells using a luciferase reporter assay. Cells were treated with CellTiter-Glo and varying concentrations of NSC 202705 from 0 to 80 μM. Following incubation for 1 h or 4 h at 37 °C, ATP-dependent luminescence was measured. Cellular ATP levels were then interpolated from an ATP standard curve (figure 2.17)

(A)

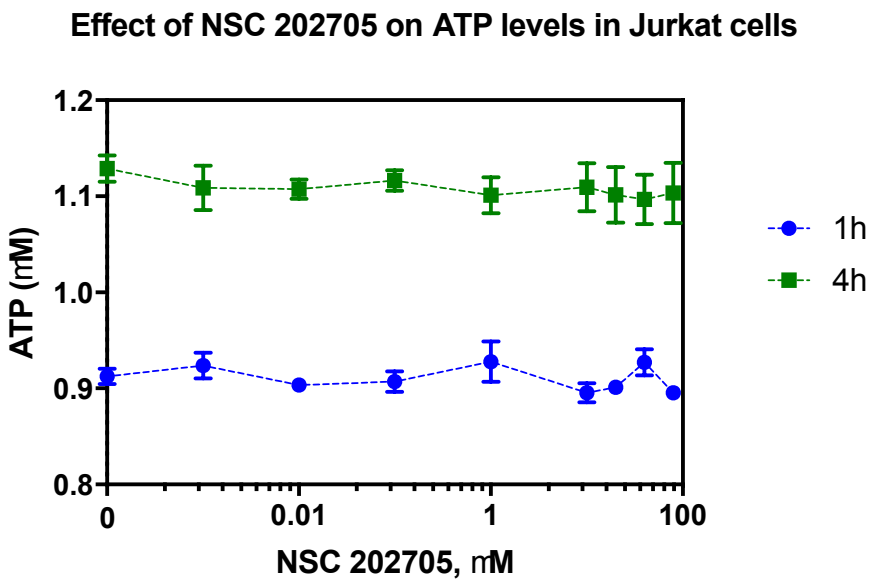

(B)

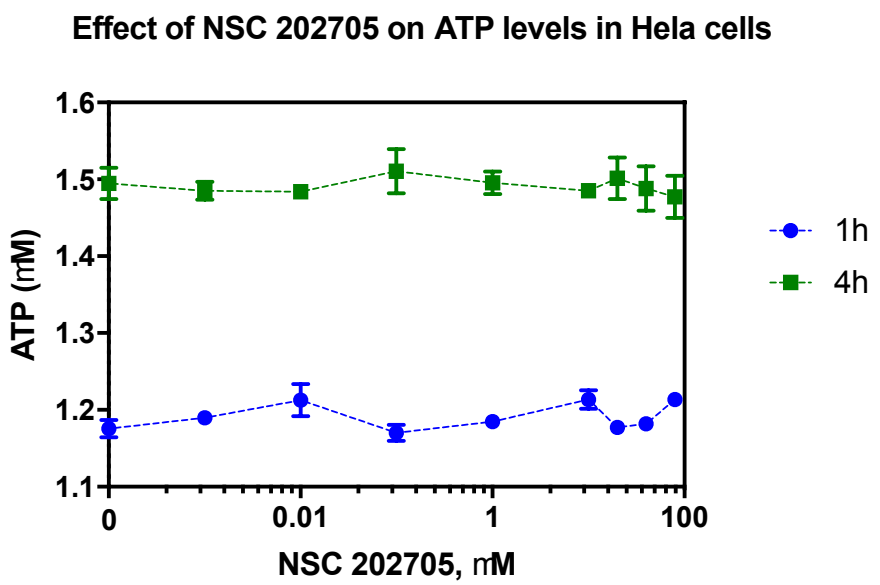

Figure 2.17. Effects of NSC 202705 on cellular ATP levels. (A) Jurkat lymphocytes were treated with CellTiter-glo and increasing amounts of NSC 202705. (B) HeLa cells were treated with CellTiter-glo and increasing amounts of NSC 202705.

Surprisingly, no correlation between ATP-levels and the concentration of NSC 202705 in either cell line was observed in glucose-rich media. ATP-levels remained constant when dosed with high concentrations of NSC 202705, indicating that the depletion of cellular ATP was not the mechanism of inhibition. However, this assay was run in high-glucose media, and the ATP consumed in this assay did not necessarily originate from mitochondria. This assay was ran again in media supplemented with low glucose and D-galactose supplemented media to further determine whether NSC 202705 affects ATP production via inhibition of mitochondrial oxidative phosphorylation.

(A)

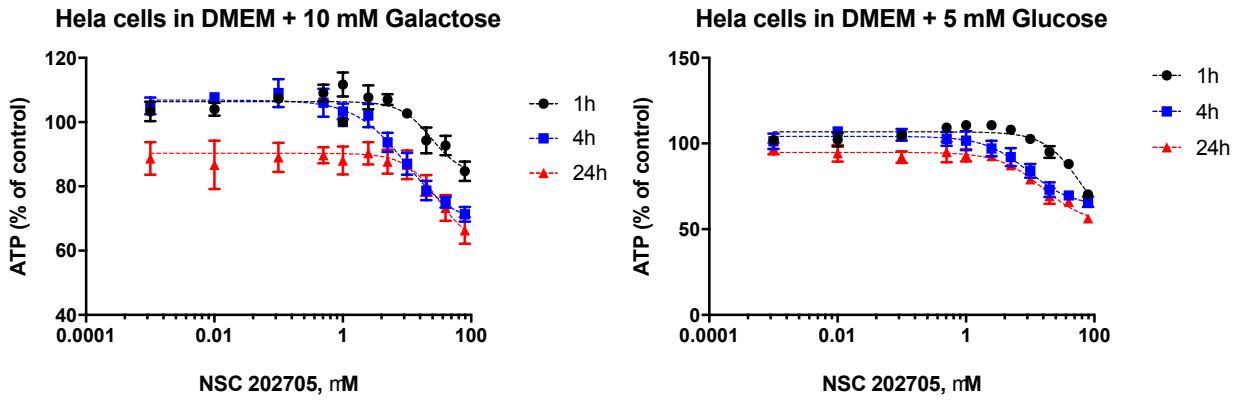

(B)

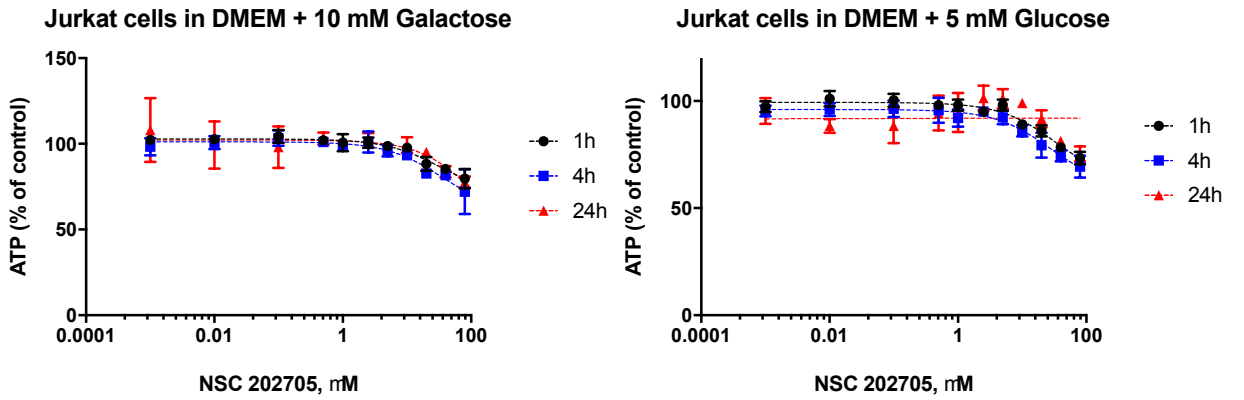

Figure 2.18. Effects of NSC 202705 on cellular ATP levels in glucose deficient media. (A) HeLa cells were treated with CellTiter-glo and increasing amounts of NSC 202705 in galactose and low glucose supplemented media. (B) Jurkat Lymphocytes were treated with CellTiter-glo and increasing amounts of NSC 202705 in galactose and low glucose supplemented media.

These studies showed that NSC 202705 was not a potent inhibitor of ATP production in glucose deficient media. However, high concentrations of NSC 202705 slightly decreased cellular ATP levels when compared to the negative control. Further studies are needed to determine how/if these two phenotypes are linked and might confirm that these compounds represent a novel chemotype and mechanism of action as cellular efflux inhibitors.

2.5 Conclusions

In summary, a high-content assay utilizing flow cytometry and a fluorescent mimic of Taxol was developed with an automated screening platform to detect inhibition of cellular efflux. A pilot screen of 1584 diverse small molecules was performed to identify inhibitors of efflux involving P-gp. From this phenotypic screen, we identified 23 compounds that increase the cellular fluorescence of Jurkat lymphocytes. Two families of compounds identified from the primary screen, phenothiazines and carbazoles, are already well studied P-gp inhibitors and substrates, providing evidence that this assay can identify inhibitors of P-gp. Additionally, a novel chemotype of diarylureas, carbamates, and amides was found to inhibit cellular efflux. The diarylureas were studied further to determine a possible mechanism of inhibition. Through the use of confocal laser scanning microscopy, we found that these diarylureas do not appear to be substrates of P-gp, nor do they appear to bind directly to P-gp. Further studies found that these diarylureas appear to disrupt the structures of mitochondria and can slightly decrease ATP levels in cells supplemented with glucose deficient media. The mechanism of cellular efflux inhibition for these compounds still remains to be determined, however, further studies to investigate how/if these two phenotypes are related could lead to a novel method to modulate P-gp mediated cellular efflux.

2.6 Experimental section

General: Chemicals were obtained from Sigma Aldrich or the National Cancer Institute (NCI) and were used without further purification. PB-Gly-Taxol was prepared by Dr. Bailin Lei, a former postdoctoral fellow in the Peterson laboratory, as previously reported.[15] The

GF Urea analogue of NSC 202705 was prepared by the KU Synthetic Chemical Biology Core.

Cell culture: Jurkat lymphocytes, ATCC TIB-152, were cultivated in Roswell Park Memorial Institute (RPMI) 1640 medium. HeLa cells, ATCC CCL-2, were cultivated in Dulbecco's Modified Eagle Medium (DMEM) medium. PC-3 cells, a gift from Dr. Matthew Levy, were cultivated in Dulbecco's Modified Eagle Medium/Nutrient Mixture F-12 (DMEM/F-12) medium. All media was supplemented with Fetal Bovine Serum (FBS, 10%), penicillin (100 units/mL), and streptomycin (100 µg/mL). Cells were maintained in a humidified 5% CO_2 incubator at 37 °C.

Confocal Microscopy: Cells were seeded on an 8-well Ibidi µ-slide (300 µL, 20,000 cells/well) 24 hours prior to analysis with the confocal microscope. All compounds were dosed in 1:1000 dilutions in complete medium (0.1% DMSO). This media was then swapped with the media in the Ibidi µ-slide. After dosing, cells were incubated for 1 hour (unless otherwise noted) at 37 °C then analyzed on a Leica SPE2 confocal laser scanning microscope. Fluorophores were excited at 405 nm, 488 nm, and/or 635 nm. Emitted photons were collected from 420-470 nm, 500-600 nm, and/or 645-700 nm unless otherwise noted.

Flow Cytometry: Cells were analyzed using a Beckman Coulter CytoFLEX S (B2-R0-V2-Y2) flow cytometer. 405 nm and 488 nm diode lasers were used to excite the fluorophores. Emitted photons were collected with 450/45 nm PB filter or 525/40 nm FITC

filter. Flow speed = fast, backflush = 3 s, mixing time = 3 s, and cells were collected until 5000 cells were counted or until a time limit of 120 s was reached.

Comparison of PBGT to calcein-AM: 200 µL of Jurkat lymphocytes (7.5×10^5 cells/ml) in RPMI media were seeded in 15 wells of a 96 well plate (200 µL/well). 10 mL of the Jurkat lymphocytes were split into two conical tubes (5 mL each). To one tube, 5 µL of 1 mM PBGT in DMSO was added to afford a final concentration of 1 µM. To the other tube, 5 µL of 0.25 mM Calcein-AM in PBS was added to afford a final concentration of 0.25 µM Calcein-AM. 200 µL of each solution was seeded in 18 wells of a 96 well plate (9 wells each). 0.2 µL of 25 mM and 100 mM verapamil were dosed in triplicate in wells containing 1 µM PBGT, 0.25 µM calcein-AM, and only cells. 9 wells were left with only 1 µM PBGT, 0.25 µM Calcein-AM, or 0.1% DMSO. Cells were incubated for 1 hour at 37 °C and subsequently analyzed with a Beckman Coulter CytoFLEX S (B2-R0-V2-Y2) flow cytometer. 5000 cells were counted for each sample. Photons emitted by PBGT were collected after passing through a Pacific Blue filter (450/40). Photons emitted by calcein-AM were collected after passing through a FITC filter (520/40).

Primary screening assay by flow cytometry: Jurkat lymphocytes (7.5×10^5 cells/ml) in RPMI media (25 mL) were placed in a 25 mL integra multichannel reservoir. 25 µL of 1 mM PBGT in DMSO was added to the reservoir for a final concentration of 1 µM (0.1% DMSO). Solution was mixed by pipetting then transferred to a 96 well plate (200 µL/well) using an Integra ASSIST PLUS pipetting robot. Library compound (0.5 µL,10 mM in DMSO) was transferred from the NCI diversity set VI library plate to the assay plate for a

final concentration of 25 μM (0.35% DMSO). Compounds were transferred into the same well on the assay plate as the well it is stored on the library plate to encode what is in each assay well. Positive controls (25 and 100 μM verapamil) and negative controls (DMSO) were added manually. Plates were incubated for 1 hour at 37 °C then analyzed with a Beckman Coulter CytoFLEX S (B2-R0-V2-Y2) flow cytometer. 5000 cells were counted for each sample. Library compounds were tested as singlets while controls were tested in triplicate. Photons emitted by PBGT were collected after passing through a Pacific Blue filter (450/40). To assess the intrinsic fluorescence of library members the same assay was ran, but PBGT was not added to the reservoir.

Generation of dose response curves: Jurkat lymphocytes (7.5×10^5 cells/ml) in RPMI media (25 mL) were placed in a 25 mL integra multichannel reservoir. 25 μL of 1 mM PBGT in DMSO was added to the reservoir for a final concentration of 1 μM (0.1% DMSO). Solution was mixed by pipetting then transferred to a 96 well plate (200 μL/well) using an Integra ASSIST PLUS pipetting robot. Inhibitors were dosed in duplicate in 1:1000 dilutions to keep DMSO concentration constant. After dosing, plates were incubated for 1 hour at 37 °C then analyzed with a Beckman Coulter CytoFLEX S (B2-R0-V2-Y2) flow cytometer. 5000 cells were counted for each sample. Photons emitted by PBGT were collected after passing through a Pacific Blue filter (450/40).

Cellular uptake of PBGT mediated by the GF Urea: 200 μL of Jurkat lymphocytes (7.5×10^5 cells/ml) in RPMI media were seeded in 12 wells of a 96 well plate (200 μL/well). 5 mL of the Jurkat lymphocytes were placed in a 15 mL conical tube. 5 μL of 1 mM PBGT

in DMSO was added to afford a final concentration of 1 μM. 200 μL of the solution was seeded in 12 wells of a 96 well plate. 0.2 μL of 25 mM a verapamil in DMSO was dosed in triplicate to wells containing 1 μM PBGT and only cells. 0.2 μL of 10 mM and 25 mM GF urea in DMSO were dosed in triplicate to wells containing 1 μM PBGT and only cells. 6 wells were left with only 1 μM PBGT and 0.1% DMSO. Cells were incubated for 1 hour at 37 °C then analyzed with a Beckman Coulter CytoFLEX S (B2-R0-V2-Y2) flow cytometer. 5000 cells were counted for each sample. Photons emitted by PBGT were collected after passing through a Pacific Blue filter (450/40).

Transient transfection of PC-3 cells with pHaMDR-EGFP: This transfection assay was adapted from the previously reported protocol.[15] PC-3 cells in DMEM/Ham's F-12 medium were seeded into a 8-well Ibidi μ-slide (300 μL, 20,000 cells/well) and incubated for 16 h at 37 °C. Plasmid pHaMDR-EGFP (2 μg, a gift from Dr. Michael M. Gottesman, NCI) was incubated in 200 μL serum free DMEM/Ham's F-12 medium at 22 °C with the DNA transfection reagent X-tremeGENE HP (2 μL, Roche) for 30 minutes. After incubation, 20 μL of the DNA complex was added to each desired well of the Ibidi μ-slide. The slide was incubated for another 48 hours then washed with complete medium, treated with probes and imaged using the confocal microscopy protocol.

ATP-Depletion analysis: Jurkat cells (4000 cells/well) and Hela cells (3000 cells/well) in DMEM media (high glucose, low glucose, or galactose supplemented), were exposed to various concentrations of NSC 202705 (0, 0.001, 0.01, 0.1, 1, 10, 20, 40 and 80 μM) for 1h, 4h, and/or 24h at 37 °C, 5% CO2. Cell-Titer Glo (promega) was added to the cells

and to a freshly plated ATP concentration curve (0,0.01, 0.1, 1, 10, 100, 1000, 2000 and 5000 nM), After 10 min of incubation at room temperature, luminescence was read using Perkin Elmer Enspire. ATP levels were interpolated from the ATP standard curve.

Compound characterization data

1-(4-chlorophenyl)-3-(7-nitrobenzo[c][1,2,5]oxadiazol-4-yl)urea (GF Urea):

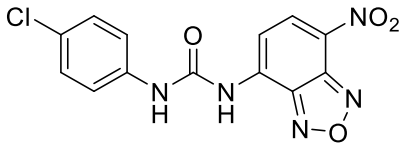

^{1}H NMR (400 MHz, DMSO-d_6): δ 10.35 (s, 1H), 9.69 (s, 1H) 8.76 (d, *J* = 8.6 Hz, 1H), 8.20 (d, *J* = 8.5 Hz, 1H), 7.54 (d, *J* = 8.7 Hz, 2H), 7.41 (d, *J* = 8.8 Hz, 2H). ^{13}C NMR (126 MHz, DMSO-d_6): δ 151.5, 145.9, 143.8, 137.7, 137.1, 136.4, 129.4, 129.1, 128.7, 127.3, 120.7, 120.3, 110.6. HRMS calculated for C13H8ClN5O4 $(M-H)^+$ 331.98; found 331.99 (TOF MS ES+).

2.7 References

1. What is cancer? www.cancer.gov. National Cancer Institute. www.cancer.gov/about-cancer/understanding/what-is-cancer.

2. Devita, V.T.; Chu, E., A history of cancer chemotherapy. *Cancer Res.* **2008,** 68(21), 8643-8653.

3. History of Cancer. www.cancer.org. American Cancer Society. www.cancer.org/cancer/cancer-basics/history-of-cancer.html.

4. Arruebo, M.; Vilaboa, N.; Saez-Gutierrez, B.; Lambea, J.; Tres, A.; et al., Assessment of the evolution of cancer treatment therapies. *Cancers*. **2011,** 3(3), 3279-3330.

5. Kufe, D.W.; Pollock, R.E.; Weichselbaum, R.R., et al., Alkylating agents. *Cancer Medicine.* **2003,** 6th edition.

6. Gonen, N.; Assaraf, Y.G., Antifolates in cancer therapy: structure, activity and mechanisms of drug resistance. *Drug. Resist. Updat.* **2012,** 15(4), 183-210.

7. Wheate, N.J.; Brodie, C.R.; Collins, J.G.; Kemp, S.; Aldrich-Wright, J.R. DNA intercalators in cancer therapy: organic and inorganic drugs and their spectroscopic tools of analysis. *Mini.* Rev. *Med. Chem.* **2007,** 7(6), 627-648.

8. Hartmann, J.T.; Haap, M.; Kopp, H.G.; Lipp, H.P; Tyrosine kinase inhibitors - a review on pharmacology, metabolism and side effects. *Curr. Drug Metab.* **2009,** 10(5), 470-481.

9. Dumontet, C.; Jordan, M.A., Microtubule-binding agents: a dynamic field of cancer therapeutics. *Nat. Rev. Drug Discov.* **2011,** 9(10), 790-803.

10. Holohan, C.; Schaeybroeck, S.V.; Longley, D.B.; Johnston, P.G., Cancer drug resistance: an evolving paradigm. *Nat. Rev. Cancer.* **2013,** 13, 714-726.

11. Volm, M.; Efferth, T., Role of P-glycoprotein for resistance of tumors to anticancer drugs: from bench to bedside. *Resitance to Targeted ABC Transports in Cancer.* **2014,** 4, 1-26.

12. Kim, Y.; Chen, J., Molecular structure of human P-glycoprotein in the ATP-bound, outward facing conformation. *Science.* **2018,** 359, 915-919.

13. Kwon, H.; Lionberger, R.A.; Yu, L.X, Impact of P-glycoprotein-mediated efflux kinetics on oral bioavailability of P-glycoprotein substrates. *Mol. Pharmaceutics.* **2004,** 1(6), 455-465.

14. Chung, F.S.; Santiago, J.S.; De Jesus, F.M.; Trinidad, C.V.; See, M.F.E., Disrupting P-glycoprotein function in clinical settings: what can we learn from the fundamental aspects of this transporter. *Am. J. Cancer Res.* **2016,** 6(8), 1583-1598.

15. Sparreboom, A.; Asperen, J.V.; Mayer, U.; Schinkel, A.H.; Smit, J.W.; et al., Limited oral bioavailability and active epithelial excretion of paclitaxel (Taxol) caused by P-glycoprotein in the intestine. *Proc. Natl. Acad. Sci. USA.* **1997,** 94(5), 2031-2035.

16. Lee, M.M.; Gao, Z.; Peterson, B.P., Synthesis of a fluorescent analouge of paclitaxel that selectively binds microtubules and sensitively detects efflux by P-glycoprotein. *Angew. Chem. Int. Ed. Engl.* **2017,** 56(24), 6927-6931.

17. Twentyman, P.R.; Rhodes, T.; Rayner, S., A comparison of rhodamine 123 accumulation and efflux in cells with P-glycoprotein-mediated and MRP-associated multidrug resistance phenotypes. *Eur. J. Cancer.* **1994,** 30A(9), 1360-1369.

18. Jouan, E.; Vee, M.L.; Mayati, A.; Denizot, C.; Parmentier, Y., Evaluation of P-glycoprotein inhibitory potential using a rhodamine 123 accumulation assay. *Pharmaceutics.* **2016,** 8(2), 12.

19. Legrand, O.; Simonin, G.; Perrot, J.Y.; Zittoun, R. Marie, J.P., Both P-gp and MRP1 activities using calcein-AM contribute to drug resistance in AML. *Adv. Exp. Med. Biol.* **1999,** 457, 161-175.

20. Dandapani, S.; Rosse, G.; Southall, N.; Salvino, J.M.; Thomas, C.J., Selecting, acquiring, and using small molecule libraries for high-throughput screening. *Curr. Protoc. Chem. Biol*. **2012,** 4, 177-191.

21. Baell, J.B.; Nissink, J.W.M., Seven year itch: pan-assay interference compounds (PAINS) in 2017 - utility and limitations. *ACS Chem. Biol.* **2018,** 13(1), 36-44.

22. Harris, C.J.; Hill, R.D.; Sheppard, D.W.; Slater, M.J.; Stouten, P.F.W.; The design and application of target-focused compound libraries. *Comb. Chem. High Throughput Screen.* **2011,** 14(6), 521-531.

23. Developmental therapeutics program: available plates. www.cancer.gov. National cancer institute. www.dtp.cancer.gov/organization/dscb/obtaining/available_plates.html

24. Ren, S.; Frymier, P.D., Reducing bioassay variability by indentifying sources of variation and controlling key parameters in assay protocol. *Chemosphere.* **2004,** 57(2), 81-90.

25. Postnikova, E.; Cong, Y.; DeWald, L.I.; Dyall, J.; Yu, S.; et al., Testing therapeutics in cell-based assays: factors that influence the apparent poency of drugs. *PLOS ONE.* **2018,** 1-18.

26. Evelyn, C.R.; Biesiada, J.; Duan, X.; Tang, H.; Shang, X.; et al., Combined rational design and a high throughput screening platform for identifiying chemical inhibitors of a Ras-activating enzyme. *J. Biol. Chem.* **2015,** 290, 12879-12898.

27. Subramanian, N.; Condic-Jurkic, K.; O'Mara, M.L., Structural and dynamic perspectives on the promiscuous transport activity of P-glycoprotein. *Neurochem. Int.* **2016,** 98, 146-152.

28. Varga, B.; Csonka, A.; Csonka, A.; Molnar, J.; Amaral, L., *Anticancer Res.* **2017,** 37(11), 5983-5993.

29. Spengler, G.; Takacs, D.; Horvath, A.; Riedl, Z.; Hajos, G.; et al., Multidrug resistance reversing activity of newly developmed phenothiazines on P-glycoprotein (ABCB1)-related resistence of mouse T-lymphoma cells. *Anticancer Res.* **2014,** 34(4), 1737-1741.

30. Kristiansen, J.E.; Dastidar, S.G.; Palchoudhuri, S.; Roy, D.S.; Das, S.; et al., Phenothiazines as a solution for multidrug resistant tuberculosis: from the origin to present. *Int. Microbiol.* **2015,** 18, 1-12.

31. Wesolowska, O.; Molanar, J.; Ocsovszki, I.; Michalak, K., Differential effect on phenothiazines on MRP1 and P-glycoprotein activity. *In Vivo.* **2009,** 23(6), 943-947.

32. Miller, B.R.; Farmer, S.C., Modified methods for the synthesis of carbazole from phenothiazine. *Molecules.* **2001,** 6(8), 668-672.

33. Bachmakov, I.; Werner, U.; Endress, B.; Auge, D.; Fromm, M.F., Characterization of beta-adrenoceptor antagonists as substrates and inhibitors of the drug transporter P-glycoprotein. Fundam. *Clin. Pharmacol.* **2006,** 20(3), 273-282.

34. Saengkhae, C.; Salerno, M.; Ades, D.; Siove, A.; Moyec, L.L.; et al., Ability of carbazole salts, inhibitors of Alzeimer β-amyloid fibril formation, to cross cellular membranes. *Eur. J. Pharmacol.* **2007,** 559(2-3), 124-131.

35. Zhou, W.; Hu, X.; Tam, K.Y., Systemic clearance and brain distribution of carbazole-based cyanine compounds as Alzeimer's disease drug candidates. *Nature Sci. Rep.* **2017,** 1-10.

36. Bennion, B.J.; Daggett, V., The molecular basis for the chemical denaturation of proteins by urea. *PNAS.* **2003,** 100(9), 5142-5147.

37. Stumpe, M.C.; Grubmuller, H., Interaction of urea with amino acids: implications for urea-induced protein denaturation. *J. Am. Chem. Soc.* **2007,** 129(51), 16126-161131.

38. Gandin, V.; Ferrarese, A.; Dalla Via, M.; Marzana, C.; Chilin, A.; et al., Targeting kinases with anilinopyrimidines: discovery of N-phenyl-N'-[4-(pyrimidin-4-ylamino)phenyl]urea derivatives as selective inhibitors of class III receptor tyrosine kinase subfamily. *Nature Sci. Rep.* **2015,** 5, 1-16.

39. Wrobel, T.A.; Kielbus, M.; Kaczor, A.A.; Krystof, V.; Karczmarzky, Z.; et al., Discovery of nitroaryl urea derivatives with antiproliferative properties. *J. Enzyme Inhib. Med. Chem.* **2015,** 31(4), 608-618.

40. Jiang, N.; Bu, Y.; Wang, Y.; Nie, M.; Zhang, D.; et al., Design, synthesis, and structure-activity relationships of novel diaryl urea deriviatives as potential EGFR inhibitors. *Molecules.* **2016,** 21(11), 1-12.

41. Houghton, P.J.; Bailey, F.C.; Houghton, J.A.; Murti, G.; Howbert, J.J.; et al., Evidence for mitochondrial localization of N-(4-methylphenylsulfonyl)-N'-(4-chlorophenyl)urea in human colon adenocarcinoma cells. *Cancer Res.* **1990,** 50, 664-668.

42. Houghton, P.J.; Sosinski, J.; Thakar, J.H.; Boder, G.B.; Grindey, G.B., Characterization of the intracellular distribution and binding in human adenocarcinoma cells of N-(4-azidophenyl-sulfonyl)-N'-(4-chlorophenyl)urea (LY219703), a photoaffinity analogue of the antitumor diarylsulfonylurea sulofenur. *Biochemical Pharmacol.* **1995,** 49(5), 661-668.

43. Chen, J.N.; Wang, X.F.; Li, T.; Wu, D.W.; Fu, X.B., et al., Design, synthesis, and biological evaluation of novel quinazolinyl-diaryl urea derivatives as potential anticancer agents. *Eur. J. Med. Chem.* **2015,** 107(2016), 12-25.

44. Karbowski, M.; Youle, R.J., Dynamics of mitochondrial morphology in healthy cells and during apoptosis. *Cell Death Differ.* **2003,** 10, 870-880.

45. Wang, H.; Gao, Z.; Liu, X.; Agarwal, P.; Zhao, S.; et al., Targeted production of reactive oxygen species in mitochondria to overcome cancer drug resistance. *Nat. Commun*. **2018,** 9(562), 1-16.

Appendix A

Plate map and raw screening data

PLATE	WELLID	NSC #	MW	Assay Fluor.	Intrinsic Fluor.	Viability
4860	A02	18473	125	21666.3	1875.9	90%
4860	B02	30041	136	21481.9	1774.3	89%
4860	C02	38968	129.2	20639.6	1733.8	89%
4860	D02	41833	125	19459.4	1701.8	90%
4860	E02	42633	149	20297.4	1681.3	88%
4860	F02	47881	145	17636.6	1618.8	90%
4860	G02	48231	138	16775.5	1613.1	89%
4860	H02	51787	145	17232.4	1934.6	87%
4860	A03	54260	150	20823.7	1627.4	88%
4860	B03	65248	150	22722.5	1568.9	88%
4860	C03	75071	131	20601	1569.6	88%
4860	D03	113532	145	19269.7	1574.3	90%
4860	E03	122276	150	18469.4	1541.1	89%
4860	F03	123797	150	16924	1512.6	89%
4860	G03	135857	142	16823.8	1511.9	90%
4860	H03	148304	144	15897.9	1514.6	89%
4860	A04	149877	122	20561.8	1555.3	89%
4860	B04	173969	146	20218.2	1581.1	89%
4860	C04	200686	138	20240.2	1537.4	89%
4860	D04	679449	136	18726.6	1509	89%
4860	E04	4135	190	19867.8	1514.4	88%
4860	F04	4426	191	16973.3	1525.5	89%
4860	G04	4936	165	16471.6	2249.4	89%
4860	H04	5784	180	15777	1519.5	89%
4860	A05	7606	158	20187.5	1551.6	89%
4860	B05	7950	185	21227.6	2753	88%
4860	C05	9441	190	22006.9	1528.1	89%
4860	D05	9489	182	20624.1	1524.6	90%
4860	E05	10427	188	19093.5	1499.8	90%
4860	F05	10772	178	17056.4	1472.4	89%
4860	G05	11128	197	16119.2	1502.4	88%
4860	H05	11141	163	15830.7	1475.2	88%
4860	A06	11470	182	21422.6	1535.9	88%
4860	B06	12588	158	21394.9	1513.9	88%
4860	C06	13213	187	21167.1	2069.1	89%
4860	D06	14767	185	19833.1	1539	89%
4860	E06	14771	198	17958.1	1482.7	88%

4860	F06	15133	171	16294.8	1462.8	89%
4860	G06	15776	193	16307.1	3709.1	87%
4860	H06	16021	164	16379.5	1502.3	89%
4860	A07	16162	165	21916.6	1940.6	89%
4860	B07	16631	154	21150.1	1534.9	89%
4860	C07	16646	180	21504.9	1518.5	88%
4860	D07	16873	190	20999.6	1615.9	89%
4860	E07	17796	162	17965.6	1538	89%
4860	F07	18415	191	19270.3	1517.8	89%
4860	G07	19219	198	21875.7	7996.8	88%
4860	H07	19848	188	16824.8	2149.1	88%
4860	A08	20559	193	20519.1	1610.9	88%
4860	B08	22847	171	21096.8	1527	87%
4860	C08	23225	156	20930.4	1550.6	87%
4860	D08	27389	180	20532.7	1517.9	88%
4860	E08	27626	194	17621.5	1502.3	88%
4860	F08	28011	154	17043.7	1490	89%
4860	G08	28837	161	15949.8	1479.3	88%
4860	H08	29193	184	15580.9	1479.9	88%
4860	A09	29629	163	21895.6	1521.6	87%
4860	B09	29851	155	20681	1543.9	89%
4860	C09	29874	185	20315.2	1499	87%
4860	D09	31712	174	19707.4	1489.7	88%
4860	E09	34012	157	17936.1	1486.4	88%
4860	F09	34210	157	16231.1	1485.9	88%
4860	G09	34794	160	14944.3	1449.1	89%
4860	H09	34983	191	15679.4	1466.5	88%
4860	A10	35534	181	21323.1	1542.1	88%
4860	B10	35679	180	21431.3	1742.9	88%
4860	C10	37408	166	21358.2	1482.4	88%
4860	D10	37883	187	20436.6	1472.3	88%
4860	E10	40817	193	37130.1	15733.8	88%
4860	F10	40840	156	15948.1	1534.5	88%
4860	G10	41331	199	15532.2	1476.2	89%
4860	H10	42021	197	15805.6	1554.9	88%
4860	A11	42028	158	21502.4	1536.3	89%
4860	B11	42231	182	22542.1	2345.6	88%
4860	C11	42774	172	21060.6	1493.4	88%
4860	D11	43013	172	20384.2	1484.1	87%
4860	E11	43512	200	19452.8	1568.6	88%
4860	F11	43546	156	16078.7	1465.8	89%
4860	G11	43805	184	14768.6	1492.3	87%
4860	H11	44680	155	23628.7	1599.3	86%

4861	A02	44819	199	20787.6	1608.6	92%
4861	B02	45117	181	21830.4	1764.4	93%
4861	C02	45641	190	20587.7	1610.1	91%
4861	D02	45719	177	20766.4	1526.1	93%
4861	E02	46273	198	21035.4	1514.8	92%
4861	F02	47496	188	19066.7	1511.1	92%
4861	G02	48422	173	16545.4	1620.2	93%
4861	H02	49252	156	16465.6	1481.2	92%
4861	A03	50751	186	22187.1	1772.6	92%
4861	B03	50858	182	20953.6	1506.1	92%
4861	C03	51093	180	19629.6	1490.8	92%
4861	D03	53506	179	20165.6	1496.7	93%
4861	E03	54834	181	19107.4	1621.3	92%
4861	F03	55459	189	18135	1491.8	92%
4861	G03	55573	171	16567.3	1508.8	92%
4861	H03	55957	198	28480.1	1779.6	90%
4861	A04	56914	184	21108.6	1549.1	91%
4861	B04	57741	174	26434.2	7339	92%
4861	C04	57890	194	20202.3	1574.8	92%
4861	D04	60239	192	20399.7	1552.4	92%
4861	E04	60373	183	19514.1	1498.6	92%
4861	F04	60377	169	17984.7	1572.9	93%
4861	G04	60530	151	16748.3	1467.8	93%
4861	H04	60548	175	15933.8	1479.5	92%
4861	A05	62129	184	19107.3	1802.1	90%
4861	B05	62318	194	21403.8	1530.9	92%
4861	C05	62511	190	20642.4	1506.1	92%
4861	D05	62609	195	20154.1	1834.8	92%
4861	E05	62840	171	17673.9	1530.5	91%
4861	F05	63311	189	20039.5	1973.1	93%
4861	G05	63314	189	18154.6	1831	91%
4861	H05	64952	154	28689.1	13602.2	92%
4861	A06	66241	200	21706.4	1943.9	92%
4861	B06	67307	186	22721.7	1600.1	92%
4861	C06	68657	178	20757.3	1565.7	92%
4861	D06	70717	165	20834.6	1616.8	92%
4861	E06	72292	198	1031910	867511.6	92%
4861	F06	73482	179	21538.2	3129.1	91%
4861	G06	75585	171	16624.6	1767.3	91%
4861	H06	75786	159	16306.8	1663.6	91%
4861	A07	75846	157	20745.6	1633.7	92%
4861	B07	77422	200	22083	2026.5	92%
4861	C07	77913	194	21591.1	1699.2	92%

4861	D07	78609	173	19097.8	1535.8	90%
4861	E07	78999	173	18833.1	1500.8	92%
4861	F07	79010	161	16852.6	1476.7	92%
4861	G07	79582	196	15933.5	2248.6	91%
4861	H07	80807	198	15453.5	1581.8	92%
4861	A08	81462	182	21029.1	1602.4	92%
4861	B08	82339	189	21680.5	1586.3	92%
4861	C08	82769	172	21325.9	1547.1	91%
4861	D08	83076	151	19216.8	1508	91%
4861	E08	83237	191	18220.4	1651.3	91%
4861	F08	83339	191	16903.4	1542.1	91%
4861	G08	83345	199	15453	1478.2	91%
4861	H08	84200	169	15300	1474.2	91%
4861	A09	85331	177	20172.8	1575	92%
4861	B09	88882	196	19558.2	1625.5	91%
4861	C09	89720	151	20573.7	1553	92%
4861	D09	91438	194	20013.6	1531.5	91%
4861	E09	92264	176	18160.4	1808.9	91%
4861	F09	92753	187	16749	1507	92%
4861	G09	93260	157	15050.3	1519.8	91%
4861	H09	96979	152	15390.7	1585.5	91%
4861	A10	97090	151	20306	1610.4	91%
4861	B10	97104	192	54052.4	36748.2	91%
4861	C10	97538	157	23531.8	3319	91%
4861	D10	99756	196	20473.8	1815.8	91%
4861	E10	100729	162	18299.4	1642.5	91%
4861	F10	102025	198	16888.8	1682.7	91%
4861	G10	102509	180	15295.2	1870.2	91%
4861	H10	104969	195	15744	1659.6	90%
4861	A11	106045	187	20479.6	1625.5	92%
4861	B11	106261	179	21164.4	1605.2	90%
4861	C11	108655	167	21114.1	1894.8	91%
4861	D11	109176	168	19973.7	1550.3	91%
4861	E11	109231	197	18501.5	1539.8	91%
4861	F11	109528	195	18932.8	4358	91%
4861	G11	109813	187	24246.8	1630.9	90%
4861	H11	20586	192	14651	1535.1	91%
4862	A02	109885	181	21512.8	1707.6	91%
4862	B02	111107	184	21617.8	1729.6	91%
4862	C02	116565	199	22980.3	1725.5	91%
4862	D02	117386	170	21234.2	1634.6	92%
4862	E02	118832	191	21613.9	1714.8	92%
4862	F02	119969	188	21565	1918.9	92%

4862	G02	120312	196	20572.4	1641.2	92%
4862	H02	122131	173	116684.6	120008.1	91%
4862	A03	123458	193	21361.4	5153	90%
4862	B03	125197	193	21270.6	2279.2	91%
4862	C03	127216	162	21218.7	2067.8	92%
4862	D03	127458	195	22709.3	3281.7	91%
4862	E03	127947	199	21530	1885.9	90%
4862	F03	128068	183	22190.4	2778.4	91%
4862	G03	131982	194	20979.5	1756.8	92%
4862	H03	134577	164	20787.8	1761.4	90%
4862	A04	134580	167	21305.2	1803.2	92%
4862	B04	134784	182	21174.6	1825.4	91%
4862	C04	134785	197	21317.5	1748.8	91%
4862	D04	135351	151	21269.8	1729.7	91%
4862	E04	136065	191	21150	1793.7	91%
4862	F04	145180	167	21071.1	1683.6	92%
4862	G04	147829	186	19816.3	1740.8	91%
4862	H04	150982	188	34356.2	4433.4	90%
4862	A05	151901	189	21355.4	1830.4	92%
4862	B05	152632	174	20747	1727.5	91%
4862	C05	154316	153	20549	1739.5	92%
4862	D05	154718	183	21067.5	1952.9	91%
4862	E05	155196	169	21585.4	1839.6	91%
4862	F05	155698	200	30637.5	8143.9	90%
4862	G05	155703	196	20676.2	2077.3	90%
4862	H05	156571	171	20283.8	1778.5	91%
4862	A06	160005	168	21207.9	1756	92%
4862	B06	162292	196	20251.8	1787.9	91%
4862	C06	162915	197	21114.4	1950.1	92%
4862	D06	163104	198	22551.4	1785.7	92%
4862	E06	163158	165	21575	1716.7	90%
4862	F06	163920	184	17914.8	1912.6	89%
4862	G06	164965	187	20571.8	1707	91%
4862	H06	166900	156	20870.4	1693.7	91%
4862	A07	169458	185	21099	1740.2	90%
4862	B07	169566	151	20104.4	1755.6	90%
4862	C07	173101	193	20359.3	1769.4	90%
4862	D07	176324	195	20552.1	1747.5	91%
4862	E07	177952	156	20232	1702.8	90%
4862	F07	191029	183	20765.9	1702.3	90%
4862	G07	194242	161	19880.2	1673.3	89%
4862	H07	194243	176	20084.1	1711.3	90%
4862	A08	195031	185	21540.3	1772.9	91%

4862	B08	203065	191	21973.5	1690.3	90%
4862	C08	206630	172	20531.7	1734	90%
4862	D08	227309	189	21463.3	1879.3	90%
4862	E08	234764	196	19978.9	1713.6	90%
4862	F08	246415	200	18536.3	1616.4	79%
4862	G08	269905	188	20202.4	1692.7	89%
4862	H08	272275	159	23290.3	4030.3	90%
4862	A09	276369	182	22873.4	1789.3	91%
4862	B09	278741	177	20326.3	1726.9	89%
4862	C09	279834	187	21651.2	1752	89%
4862	D09	284701	152	20691.6	1744.8	90%
4862	E09	287065	178	19573	1731.1	89%
4862	F09	287495	182	20525.6	1713.9	90%
4862	G09	288686	189	18939.5	1789.8	89%
4862	H09	295701	189	20187.9	1866.2	89%
4862	A10	303244	199	28558.1	4838.1	89%
4862	B10	303603	200	21169.4	1945.8	90%
4862	C10	303800	171	21038.1	1752.2	90%
4862	D10	304902	186	20637	2650.8	90%
4862	E10	311723	189	20545.9	1831.8	89%
4862	F10	321484	165	20722.6	1759.7	89%
4862	G10	331198	155	20130.1	1735.8	89%
4862	H10	331208	175	19588.3	1746.1	90%
4862	A11	335649	166	21973.7	1785.6	89%
4862	B11	338205	175	21280.8	1750.7	90%
4862	C11	339578	199	26504.6	10117.3	84%
4862	D11	341902	178	20732.4	1796.9	89%
4862	E11	342460	183	20641.6	1917.1	90%
4862	F11	344494	175	28250.1	3016.5	87%
4862	G11	351110	183	19973.2	1809.6	88%
4862	H11	361056	198	20404.1	1778.3	89%
4863	A02	366808	197	19565.8	1632.2	91%
4863	B02	370387	161	18953.2	1564.7	91%
4863	C02	372063	191	19949.9	2476.4	90%
4863	D02	407282	190	18609.6	1538.2	90%
4863	E02	513815	178	18838	1518.9	89%
4863	F02	650438	179	52841.4	29379.8	88%
4863	G02	664971	169	18342.4	1494.1	92%
4863	H02	672441	158	18854.1	1474.8	91%
4863	A03	1451	239	19901.8	1584.1	90%
4863	B03	1620	215	17904.3	1561.8	92%
4863	C03	1751	224	18774	1527.2	92%
4863	D03	2561	240	18957.5	1523.6	90%

4863	E03	2805	246	42000.1	4382.7	87%
4863	F03	3001	214	19579.6	1483	90%
4863	G03	4263	225	18623.9	1475.1	91%
4863	H03	4921	214	18011.1	1487.8	91%
4863	A04	5995	213	18064.1	1579.9	86%
4863	B04	6866	232	19786.1	1552.7	91%
4863	C04	6910	250	19901.8	1552.9	89%
4863	D04	8090	247	19009.7	1601.4	91%
4863	E04	8179	203	18730.4	1498.7	89%
4863	F04	8481	208	17387.6	1519.5	91%
4863	G04	8813	238	18934.2	1484.4	90%
4863	H04	9064	204	19309.6	1482.8	90%
4863	A05	9341	237	19032	1613.5	90%
4863	B05	9358	226	14857.5	1362.6	89%
4863	C05	9461	202	18464.8	1530.5	90%
4863	D05	10091	240	36115.1	15823.3	89%
4863	E05	10416	243	20971.7	4384.7	71%
4863	F05	10428	204	18415.1	2131.6	90%
4863	G05	10995	241	17622.7	1828.7	90%
4863	H05	11149	235	14865.3	1708.4	89%
4863	A06	11150	235	16403.3	1804	89%
4863	B06	11826	228	18597.6	1765.1	85%
4863	C06	11891	225	19463.9	1752.9	90%
4863	D06	11991	226	19886.6	1586.1	89%
4863	E06	13653	218	17816.9	1565.2	90%
4863	F06	13974	247	14053.8	1744.2	92%
4863	G06	14304	222	15054.5	1720.4	89%
4863	H06	14540	219	17651.1	1727.8	90%
4863	A07	15362	227	18044.5	1800.1	91%
4863	B07	15364	242	17717.4	1647.9	88%
4863	C07	15372	235	56089.1	38670.3	90%
4863	D07	15571	246	20461.7	3355.5	90%
4863	E07	16416	234	19156.6	1928.3	88%
4863	F07	16813	216	25841.5	1685.1	88%
4863	G07	17129	242	18985.6	1667.7	89%
4863	H07	19063	230	20054.9	1620.9	89%
4863	A08	19096	222	20268.9	1791.1	88%
4863	B08	19108	244	18561.6	1639.8	89%
4863	C08	19115	217	18804.9	1783.7	88%
4863	D08	19487	220	20335.4	1664.7	89%
4863	E08	19637	226	30047.7	1588.2	90%
4863	F08	20045	205	18735.6	1584.3	89%
4863	G08	21034	237	19780.3	1634.3	89%

4863	H08	21678	232	14426.5	1272.6	87%
4863	A09	22939	224	21373.5	2414.6	89%
4863	B09	23123	240	20130.3	2127.9	91%
4863	C09	23247	237	19638.2	1668.9	88%
4863	D09	23248	227	19087.3	1658.3	90%
4863	E09	23672	222	17537.2	1608.7	89%
4863	F09	23895	221	19096	2074.5	89%
4863	G09	23906	201	53528.5	38112.3	89%
4863	H09	24035	227	15158.1	1750.6	89%
4863	A10	25368	216	18086.8	1811.9	88%
4863	B10	26744	238	63466.5	1781.9	86%
4863	C10	27032	223	16405	5208.3	86%
4863	D10	27628	208	17379.3	1781.6	86%
4863	E10	28341	210	20643.4	4483.7	89%
4863	F10	29471	213	19986.6	1698.3	89%
4863	G10	29620	212	16605.7	1611	89%
4863	H10	112975	191	17890.3	1746.3	89%
4863	A11	173103	196	17756.3	1684.6	88%
4863	B11	281639	156	17392.6	1659.5	88%
4863	C11	365560	187	24941.2	1580.3	87%
4863	D11	3961	228	21403.1	1775.6	84%
4863	E11	9852	240	21750	3142.9	86%
4863	F11	14303	222	17993.2	2186.5	88%
4863	G11	21725	244	17033.9	1679.1	88%
4863	H11	17339	213	18009	2198.1	88%
4864	A02	31208	248	23950.1	6706.3	92%
4864	B02	31664	233	21576.1	2500.6	91%
4864	C02	31741	203	21613	2329.7	91%
4864	D02	32838	202	21761.7	2316.4	90%
4864	E02	33005	243	53316.4	16828.6	91%
4864	F02	34488	239	23943.8	2920.3	89%
4864	G02	34769	218	21150.4	2419.5	91%
4864	H02	34774	230	20798.2	2389.3	90%
4864	A03	34777	214	21830.3	2322.6	89%
4864	B03	35676	220	21108.3	2480.4	90%
4864	C03	35964	238	22127.9	2343.7	90%
4864	D03	36425	241	20856.5	2323.3	90%
4864	E03	36520	238	22038	2405.6	90%
4864	F03	36582	219	20951.4	2353.7	89%
4864	G03	37003	244	20390	2335.8	90%
4864	H03	37812	212	25975.8	13721.9	88%
4864	A04	38042	237	21295.1	2426.1	89%
4864	B04	38490	249	29190.1	9767.4	86%

4864	C04	38743	248	21665.9	2362.8	91%
4864	D04	38845	242	21682.4	2364.3	90%
4864	E04	38983	224	25062.3	2395.5	90%
4864	F04	39336	223	21230.4	2363.5	90%
4864	G04	40467	224	15053.4	2007.9	87%
4864	H04	40500	237	18733.3	2281.7	90%
4864	A05	40614	224	22880.7	2403.2	90%
4864	B05	40669	209	21446.5	2340.5	89%
4864	C05	41092	215	21186.6	2465.9	79%
4864	D05	42014	228	21856.1	2336.2	89%
4864	E05	44688	232	21127.8	2464.6	90%
4864	F05	45153	222	20755.6	2351.7	90%
4864	G05	45291	214	20987.6	2670.5	83%
4864	H05	46615	233	19032.7	2361.5	90%
4864	A06	47617	248	21620.1	2417.4	89%
4864	B06	47619	216	20433.3	2403.7	90%
4864	C06	48964	210	21923.3	3478.7	91%
4864	D06	49652	225	35827.9	3091.3	86%
4864	E06	49701	230	19434.8	2397.9	90%
4864	F06	50633	237	20239.1	2395.6	91%
4864	G06	51331	238	18868.5	2548	91%
4864	H06	51936	214	20074.6	2413.8	91%
4864	A07	55770	206	21500.7	2396.6	89%
4864	B07	56455	235	22595.8	2399.9	90%
4864	C07	57103	235	28362.8	2329.9	88%
4864	D07	57165	202	21730.7	2379.4	88%
4864	E07	57318	225	21364.9	2477.6	89%
4864	F07	57345	226	22697.4	2968.2	90%
4864	G07	57794	219	20503.8	2455.4	90%
4864	H07	58907	237	20637.2	2479.2	89%
4864	A08	59776	220	23141.7	2422.7	88%
4864	B08	60034	244	21739.8	2453.8	90%
4864	C08	60266	228	21392.8	2440.9	89%
4864	D08	60419	203	30584.1	5908.4	86%
4864	E08	61888	207	21190.9	4323.8	86%
4864	F08	61910	231	20768.7	2696.6	88%
4864	G08	62665	205	23031.8	2671.1	89%
4864	H08	63001	236	30501.8	5990.4	87%
4864	A09	63865	244	22578.3	2910.9	88%
4864	B09	63963	248	23573.3	5353.5	89%
4864	C09	66837	230	21479.7	2607.7	89%
4864	D09	67546	203	20933.6	2580.3	90%
4864	E09	69421	250	22300.8	2586.2	90%

4864	F09	70534	240	18784.4	2379.5	89%
4864	G09	73170	244	20960.8	2553.8	89%
4864	H09	75241	247	20728.3	2536.8	89%
4864	A10	75885	234	22219.6	2528.4	88%
4864	B10	77596	244	21556.7	2453.3	88%
4864	C10	78130	243	13096.5	1897.2	86%
4864	D10	79139	246	176435.3	171734.6	81%
4864	E10	79253	244	59332.5	49958.7	92%
4864	F10	79538	205	38894	25119.9	88%
4864	G10	80141	250	29702.8	17480.4	86%
4864	H10	81018	242	29774.6	13818.5	88%
4864	A11	81120	249	27328.5	15260.9	81%
4864	B11	81213	237	26583.6	9231.1	90%
4864	C11	81660	217	25379.7	5879	88%
4864	D11	81703	224	27483.9	4227.3	66%
4864	E11	83715	247	30633.9	3551.8	81%
4864	F11	85179	220	22654.6	3910.9	89%
4864	G11	85326	211	21635.5	3774.2	88%
4864	H11	87352	212	21019.5	3625.4	89%
4865	A02	87822	244	23757.8	2170.9	94%
4865	B02	88811	212	27277.1	2164.9	93%
4865	C02	88883	215	23413.9	2441.8	95%
4865	D02	88962	210	22592.8	2185.1	94%
4865	E02	88998	236	23302.1	2115.1	94%
4865	F02	89249	224	22340.8	2110.2	94%
4865	G02	89258	218	96456.4	80012.8	92%
4865	H02	89723	232	22714	3157.9	95%
4865	A03	91516	212	24813	2454.5	92%
4865	B03	92207	208	21878.7	2121.3	93%
4865	C03	92794	245	20941.6	1572	94%
4865	D03	93817	227	22627.1	2181.9	94%
4865	E03	96491	241	22712	2134.4	95%
4865	F03	98683	211	21850.4	2131.5	94%
4865	G03	98857	211	19600.1	2178.6	90%
4865	H03	99796	230	23658.9	2358	94%
4865	A04	100120	241	23405.4	2217.3	95%
4865	B04	101266	219	19812.4	2157.6	95%
4865	C04	101777	250	22188.4	2121.6	94%
4865	D04	102086	237	26834.9	2112.4	94%
4865	E04	102288	205	21812.2	2127.1	94%
4865	F04	103770	213	22492.1	2108.3	94%
4865	G04	103775	228	21596.2	2104.9	94%
4865	H04	106208	248	10674.3	1410.7	92%

4865	A05	106282	249	19980.2	1766.4	94%
4865	B05	106461	240	19797.3	1984.2	93%
4865	C05	106506	224	88204.1	95867.1	89%
4865	D05	106570	238	20722.9	2092.6	95%
4865	E05	106863	242	21834	2125.3	94%
4865	F05	108235	229	15610.8	1768.2	93%
4865	G05	108750	250	24366	4067.9	93%
4865	H05	108753	209	22883.8	5483.5	92%
4865	A06	108972	223	23557.9	2202.8	94%
4865	B06	109084	214	25517.4	2091.6	94%
4865	C06	109086	228	39900.6	2804.2	93%
4865	D06	109466	245	23061.2	3005.3	92%
4865	E06	109719	204	22000.1	2185.5	95%
4865	F06	111552	202	35444.5	6375.3	83%
4865	G06	112677	240	34060.8	12955.8	95%
4865	H06	114490	226	23006.4	2534.2	94%
4865	A07	114831	243	23469.8	2220	94%
4865	B07	117554	250	27835.8	2172.6	94%
4865	C07	117741	217	22346.1	2188.8	94%
4865	D07	117922	210	22757	2164.8	94%
4865	E07	118723	239	36498.7	15296.2	94%
4865	F07	120286	220	21937	2479.2	93%
4865	G07	120307	227	36233.6	17366.1	93%
4865	H07	120844	210	22149.5	2480.6	94%
4865	A08	121781	240	22179.2	2307.5	93%
4865	B08	122280	204	27079.5	6729.6	93%
4865	C08	122297	239	23189.1	2330.6	93%
4865	D08	122376	226	24271.9	2331.3	94%
4865	E08	122987	212	22743.6	2211.1	94%
4865	F08	123141	214	23152.8	2227.4	93%
4865	G08	124146	245	22334.1	2233.2	93%
4865	H08	125043	212	22136.4	2184	93%
4865	A09	125727	226	23244.2	2244.9	93%
4865	B09	126405	232	31137.1	1801.9	89%
4865	C09	126757	220	20352.8	3521	93%
4865	D09	128141	236	22909.5	2200.7	94%
4865	E09	128737	210	30621.3	10278.5	93%
4865	F09	128751	229	23806.4	2554.9	94%
4865	G09	129260	241	23227.9	2745.1	93%
4865	H09	130872	236	28113.6	4359.5	93%
4865	A10	40383	226	22804.6	2515.9	93%
4865	B10	42846	213	28702.2	3638.3	93%
4865	C10	53710	204	23036.5	2391.7	93%

4865	D10	57670	230	26338.4	2857.6	89%
4865	E10	62611	212	22767.2	3096.9	93%
4865	F10	68982	231	19175.8	2221.7	92%
4865	G10	70959	201	32224.2	2463.4	93%
4865	H10	71795	246	700715.8	261600.7	20%
4865	A11	101653	209	72173.8	47282.3	93%
4865	B11	109174	241	39379.7	17166.9	92%
4865	C11	42212	223	30027.1	8078.8	91%
4865	D11	50405	202	28022.3	6789	93%
4865	E11	50572	248	35475.8	7735.4	92%
4865	F11	56906	214	27134.4	5888.6	93%
4865	G11	113486	209	25635.1	4903.5	92%
4865	H11	73054	234	22429.3	4440.2	90%
4866	A02	131986	208	19117.1	1801.8	89%
4866	B02	133195	229	18821.7	1759.6	88%
4866	C02	133356	214	19331.8	1767.1	89%
4866	D02	139257	235	21309.1	1853.9	85%
4866	E02	140892	244	20537.6	1783.1	89%
4866	F02	143348	243	21954.3	2150.6	88%
4866	G02	144958	242	20030.1	1960.1	89%
4866	H02	144982	226	21365.2	1804.8	88%
4866	A03	149046	228	21060.8	1927.8	87%
4866	B03	149286	236	29753.4	2050.4	88%
4866	C03	150954	231	80699.8	1746.3	89%
4866	D03	152551	236	22894.8	3860.1	89%
4866	E03	153330	220	20323.4	2015	89%
4866	F03	153365	249	20053.5	1824.5	90%
4866	G03	153399	237	20280	2128.6	89%
4866	H03	154295	231	20440	1794.2	90%
4866	A04	156616	215	19642	1790.1	89%
4866	B04	157767	211	18456.8	2760	89%
4866	C04	157940	250	18391.2	1849.8	89%
4866	D04	159031	223	16688.9	2067.5	87%
4866	E04	163144	211	24313.9	9545.2	89%
4866	F04	164208	220	20855.8	1885.1	89%
4866	G04	164511	206	21110	1783.6	89%
4866	H04	164678	203	20847.1	1880.8	90%
4866	A05	165883	227	18475.4	1829.7	90%
4866	B05	166583	219	19139.2	2465.8	89%
4866	C05	170001	206	17351.4	1956.4	89%
4866	D05	170578	245	19051.9	1761.6	89%
4866	E05	170621	202	18800.4	1787.9	89%
4866	F05	174027	212	19434.9	1897.2	90%

4866	G05	175412	238	20787.6	1762.9	90%
4866	H05	175415	216	21393.1	2164.9	89%
4866	A06	176765	217	19002.3	1887	90%
4866	B06	177989	237	17818.3	2153.3	86%
4866	C06	179818	214	20203.5	4562.2	88%
4866	D06	182400	233	19919.4	2477.2	89%
4866	E06	190336	244	19208.5	1783.1	89%
4866	F06	193043	221	20275.9	2186.2	89%
4866	G06	196148	201	19304.3	1756.6	89%
4866	H06	197049	221	20492.6	1763.2	89%
4866	A07	202883	203	17272.3	1833.1	90%
4866	B07	204920	226	23539.9	1789.9	89%
4866	C07	204976	212	17387.4	1818.7	90%
4866	D07	205843	244	19096	2078	90%
4866	E07	210816	243	18487.1	1729	89%
4866	F07	215276	206	20534	2665.6	89%
4866	G07	220030	217	20535.1	1754.4	90%
4866	H07	227383	211	19657.3	1746.6	89%
4866	A08	234945	223	17986.6	1749.9	89%
4866	B08	236246	233	17936	1798.9	88%
4866	C08	240502	206	17408.1	1762	88%
4866	D08	255025	226	17733.8	1749.8	89%
4866	E08	261037	201	19451.2	1733.6	90%
4866	F08	261610	218	19339.8	1730.3	88%
4866	G08	274905	221	20917.1	2224.8	89%
4866	H08	277806	230	18467.5	1795.6	89%
4866	A09	279895	236	17058	1765.3	89%
4866	B09	282187	248	17574.1	1827.4	88%
4866	C09	284234	245	17078.9	1737	88%
4866	D09	288519	240	20021.9	1807.6	88%
4866	E09	289090	246	18933.8	1767	89%
4866	F09	289365	250	18472	1781.7	89%
4866	G09	290307	210	20263.3	1866.4	90%
4866	H09	292826	250	22188.5	2404.2	91%
4866	A10	293334	210	17103.2	1792.1	89%
4866	B10	293780	209	21553.4	1799	90%
4866	C10	294154	212	17116.7	1885.6	89%
4866	D10	294623	242	19846.8	1781.4	88%
4866	E10	295404	230	18318.6	1759.9	89%
4866	F10	298197	221	18457.1	2071.5	89%
4866	G10	298793	233	18310.5	1743.9	89%
4866	H10	301168	236	17058.3	2280.5	88%
4866	A11	309971	242	17711.2	1829.4	89%

4866	B11	311074	226	17050.6	1761.6	89%
4866	C11	311727	240	22833.1	2931.4	87%
4866	D11	319034	229	16936.8	1754.4	89%
4866	E11	321506	245	18009.1	1755.8	88%
4866	F11	327693	248	18919.9	1731.8	88%
4866	G11	329676	214	18248.3	1730.8	88%
4866	H11	330497	206	18661.5	1783.3	89%
4867	A02	332473	220	28181.3	2182.3	94%
4867	B02	335048	239	27568.8	2123.8	93%
4867	C02	338106	240	25379.1	4411.7	94%
4867	D02	341074	241	26282.3	2117.1	94%
4867	E02	343343	224	29616.2	3679.7	94%
4867	F02	343344	204	24971.4	2621.5	94%
4867	G02	343783	238	35638.2	14506	93%
4867	H02	353451	243	25078.7	2297.3	93%
4867	A03	357683	223	34276.3	6735.5	94%
4867	B03	366807	223	27482.5	2209.6	93%
4867	C03	367428	220	26717.7	2172.9	94%
4867	D03	367487	205	26949.9	2197.9	94%
4867	E03	370367	211	25391.8	2186.6	93%
4867	F03	372134	243	25663.4	2183.6	94%
4867	G03	372221	230	25017.2	2168.6	93%
4867	H03	373427	245	23543	2131.1	93%
4867	A04	373535	232	27347.8	2182.3	94%
4867	B04	375392	210	26291.2	2249	94%
4867	C04	375997	241	28856.2	2278.9	92%
4867	D04	382059	220	26585.8	2183.7	92%
4867	E04	403374	229	24595	2150.8	94%
4867	F04	503425	202	26687.8	2190.2	93%
4867	G04	509563	243	24363.4	2129.3	93%
4867	H04	515893	238	24780.9	2306.4	91%
4867	A05	601351	240	27028.6	2189.4	93%
4867	B05	605333	223	22821.1	2214.5	89%
4867	C05	622175	203	26213.8	2254.3	93%
4867	D05	636717	250	43134.2	13017.1	92%
4867	E05	637290	215	30620.8	3387.6	92%
4867	F05	638080	220	25805.2	3023.3	92%
4867	G05	638134	203	26134.5	2446.6	93%
4867	H05	643150	222	28494.9	8772.4	93%
4867	A06	645987	242	385275.1	56014.3	54%
4867	B06	646976	233	27673.2	2521.6	92%
4867	C06	659107	244	28137.9	3735.6	88%
4867	D06	660300	249	26104.1	2295.1	93%

4867	E06	479	267	25592.6	2250.6	93%
4867	F06	1847	262	23808.5	2235.2	93%
4867	G06	3076	265	21591.6	2341.1	94%
4867	H06	3193	270	24912.4	2264.9	92%
4867	A07	3247	275	27629.8	2273.4	94%
4867	B07	4429	296	26860	2278.9	92%
4867	C07	5426	258	27958.6	2996.5	92%
4867	D07	5564	275	26964.1	2216.7	92%
4867	E07	6137	263	25996.8	2181.3	93%
4867	F07	6145	286	32398.7	3843	93%
4867	G07	6731	254	27627.2	2294.3	82%
4867	H07	6821	289	33455.3	2305.3	90%
4867	A08	6844	292	32071.3	2403.5	93%
4867	B08	7218	293	89906.3	67872.4	91%
4867	C08	7420	298	36996.4	2222.4	83%
4867	D08	7572	278	27353.8	2807.7	92%
4867	E08	7745	268	25343	2251.5	93%
4867	F08	7962	284	23845.3	2206.3	90%
4867	G08	9782	282	36872	2454.4	91%
4867	H08	10173	278	64683.3	47267.4	92%
4867	A09	10211	287	30558	2334.8	91%
4867	B09	10768	255	28483.3	3074.9	93%
4867	C09	11296	286	33354.6	2367.5	91%
4867	D09	131388	209	26197.8	2241	91%
4867	E09	148170	227	25796.9	2295	88%
4867	F09	154587	219	25957	2241.8	93%
4867	G09	159632	236	54350.6	33790.3	92%
4867	H09	166547	229	26798.4	2695.1	91%
4867	A10	294161	238	29946	2257.1	92%
4867	B10	329284	212	47501.9	2286.1	91%
4867	C10	343230	226	27842.3	2203.3	92%
4867	D10	7867	294	29995.8	2329.9	92%
4867	E10	8816	252	31051.4	2240.6	91%
4867	F10	11023	268	24290.5	2198.2	85%
4867	G10	11275	266	31263.8	2267.5	90%
4867	H10	11643	288	48481.6	2349.9	91%
4867	A11	306752	238	29115.6	2228.1	91%
4867	B11	10865	260	28006.8	2246.9	91%
4867	C11	379639	245	28506.1	3408.5	79%
4867	D11	402843	244	26436.8	2204.5	92%
4867	E11	403379	203	25307.8	2233.4	91%
4867	F11	647136	238	28938.4	3255.4	92%
4867	G11	11276	266	31599.1	2450.6	91%

4867	H11	11624	277	24422.1	2314.6	91%
4868	A02	11664	295	193144.8	4174	85%
4868	B02	11912	274	945765.6	958155.3	77%
4868	C02	12028	286	111994.5	79605.3	94%
4868	D02	12488	271	61867.6	29786.1	63%
4868	E02	12633	275	42841.3	16004.7	92%
4868	F02	12644	289	39124.4	11594.3	93%
4868	G02	12646	267	36351.6	9985.2	93%
4868	H02	13151	259	69867.8	9976.7	86%
4868	A03	13248	290	34539.2	9393.2	91%
4868	B03	13345	254	27583.7	6165.9	93%
4868	C03	13434	269	28616.9	5888.3	93%
4868	D03	13579	268	30011.7	5299.6	93%
4868	E03	13658	264	33047.9	5264.9	93%
4868	F03	13785	267	30087.4	4964	93%
4868	G03	13800	254	29712.6	7344.6	92%
4868	H03	14380	266	46454.4	5302.7	92%
4868	A04	14396	284	33792.1	4979.4	93%
4868	B04	14398	299	27368.1	4439.4	92%
4868	C04	15358	293	24199.8	3203.5	93%
4868	D04	15359	264	25507	4005.1	92%
4868	E04	15784	266	504816.5	4213.5	89%
4868	F04	17148	286	26311.5	3682.6	92%
4868	G04	17362	266	33010.2	3728.6	91%
4868	H04	17507	253	35709.2	4109.5	90%
4868	A05	19125	276	24751.5	3850.1	93%
4868	B05	19136	273	32805.3	6084.6	90%
4868	C05	19141	288	28331	3734.7	92%
4868	D05	19824	275	27323	5432.2	92%
4868	E05	19962	274	33986.4	3614.2	92%
4868	F05	21333	260	32453.4	4244.2	92%
4868	G05	21603	290	32286.2	3569.4	85%
4868	H05	21683	292	17229.3	2867.9	90%
4868	A06	21709	279	29121	3399	91%
4868	B06	21710	277	41637.8	3275	91%
4868	C06	22801	280	23746.6	3411.9	91%
4868	D06	22806	262	22800.8	3340.4	93%
4868	E06	22881	266	24451	2669.7	91%
4868	F06	25678	277	29447	3737.5	92%
4868	G06	25740	298	26944.3	3108.9	91%
4868	H06	26692	296	30437.9	7544.7	91%
4868	A07	28377	269	23468.4	3432.8	93%
4868	B07	29073	276	21531.3	3252.7	92%

4868	C07	30813	272	20785.6	3563.4	93%
4868	D07	30930	267	22704.1	4622.8	91%
4868	E07	31069	297	21848.9	3310.5	90%
4868	F07	31698	265	30911.8	6889.8	92%
4868	G07	31703	295	79418.3	3523.3	86%
4868	H07	33010	253	35941.4	3393.8	87%
4868	A08	34875	272	28994	3354.9	91%
4868	B08	34879	267	28025.1	3401.1	92%
4868	C08	34910	291	44710.6	3466.3	87%
4868	D08	36586	270	30650.4	3328.7	89%
4868	E08	36753	274	24236.6	3047.5	91%
4868	F08	36815	264	33174.6	3000.4	91%
4868	G08	37612	269	46333.3	9976	91%
4868	H08	37955	261	38882.4	4728.8	89%
4868	A09	38352	295	24026.5	3573.7	93%
4868	B09	39047	256	22394.6	3323.2	91%
4868	C09	39938	281	26350.2	6264.7	91%
4868	D09	40275	263	24319.9	3364.5	91%
4868	E09	40306	298	30544.8	3341.4	90%
4868	F09	41066	286	27235.2	3015.1	91%
4868	G09	41376	278	27749.6	2950.1	91%
4868	H09	41378	277	28814.6	2973.3	91%
4868	A10	41649	260	29504.5	3166.5	91%
4868	B10	41805	300	23932.6	3224.2	92%
4868	C10	42096	294	23056.3	2978.7	93%
4868	D10	42135	280	23452.2	3808.5	92%
4868	E10	43308	288	55065.1	3194.7	73%
4868	F10	43344	300	29234.5	2895.9	91%
4868	G10	44556	287	26574	2951.6	90%
4868	H10	45086	261	44399.6	2995.7	91%
4868	A11	45536	266	13826.5	2167.1	81%
4868	B11	45745	261	22678.2	2847.7	92%
4868	C11	46212	298	20977.6	2853.5	80%
4868	D11	47522	255	31265.2	3454.4	91%
4868	E11	49643	292	25203.9	2839	91%
4868	F11	49847	274	27197.2	2881.7	91%
4868	G11	50199	260	120586.4	64337.9	89%
4868	H11	51349	283	46718.4	3065.5	90%
4869	A02	51351	284	105235.6	1585.6	49%
4869	B02	52241	284	50834.6	1895.3	91%
4869	C02	55172	285	26449.1	1986.6	92%
4869	D02	55453	272	33817.3	2001.1	91%
4869	E02	55845	285	33166.5	2039.6	92%

4869	F02	55862	298	28609.1	2919.6	93%
4869	G02	58347	281	29488.1	2232.5	91%
4869	H02	58724	256	28202.2	2449	92%
4869	A03	59430	284	24729.1	2047.8	92%
4869	B03	59782	252	25414.9	1958	92%
4869	C03	59984	265	42740.6	2915.1	91%
4869	D03	60303	278	31815.4	3199.9	91%
4869	E03	61929	294	27737	2020.3	91%
4869	F03	62901	259	27006.9	1983	92%
4869	G03	63161	264	27353.3	2163	92%
4869	H03	66020	259	27916.7	2014.8	91%
4869	A04	68841	267	29063.2	2066.6	92%
4869	B04	68971	273	25836.1	2017.5	92%
4869	C04	70307	267	24366.6	1961.8	90%
4869	D04	72947	282	30012.5	1977.1	92%
4869	E04	73295	252	25721.5	1992.8	92%
4869	F04	73753	289	28806.6	2032.9	92%
4869	G04	76549	261	25499.8	2059.8	92%
4869	H04	76747	272	111768.8	106674	90%
4869	A05	78623	292	24749.5	2067	91%
4869	B05	78697	264	21726.6	2527.2	88%
4869	C05	82269	272	27370.9	3070.3	92%
4869	D05	87008	293	26020.9	1986.8	92%
4869	E05	87690	271	25136.1	1997.6	90%
4869	F05	88324	251	23614.3	2015	91%
4869	G05	88349	254	26679.3	1967.1	91%
4869	H05	88402	292	31919.8	2504.2	90%
4869	A06	88795	253	30062.2	2080.3	92%
4869	B06	89349	284	23057.5	2330.1	92%
4869	C06	89429	296	29576.6	1984.5	93%
4869	D06	89759	258	26248.6	1929.4	93%
4869	E06	92849	278	24461	1947.6	93%
4869	F06	93427	286	8841.9	1413.1	90%
4869	G06	93945	262	21994.3	1786.8	92%
4869	H06	95909	266	25223.1	1855.4	91%
4869	A07	97865	277	24524.8	1943.6	91%
4869	B07	98026	300	27507	1990	91%
4869	C07	98049	262	55043.2	2022.1	93%
4869	D07	98938	280	65154.8	5947.3	90%
4869	E07	100058	287	22969.7	2037	92%
4869	F07	100942	274	24167	1922	92%
4869	G07	101298	269	18993.6	2006.3	82%
4869	H07	101345	265	31189.5	1967.3	91%

4869	A08	101679	273	23885.4	1980.9	92%
4869	B08	101758	259	22936.6	1963.6	93%
4869	C08	102554	263	23977.5	1974.7	92%
4869	D08	103189	299	24743.4	1999.8	92%
4869	E08	105432	284	24083.5	1944.3	93%
4869	F08	108783	272	37344.6	2015.6	92%
4869	G08	109747	263	38074.1	10457	91%
4869	H08	111847	263	55884.3	8642.1	88%
4869	A09	17055	280	434677	390321.4	91%
4869	B09	20618	258	34940.5	13892.7	91%
4869	C09	20619	258	27358.7	4164.8	90%
4869	D09	23715	265	28886.3	2775	92%
4869	E09	32892	278	25939.1	2534.5	92%
4869	F09	40749	290	26604.5	1644.9	91%
4869	G09	43409	266	26305.9	2164.4	91%
4869	H09	50680	293	80936.5	6639.3	92%
4869	A10	54645	283	29598.6	2800.2	91%
4869	B10	54860	289	45893.9	3384	82%
4869	C10	79887	298	66068.4	2447.4	89%
4869	D10	107022	278	24659.3	2787.8	92%
4869	E10	33173	269	121065.7	102757.2	89%
4869	F10	38007	256	28277.7	8874	86%
4869	G10	60037	286	19303.9	1475.4	89%
4869	H10	66122	284	18016.4	2099.2	90%
4869	A11	14311	263	22185.5	2357.5	92%
4869	B11	21970	268	29951.3	13298.7	90%
4869	C11	33182	276	22834.1	2923.2	91%
4869	D11	45815	264	23094	2233	91%
4869	E11	53934	295	24950.8	2327.4	92%
4869	F11	76478	287	86441.8	2258.4	87%
4869	G11	92937	261	53571.9	36517	80%
4869	H11	110899	254	26667.4	4444.2	91%
4870	A02	112541	292	77769	2046.4	92%
4870	B02	112547	298	58009	2771.3	91%
4870	C02	112965	271	58816.6	2355.5	93%
4870	D02	116640	295	66203.9	6237.7	94%
4870	E02	116644	270	154186.4	120376.9	93%
4870	F02	117197	299	75389.7	12206.8	92%
4870	G02	117446	261	65697.9	6168.3	92%
4870	H02	117908	286	67758.5	5583.2	93%
4870	A03	118628	288	59604	3823.9	91%
4870	B03	119805	295	55381.4	3042.5	92%
4870	C03	120631	258	55727.1	2818.2	92%

4870	D03	120913	262	60256.3	2648.8	93%
4870	E03	120961	280	61946.2	2595.6	93%
4870	F03	121268	272	63111.9	2533.1	92%
4870	G03	122253	290	63686.6	2474.6	93%
4870	H03	125344	281	64625	2499.6	92%
4870	A04	125605	257	41756.7	2114.9	90%
4870	B04	126224	265	104065.8	2401	89%
4870	C04	127886	278	56751.1	2374.9	92%
4870	D04	129220	285	54884.8	2336.6	92%
4870	E04	129929	266	275645.9	244496.5	91%
4870	F04	130801	280	76635.9	21178.3	94%
4870	G04	130847	289	138334.4	6821.8	92%
4870	H04	133002	259	62643.1	4055.5	91%
4870	A05	133351	290	52907.4	3306.8	92%
4870	B05	134058	251	56314.1	3017.5	93%
4870	C05	134199	294	53508.3	3040.4	92%
4870	D05	134674	257	57954.5	2835.1	93%
4870	E05	135412	288	60664.8	2843.9	92%
4870	F05	135894	269	58415.7	2738.9	87%
4870	G05	137399	273	63542.1	2711.3	90%
4870	H05	137577	275	79689.8	2646.1	93%
4870	A06	138389	253	150212.9	2857	89%
4870	B06	138398	289	54385.8	3244.1	92%
4870	C06	139021	255	56109.5	3727.4	90%
4870	D06	140873	277	58413.5	2774.5	92%
4870	E06	140899	268	59519.9	2767.8	92%
4870	F06	141538	296	79725	2687.6	92%
4870	G06	142269	273	58509.4	2599.4	92%
4870	H06	144694	274	65965.2	2703.6	90%
4870	A07	147866	282	55340.3	2760.9	92%
4870	B07	148832	264	52247.1	2612.8	92%
4870	C07	151262	285	57940.4	3285	91%
4870	D07	153172	272	53320.5	2464.5	93%
4870	E07	153792	269	56877.6	2658.4	92%
4870	F07	154127	281	122103.7	2689.8	90%
4870	G07	156957	263	59276.5	2622.4	92%
4870	H07	157522	275	60667.1	2678.9	92%
4870	A08	158549	260	183810.3	20023.6	92%
4870	B08	159686	257	65079.4	4985.1	93%
4870	C08	162188	275	57250.1	3381.4	92%
4870	D08	163802	258	54630.3	3000.2	91%
4870	E08	164464	275	56810.8	3090.3	92%
4870	F08	165599	287	57069.9	2893.1	92%

4870	G08	165701	295	60212.7	2855.4	91%
4870	H08	166596	268	78886.5	2937.4	91%
4870	A09	166634	267	51583.1	2777	90%
4870	B09	166846	266	49905.3	2819.6	91%
4870	C09	168221	286	72395.3	3239	91%
4870	D09	168225	278	52449.9	2890	91%
4870	E09	170637	256	47748.1	2537.6	92%
4870	F09	170955	291	55153.9	3024	92%
4870	G09	174084	295	63160.2	2913.6	90%
4870	H09	175743	268	59170.7	2734.6	90%
4870	A10	176367	257	54266.4	2763.9	92%
4870	B10	177866	259	50829.1	3480	91%
4870	C10	178873	268	53575.3	2653.8	92%
4870	D10	179822	260	50091.3	2649.9	92%
4870	E10	180964	274	57042.1	2832.8	91%
4870	F10	193528	272	57785.1	2841.8	92%
4870	G10	195327	271	53657.1	2657.4	89%
4870	H10	197046	252	58911.6	2632.5	93%
4870	A11	201634	274	46142.2	3172.2	90%
4870	B11	203837	267	46641.7	2648.6	91%
4870	C11	205909	290	52590.8	3856.3	90%
4870	D11	205913	262	56058.8	4496.9	90%
4870	E11	207895	279	107272.3	2596.1	87%
4870	F11	211336	273	58479.3	2550.3	91%
4870	G11	213708	253	55709.1	2710.6	92%
4870	H11	214029	265	68725.6	16258.2	87%
4871	A02	215275	296	24821.1	1581.9	73%
4871	B02	215585	266	18579.5	1561.4	77%
4871	C02	216183	289	208936	1376.5	88%
4871	D02	216618	265	20433.5	1544.4	88%
4871	E02	236254	266	21567	1518.9	87%
4871	F02	238929	273	15242.9	1510.9	85%
4871	G02	240029	280	19049.1	1498.7	89%
4871	H02	241621	279	27228.7	10248.7	88%
4871	A03	241998	294	20366.5	1517.3	88%
4871	B03	242557	282	31208.6	1469.2	89%
4871	C03	265372	264	18496.9	1491.2	88%
4871	D03	283856	262	20090.2	1451.8	88%
4871	E03	285669	254	19954.7	1467.5	88%
4871	F03	288024	297	18862.8	1455.9	89%
4871	G03	289748	262	17023.3	1610.3	88%
4871	H03	294150	291	18540.4	1519.9	87%
4871	A04	294625	287	16943.8	1519.3	87%

4871	B04	294747	271	20333.5	1530.1	88%
4871	C04	296934	297	19867.4	1485.6	88%
4871	D04	299514	288	17713.8	1761.6	86%
4871	E04	299967	287	20791.8	1491.1	87%
4871	F04	299968	270	20319.7	1808.1	86%
4871	G04	301167	272	19462.3	1465.6	88%
4871	H04	302584	278	22306.4	1386.4	88%
4871	A05	302867	288	16864.6	1569.6	84%
4871	B05	303304	258	42408.1	1596.1	88%
4871	C05	305329	262	39333.9	19942.5	85%
4871	D05	305743	258	38021.3	1809.8	85%
4871	E05	307703	257	22400.8	1561.9	88%
4871	F05	308814	283	29509.9	14102.3	83%
4871	G05	310113	278	19170	2907.3	84%
4871	H05	311165	285	26042.7	1493.8	88%
4871	A06	312606	284	35711	8505.1	86%
4871	B06	316458	263	19188.9	2469.6	88%
4871	C06	318799	262	18675.9	1838.7	88%
4871	D06	319029	288	18959.2	1675.4	89%
4871	E06	319079	297	20766.8	1742.3	88%
4871	F06	319436	299	20696.8	1637.1	88%
4871	G06	319471	252	18291.3	1529.8	88%
4871	H06	321792	254	20270.9	1876.9	89%
4871	A07	326644	269	30811.3	1641.7	88%
4871	B07	326921	274	20690.3	1577.1	89%
4871	C07	327444	268	20492.5	2357	88%
4871	D07	328130	261	19030.3	1572.1	86%
4871	E07	331972	263	37895.6	1479.5	88%
4871	F07	332452	286	18454.8	1523.6	88%
4871	G07	338564	277	17835.5	1575.4	86%
4871	H07	343526	265	30864.7	1684.8	87%
4871	A08	343557	281	27698.3	8019.7	87%
4871	B08	348970	258	33603.7	12487.7	88%
4871	C08	351674	286	43191.2	11264.8	89%
4871	D08	351691	260	21279.7	2090.1	88%
4871	E08	352888	279	17616.2	1637.6	88%
4871	F08	358311	271	24376.8	5534.8	77%
4871	G08	361570	283	15688	1679.1	84%
4871	H08	364889	299	18113.7	2049.6	88%
4871	A09	366086	269	19731.4	1702.9	85%
4871	B09	366802	298	20445.1	1629.1	87%
4871	C09	367474	281	18400.1	1609.2	88%
4871	D09	367480	298	18188.1	1603.1	86%

4871	E09	369066	269	20730.1	1470.6	88%
4871	F09	369070	299	18115.1	1333.5	86%
4871	G09	122385	270	16950.1	1543.8	87%
4871	H09	164880	291	49016.1	2940	89%
4871	A10	228155	290	64793	7697.5	64%
4871	B10	294153	288	22312.2	1793	85%
4871	C10	362093	275	38264.2	1628.1	86%
4871	D10	363801	253	20721.2	1581.7	88%
4871	E10	367416	282	19268.6	5134.6	75%
4871	F10	217306	290	17278.9	2121.2	87%
4871	G10	276736	281	22638.9	1906.6	87%
4871	H10	283845	273	62005.4	1711.4	84%
4871	A11	116508	276	18518.6	1676.5	86%
4871	B11	149312	266	18704	1679.7	85%
4871	C11	204939	295	49529.8	1749.2	86%
4871	D11	252172	278	17658.6	1669.8	79%
4871	E11	269904	299	20709.9	1720	87%
4871	F11	280492	298	17742.1	1571.8	79%
4871	G11	330796	283	18364.1	2161.2	84%
4871	H11	331977	254	20742.8	1572.3	86%
4872	A02	370383	264	17867.9	2119.1	86%
4872	B02	372769	290	72623.4	2148.9	84%
4872	C02	373981	257	17313.6	2645.9	86%
4872	D02	374703	298	34370.3	2058	87%
4872	E02	374814	276	21505.6	2174.1	86%
4872	F02	375105	285	2515879	2676081	83%
4872	G02	378711	281	61466.9	44635.6	87%
4872	H02	379468	296	39290.6	22363.9	84%
4872	A03	379536	296	28953.9	12195.3	86%
4872	B03	379651	277	32929.6	10556.4	85%
4872	C03	380279	295	24059.6	7442.4	87%
4872	D03	400770	274	23382.6	7329.6	78%
4872	E03	400938	253	41459.7	4802.1	85%
4872	F03	403268	265	22046.6	5023.3	85%
4872	G03	408734	273	21171.1	4569	86%
4872	H03	408860	286	21712.6	4063.4	87%
4872	A04	522131	297	33494.8	6193.7	85%
4872	B04	524615	278	20499.4	3864.6	87%
4872	C04	525721	271	21470.7	3488.4	86%
4872	D04	636718	264	35887.4	3434	84%
4872	E04	637343	276	16201.4	9963.6	82%
4872	F04	637359	258	27370.6	4676.2	86%
4872	G04	637827	276	31553.8	4116.1	79%

4872	H04	638636	257	23291.1	3434.1	84%
4872	A05	641396	291	27100.6	22433.1	71%
4872	B05	643029	280	24385.7	5594.6	69%
4872	C05	645330	275	58961.8	62570.2	81%
4872	D05	661221	275	22474.7	30113.3	76%
4872	E05	680515	265	8303.4	1787.1	57%
4872	F05	689002	287	16878.4	3370.9	77%
4872	G05	3753	304	21746.4	3574.8	86%
4872	H05	5053	335	19269.9	2966.8	86%
4872	A06	5476	334	30219.1	3326.6	85%
4872	B06	6101	330	21399.4	2887.3	73%
4872	C06	7436	304	21449.7	2978.4	84%
4872	D06	7578	343	26219.7	2788.6	87%
4872	E06	9037	336	16544	2388.1	85%
4872	F06	11437	302	7708.7	1915.8	51%
4872	G06	12262	314	30966.1	2681.6	86%
4872	H06	12544	320	19698.2	2664.5	87%
4872	A07	12628	321	18904.4	2580.7	85%
4872	B07	12650	322	18527.2	2522	86%
4872	C07	13156	314	22482.4	5439.8	86%
4872	D07	13176	318	46733	2762.8	79%
4872	E07	13616	327	125306.2	9156.5	86%
4872	F07	14142	327	20478.2	2837.2	86%
4872	G07	14506	332	25981.8	2724.9	85%
4872	H07	16722	302	19966.7	2495.4	86%
4872	A08	17128	348	25037.1	2505.9	86%
4872	B08	18883	349	381837	18006	71%
4872	C08	24032	310	45071	35012.4	79%
4872	D08	24951	350	18413.5	2720.5	86%
4872	E08	25435	310	40082.4	2700.5	87%
4872	F08	25457	348	840205.3	847977.7	55%
4872	G08	26349	302	23936.6	6438.5	85%
4872	H08	26980	334	20258.5	3894.9	85%
4872	A09	27305	324	19590.4	3277.7	86%
4872	B09	28080	312	55557	19860.5	71%
4872	C09	30205	314	38236.5	12353	71%
4872	D09	30260	349	17245.8	2242.4	86%
4872	E09	32673	334	20514.8	2288.9	75%
4872	F09	32873	305	17234.2	2287.5	86%
4872	G09	33353	337	30968.3	6062.5	33%
4872	H09	33478	328	18409.6	2288.3	84%
4872	A10	33738	339	26274.9	2377.7	86%
4872	B10	34219	313	20618.6	2286.1	80%

4872	C10	34865	322	17569.3	2269.2	86%
4872	D10	35582	347	18324.9	2268.8	73%
4872	E10	36693	332	32206.3	2409.2	86%
4872	F10	36758	305	17491.3	3116.7	72%
4872	G10	36923	317	26307.4	2235	85%
4872	H10	37168	308	16229.4	1919.9	84%
4872	A11	37187	312	23663.9	5744	81%
4872	B11	38090	333	57150.5	2203.9	85%
4872	C11	39984	314	22336.8	4907.6	85%
4872	D11	40269	326	19051.2	2298.9	87%
4872	E11	41098	312	11469.1	1373.5	79%
4872	F11	43088	335	13089.9	1861	86%
4872	G11	43506	315	16851.8	2226.3	85%
4872	H11	44584	334	19553.7	2047.7	82%
4873	A02	44750	312	13034.9	2148.6	90%
4873	B02	45527	304	8881.7	1662.6	90%
4873	C02	46213	312	13983.2	1885.8	37%
4873	D02	46492	313	486339.2	2203.4	65%
4873	E02	48388	330	25045.5	2027.1	91%
4873	F02	50648	308	31237.2	1852.1	84%
4873	G02	50651	336	118219.3	9314.5	80%
4873	H02	50690	307	27259.6	4373.7	89%
4873	A03	51683	315	12778.2	2355.4	91%
4873	B03	55152	346	13536	2061.2	50%
4873	C03	59814	317	13701.1	2060.5	92%
4873	D03	60013	307	16623.3	1952.4	56%
4873	E03	60183	310	34636.2	2084.6	91%
4873	F03	60423	321	38980.6	2608.7	89%
4873	G03	61642	344	26236.6	2283	88%
4873	H03	62375	310	26724.3	2137.5	91%
4873	A04	64672	344	12703.1	2014.1	90%
4873	B04	65689	327	16591.1	3670.9	90%
4873	C04	68116	315	15322.4	2106.7	90%
4873	D04	69359	302	20803.3	2055.2	90%
4873	E04	70413	327	22501.8	2044.8	90%
4873	F04	71097	310	42280.3	8109.3	84%
4873	G04	71866	305	21888.3	2111.6	90%
4873	H04	71881	314	24974.2	2214	77%
4873	A05	76988	302	13085.3	2445.8	91%
4873	B05	79486	340	299710.5	2208.3	88%
4873	C05	79559	308	11294.2	2162.8	74%
4873	D05	81750	329	16314.3	2108.9	90%
4873	E05	82560	309	20296.6	2023.4	58%

4873	F05	83497	326	23973	1992.3	88%
4873	G05	86467	328	38563.6	2186	89%
4873	H05	87084	331	26274.8	2230.6	90%
4873	A06	87136	312	14918	2013.8	90%
4873	B06	87838	346	15052.6	2805.3	89%
4873	C06	90749	303	23697.4	5894.3	91%
4873	D06	91378	342	21136	2121.4	90%
4873	E06	91382	340	65535.5	2165.6	88%
4873	F06	92892	337	24006.6	2042.8	89%
4873	G06	93033	305	24046.7	2264.4	89%
4873	H06	95204	306	26899.6	2172.4	90%
4873	A07	95916	343	21703.2	9810	91%
4873	B07	653004	291	14588.8	3399.1	90%
4873	C07	1014	341	8845.8	2784.4	87%
4873	D07	22070	306	27953.1	2390	92%
4873	E07	26112	306	13393.6	2142.5	78%
4873	F07	33570	321	76886.2	2187	88%
4873	G07	36525	342	39587.5	2252.6	91%
4873	H07	43271	304	22335.6	2152.8	73%
4873	A08	53874	327	12162.3	2047.5	89%
4873	B08	56779	304	11805.6	2153.1	90%
4873	C08	87010	302	13463.2	2164.4	91%
4873	D08	636734	279	15065.4	2098.8	86%
4873	E08	6268	318	18263	1977.2	82%
4873	F08	11307	314	30388.7	2128.8	88%
4873	G08	26113	318	11714.6	2605.2	81%
4873	H08	35545	301	25125.3	2193.2	89%
4873	A09	43998	318	43675.7	39009.2	85%
4873	B09	47680	301	13874.6	3534.1	89%
4873	C09	48443	332	57019.6	27230.6	79%
4873	D09	66695	340	15122.6	2332	88%
4873	E09	73254	347	22746.8	2298.1	88%
4873	F09	80313	325	30849.6	2257.7	88%
4873	G09	94600	348	34403.6	7157.4	85%
4873	H09	524385	268	34397.1	2472.4	88%
4873	A10	680516	290	148797.9	1491.6	87%
4873	B10	30622	333	11039	2048.3	90%
4873	C10	19123	305	12603.8	2829.7	62%
4873	D10	3064	328	21152.7	3732.3	88%
4873	E10	33575	345	10480.3	1787.6	89%
4873	F10	45545	308	23011.3	2738.4	81%
4873	G10	48617	312	61485.4	2384.4	89%
4873	H10	60659	312	34862.6	2493.9	87%

4873	A11	63543	326	17179.7	2193	86%
4873	B11	64859	328	19149.2	2186.1	87%
4873	C11	70895	316	15560.1	2251.9	87%
4873	D11	76015	344	15784	2179.1	87%
4873	E11	81493	303	20812.6	2216.7	87%
4873	F11	81856	327	25890.7	2021.6	85%
4873	G11	83961	303	53035.8	2290	87%
4873	H11	25673	347	30092.9	2368.9	86%
4874	A02	96541	310	18282.4	2747.3	93%
4874	B02	96996	339	24736.6	2077.9	92%
4874	C02	99634	322	16764.8	1768.1	93%
4874	D02	99660	339	20383.4	1968.6	93%
4874	E02	99663	319	20131.5	1791.8	92%
4874	F02	101789	311	18862.7	1647	85%
4874	G02	105348	330	14058.3	1748	71%
4874	H02	105781	304	217366	3894.7	91%
4874	A03	105798	328	37608.4	24039.8	94%
4874	B03	105827	325	25710.3	9102.8	88%
4874	C03	106464	332	21635.7	6068.9	94%
4874	D03	110332	303	20418.3	5251	93%
4874	E03	110562	302	19418.2	4284	93%
4874	F03	111194	347	16465.4	3731.8	91%
4874	G03	112203	311	18413.9	4182.9	92%
4874	H03	114449	338	17672.1	3818.6	85%
4874	A04	114997	326	21216	3209.4	93%
4874	B04	116397	329	18546.3	2939.5	93%
4874	C04	120290	332	17916.1	2661.1	88%
4874	D04	120622	316	16681.3	2501.5	89%
4874	E04	121908	306	16756.2	2421.6	88%
4874	F04	123389	325	107561.2	89006.8	91%
4874	G04	126226	302	32410.1	15577.9	92%
4874	H04	126347	328	30047.2	3742.5	92%
4874	A05	129536	310	20654.8	3730.9	93%
4874	B05	133114	346	20709.6	3034.3	79%
4874	C05	135184	308	19438.9	2745.4	93%
4874	D05	137112	347	19438.4	2552.1	91%
4874	E05	142277	320	16785.6	2317.8	91%
4874	F05	143974	336	20428.9	2446.1	92%
4874	G05	146071	320	21223.6	2095.8	68%
4874	H05	146554	350	22834.2	3666.4	92%
4874	A06	146769	334	15099.6	1970.8	87%
4874	B06	146770	304	16807.4	2086.9	91%
4874	C06	147358	301	151557.6	2592.6	90%

4874	D06	149054	307	17488.2	2057.7	93%
4874	E06	153391	328	17310.2	2082.3	91%
4874	F06	154585	335	16963	2013.9	91%
4874	G06	157725	329	16636.6	1987.4	93%
4874	H06	158959	316	27423.8	3590.3	73%
4874	A07	159092	332	17281.7	2088.1	85%
4874	B07	159398	347	19510.7	1964.1	92%
4874	C07	164435	338	17833.6	2109.3	93%
4874	D07	164459	305	17854.4	2044.9	92%
4874	E07	165704	336	17552.5	2041.7	91%
4874	F07	169409	339	23238.8	2002.5	92%
4874	G07	176736	335	62722.2	1834.7	80%
4874	H07	177407	333	53720.7	3514.2	91%
4874	A08	186067	339	20298.1	2711.1	92%
4874	B08	186194	324	20402	2045.8	92%
4874	C08	186200	340	35944.4	2042.5	90%
4874	D08	190501	326	36310.8	2050.7	88%
4874	E08	191441	347	16481.2	1926.1	92%
4874	F08	194308	306	26002.9	2187	91%
4874	G08	201659	323	17482.6	2307.2	90%
4874	H08	201989	343	18667.8	3438.1	91%
4874	A09	202705	305	287410.8	104150.3	91%
4874	B09	205827	301	36839.1	22853.6	82%
4874	C09	205832	350	35787.6	18459.3	50%
4874	D09	205842	319	21929.8	6529.9	92%
4874	E09	205912	325	19734.9	5195.2	91%
4874	F09	211340	303	20683.9	4389	91%
4874	G09	211787	326	32586.8	3661.3	93%
4874	H09	215684	318	21517.3	3361.9	92%
4874	A10	215689	345	18463.5	3083.3	92%
4874	B10	216607	320	25330.1	3087.8	91%
4874	C10	216621	350	29739.3	3097.6	90%
4874	D10	216623	301	18310.3	2802.4	84%
4874	E10	228137	334	16414	2284	89%
4874	F10	228150	303	18501.9	8932.3	84%
4874	G10	241619	305	23096.6	2383.8	92%
4874	H10	241624	332	78058.5	3285.8	92%
4874	A11	244387	328	20199.6	2272	91%
4874	B11	246999	331	19365.9	2340.9	67%
4874	C11	270063	308	22015.6	4898.9	90%
4874	D11	270916	337	40144.8	2458.4	91%
4874	E11	281307	331	18132.6	2144.7	91%
4874	F11	281383	319	18583.4	2074.4	92%

4874	G11	281623	340	15795.5	2875.7	84%
4874	H11	281624	310	16883.4	3209.7	89%
4875	A02	282137	314	23366.8	2308.6	92%
4875	B02	283849	328	36016.5	2281.5	93%
4875	C02	288387	348	28733.1	6203.2	94%
4875	D02	293360	343	55927.9	2005.2	93%
4875	E02	294750	310	22607.2	2221	92%
4875	F02	294756	333	43394.9	2003.9	92%
4875	G02	295300	330	39635.9	2360.4	95%
4875	H02	299119	312	19785.9	1897.5	92%
4875	A03	300540	331	22037.5	2469.2	91%
4875	B03	303294	347	28754.3	2121	93%
4875	C03	303612	322	230718	2317.1	68%
4875	D03	305780	341	205108.1	7592.6	4%
4875	E03	308848	311	22072.9	4041.4	88%
4875	F03	308849	309	24890	3108.6	75%
4875	G03	319012	321	30977	2070.3	93%
4875	H03	319424	309	25138.4	2030.1	93%
4875	A04	319449	341	31144.6	11195.8	93%
4875	B04	321517	313	41222.1	2380.6	93%
4875	C04	326182	309	30147.4	2250.7	91%
4875	D04	326385	334	23414.6	2201.9	93%
4875	E04	326422	306	19788.1	2053.9	92%
4875	F04	326757	318	20206.6	1975	88%
4875	G04	328010	336	32523.8	2067.7	95%
4875	H04	328111	325	131863.4	106392.4	94%
4875	A05	329052	322	23274.5	2398	93%
4875	B05	329255	329	25398.1	2365.5	82%
4875	C05	330770	311	346925.6	323595.4	67%
4875	D05	332670	310	153482.6	96031.5	93%
4875	E05	333544	336	39406	17596.8	92%
4875	F05	335504	337	34893.6	11345.2	92%
4875	G05	339589	322	57811.9	9690.3	94%
4875	H05	339594	339	51710.9	6702.2	93%
4875	A06	339630	339	31293.4	7189.3	92%
4875	B06	341956	307	34541.4	6218.8	95%
4875	C06	343550	309	36134.8	5895.8	93%
4875	D06	345850	332	25006.4	5624.8	93%
4875	E06	346578	339	112780	49034.2	91%
4875	F06	349156	325	28323.8	10573.8	89%
4875	G06	352890	302	25765.8	7256	92%
4875	H06	362639	344	25350.3	6442.6	91%
4875	A07	366289	303	46590.1	15755.1	89%

4875	B07	366801	333	23842.3	5712	90%
4875	C07	369986	329	26132.7	6378.3	91%
4875	D07	371765	318	113425.6	5551.1	94%
4875	E07	372146	305	46317.9	4521.8	91%
4875	F07	372275	322	20720	4314.5	78%
4875	G07	372287	339	34499.9	3922.4	93%
4875	H07	135381	304	23634.8	3894.9	91%
4875	A08	145992	301	27640.1	4169.7	91%
4875	B08	187675	323	29542.7	3938.9	91%
4875	C08	201868	318	23095.5	4374.3	84%
4875	D08	209901	331	17920.2	3421.9	87%
4875	E08	217913	307	26046.3	4122.8	91%
4875	F08	326184	316	32743	3406.6	81%
4875	G08	329249	348	35313.5	3251.2	90%
4875	H08	337726	304	26169.8	3706.1	92%
4875	A09	343549	301	54451.3	3308.9	92%
4875	B09	211356	346	24307.6	3208.8	90%
4875	C09	222362	319	23674.7	3174.3	90%
4875	D09	252359	342	45442.3	3664	90%
4875	E09	300289	339	49955	2788.8	73%
4875	F09	321502	346	18446.7	2779.5	92%
4875	G09	324623	327	37296.2	16075.8	92%
4875	H09	98363	342	37173.3	3975.9	87%
4875	A10	99657	325	28017	4784.6	92%
4875	B10	111118	331	27353.2	2940	91%
4875	C10	112125	312	41059.1	3369.1	92%
4875	D10	133075	343	21438.6	3019.8	93%
4875	E10	135168	313	18910.2	2854	94%
4875	F10	142446	349	21838.6	3965.6	60%
4875	G10	150114	303	40335.4	2702.3	92%
4875	H10	156563	350	17929.3	3046.9	91%
4875	A11	197008	336	26300.4	2890.3	92%
4875	B11	245091	324	24333.8	2848.2	92%
4875	C11	278323	326	22415.9	2763.4	93%
4875	D11	326375	338	30695.8	2618.7	92%
4875	E11	329250	349	20633.3	2509.5	79%
4875	F11	331968	301	18485.3	2644.4	90%
4875	G11	338578	318	21147.3	2533.8	87%
4875	H11	339316	303	14781.4	2000.4	93%
4876	A02	372499	308	51341.4	10573.9	91%
4876	B02	375981	337	27448.8	3030.8	91%
4876	C02	375982	344	28611.7	2784.5	90%
4876	D02	378717	333	110878.9	39048.8	87%

4876	E02	379538	304	32858.2	7243.3	89%
4876	F02	379697	343	44115.6	2916	92%
4876	G02	401077	334	23587.1	3041.5	91%
4876	H02	403447	304	35955.7	2979.7	91%
4876	A03	623109	307	29144.3	2602.5	92%
4876	B03	623638	350	38656.3	3373.3	91%
4876	C03	631160	317	40762.8	2276.6	91%
4876	D03	632536	323	39450.7	2133	90%
4876	E03	637153	327	85413	2468.9	89%
4876	F03	637317	344	73199	2903	90%
4876	G03	637325	310	44794.8	3274.2	91%
4876	H03	651084	347	20516.7	2180.1	91%
4876	A04	660151	304	46999.9	5699.4	90%
4876	B04	3323	375	17473.4	1947.7	79%
4876	C04	5157	395	51746.9	2168.1	91%
4876	D04	5836	362	26017.6	2214	91%
4876	E04	7419	393	69201.5	2257	90%
4876	F04	11668	385	29811.7	3329.8	27%
4876	G04	12666	364	22836.9	2191.5	90%
4876	H04	13487	379	895945.9	860556.3	68%
4876	A05	14974	396	28654.4	3322.1	90%
4876	B05	16437	368	23057.8	2653.1	87%
4876	C05	16736	362	32057.3	2377.8	91%
4876	D05	17355	357	55586.1	2848.1	91%
4876	E05	19061	385	35004.1	11511.8	84%
4876	F05	20192	386	225175.8	2561.5	86%
4876	G05	24113	369	354566.6	19446.3	50%
4876	H05	29200	357	12992.2	2966.7	73%
4876	A06	31748	358	27302.1	2554.8	89%
4876	B06	34871	364	27193.4	2368.1	90%
4876	C06	36317	384	26744.2	2231.4	90%
4876	D06	36818	374	25862.6	2206.2	90%
4876	E06	46075	370	29154	3623.7	87%
4876	F06	46385	39	24557.6	2262.9	92%
4876	G06	49852	384	23355.1	2127.5	90%
4876	H06	50650	363	26196	10295.1	79%
4876	A07	50654	382	29878.1	12176.4	70%
4876	B07	50688	358	194231.8	6901.6	91%
4876	C07	57624	384	22008.3	2736.5	89%
4876	D07	65537	356	29658.1	1983.6	89%
4876	E07	70799	377	35967	2083.8	90%
4876	F07	73053	381	80712.3	19595.3	89%
4876	G07	76350	398	21306.8	2316.3	90%

4876	H07	78846	359	21599.1	2385.8	90%
4876	A08	80137	386	37107.5	4832.7	89%
4876	B08	81463	400	28886.4	3657.2	90%
4876	C08	81915	378	27280	2520.4	91%
4876	D08	84100	392	18944.1	2240.6	83%
4876	E08	89602	377	25776.4	2233.1	86%
4876	F08	91340	381	96052.8	2420.6	69%
4876	G08	91355	361	122952.3	2408.8	89%
4876	H08	91356	361	108461.5	2272.3	87%
4876	A09	91357	361	153760.6	2453.7	81%
4876	B09	91368	377	69436.2	2387	87%
4876	C09	91396	397	53243.8	2283.8	46%
4876	D09	91397	397	19854.5	2141.7	83%
4876	E09	97920	393	93101.2	51648.6	84%
4876	F09	99867	363	71168.5	2736.9	83%
4876	G09	99925	383	15037.3	2150.7	89%
4876	H09	100708	385	66845.8	2304.5	87%
4876	A10	103331	399	84556.5	32419.8	82%
4876	B10	106231	360	42240.3	9322.8	89%
4876	C10	107679	380	32032	4488.3	87%
4876	D10	110300	358	25453.4	2993.8	72%
4876	E10	111210	397	34530	3512.2	41%
4876	F10	114414	357	14808.9	2149.7	82%
4876	G10	117268	379	20027.1	2481	89%
4876	H10	117987	360	28606.5	2153.1	89%
4876	A11	118818	369	58711	2512.9	90%
4876	B11	124818	354	22547.4	2904.8	88%
4876	C11	126837	391	33571.1	2282.8	89%
4876	D11	131467	386	31967.1	6445.7	88%
4876	E11	131616	354	37554.8	5551.7	89%
4876	F11	134137	371	23334.4	3400.8	88%
4876	G11	139168	390	22291.1	2541.8	88%
4876	H11	151721	354	28536.2	2197.4	90%
4877	A02	151888	375	3802018.5	3758172	77%
4877	B02	154389	396	36179.5	6093.2	76%
4877	C02	156565	359	104066.3	1539.9	85%
4877	D02	159566	351	103172.2	2914.4	85%
4877	E02	163639	399	40665.5	3216.4	90%
4877	F02	163823	356	40443.1	2706.5	83%
4877	G02	164991	367	32460.6	2476.7	58%
4877	H02	166637	384	142389.5	5053.4	90%
4877	A03	177862	351	47243.3	2513.9	88%

4877	B03	191454	363	36396.9	2607.3	90%
4877	C03	201863	370	44158.2	2499.2	43%
4877	D03	204262	396	353245.4	2400.2	89%
4877	E03	204665	376	63847.4	2306.6	86%
4877	F03	215721	386	27568.5	2509.2	76%
4877	G03	216606	354	34475.1	2124.9	77%
4877	H03	217697	359	69478.5	42034.6	66%
4877	A04	250429	364	43438.2	3095.8	90%
4877	B04	263220	388	35570.1	2862.4	90%
4877	C04	270071	391	37941.6	2502	90%
4877	D04	271923	359	32344.8	1938.3	91%
4877	E04	275266	374	38269.8	3424.2	85%
4877	F04	275971	365	31163.1	2367.7	31%
4877	G04	289359	352	75436.5	37620.4	83%
4877	H04	292140	373	40589.4	5291.6	90%
4877	A05	292923	370	37368.2	4779.9	90%
4877	B05	293962	366	40004.2	3164.6	90%
4877	C05	298892	373	71797.1	2592.1	89%
4877	D05	309401	377	40307.1	12402.5	5%
4877	E05	310354	372	112120.3	3340.8	46%
4877	F05	317605	368	205572.7	19973.1	2%
4877	G05	319435	367	38110.5	4062.1	89%
4877	H05	319994	362	44703	2504.4	88%
4877	A06	320218	388	50117.1	2365	87%
4877	B06	325014	383	40433.9	2524.4	85%
4877	C06	329065	369	43485.9	2620.9	87%
4877	D06	338519	355	82736.9	64958.7	86%
4877	E06	339161	395	37125.4	13191.1	84%
4877	F06	347463	357	58762.4	5503.6	90%
4877	G06	630602	347	79652.8	3277.7	79%
4877	H06	634396	347	27715.7	2943.7	84%
4877	A07	37219	358	44145.2	3111.5	81%
4877	B07	56287	365	109489.6	3100.1	83%
4877	C07	102314	358	62073.6	2772.2	90%
4877	D07	116702	362	1692919.4	1610948.8	63%
4877	E07	116709	353	70668.1	9412.7	87%
4877	F07	120289	390	48199.9	5042.1	86%
4877	G07	372767	345	31825.4	4388.3	80%
4877	H07	407628	302	78842.5	22614.9	86%
4877	A08	32984	369	43295.2	3622.3	90%
4877	B08	37627	392	39235.5	11331.8	86%
4877	C08	45572	386	39605.4	2930	88%

4877	D08	63680	376	37584.8	2974.2	89%
4877	E08	117028	398	29063.2	4531.4	75%
4877	F08	216633	391	37508.6	2674.5	89%
4877	G08	275428	362	74961.9	4820.1	86%
4877	H08	295486	359	88018.2	8731.5	87%
4877	A09	345845	364	45356.5	3615.6	21%
4877	B09	622608	322	34129.5	3128.6	88%
4877	C09	622691	317	27735.8	2765.8	81%
4877	D09	637578	325	56493.9	2888.2	82%
4877	E09	680495	312	30874.2	2497.3	88%
4877	F09	4292	380	29143	2553.9	61%
4877	G09	9032	364	45848.6	3646.4	87%
4877	H09	11881	390	29975.9	2565.4	87%
4877	A10	60785	364	35844.5	3006.2	89%
4877	B10	62685	353	37119.1	2648.2	89%
4877	C10	84126	385	43508.4	2942.5	88%
4877	D10	88600	377	39328.8	2583.6	89%
4877	E10	88916	370	218607.3	2754.1	87%
4877	F10	125095	375	38691.7	4655.1	81%
4877	G10	142335	399	94935.1	14500.7	85%
4877	H10	163443	394	448249.7	335331.2	85%
4877	A11	178249	354	93769.7	14068.3	83%
4877	B11	214009	362	26854.5	2602.1	57%
4877	C11	280594	400	39151.2	5190	88%
4877	D11	319709	352	41692.5	4426.2	84%
4877	E11	321491	383	23475	4842.7	82%
4877	F11	327702	353	23863.6	3008.5	88%
4877	G11	338042	392	34904	3425	87%
4877	H11	54709	370	69472.4	3432.6	78%
4878	A02	350187	388	105505.6	2704.9	91%
4878	B02	354261	355	73870.3	2643.6	92%
4878	C02	359472	361	69801.8	2578.8	92%
4878	D02	367306	381	55685.3	2349.8	91%
4878	E02	367469	362	30555.4	2404.1	92%
4878	F02	379388	359	76112.3	2471.2	92%
4878	G02	379555	358	63974.1	2350.3	92%
4878	H02	382035	378	182777.6	1569.5	82%
4878	A03	601359	392	148158.3	26120.9	92%
4878	B03	603071	363	85262.6	2744.4	77%
4878	C03	607097	357	63974.8	2300.5	93%
4878	D03	614826	361	71278.3	2225.2	92%
4878	E03	622689	353	55935.8	2377.6	90%
4878	F03	661122	370	625644.8	2313.9	53%

4878	G03	665497	368	62548.7	2465.1	92%
4878	H03	670283	356	48037	2278.1	88%
4878	A04	672865	367	891522	58723.9	89%
4878	B04	5856	449	50807.1	10564.3	88%
4878	C04	12865	405	108444	4570.5	92%
4878	D04	13294	430	50460.2	5352.4	88%
4878	E04	13791	447	62316	3044.3	93%
4878	F04	30625	411	68464.8	2996.5	92%
4878	G04	41148	414	59911	2762.4	91%
4878	H04	42199	404	246912.1	2413.9	92%
4878	A05	53275	434	92047.5	5894.7	90%
4878	B05	57608	401	85061.1	2554.6	92%
4878	C05	58904	431	70687.7	2480.6	91%
4878	D05	65238	408	78456.8	4834.2	7%
4878	E05	70933	415	71625.5	2509.6	91%
4878	F05	85433	424	134046.1	2807.5	90%
4878	G05	89201	440	100772.1	2568	87%
4878	H05	89821	407	78631.8	3859.4	91%
4878	A06	105584	422	72395.8	2345.7	91%
4878	B06	107582	430	81045	1805.4	79%
4878	C06	107677	409	68175.3	2248.6	91%
4878	D06	109128	416	182675.4	2312.9	91%
4878	E06	123418	441	62411.5	2171.4	91%
4878	F06	123527	412	100735.8	2497.5	91%
4878	G06	127133	434	71185.8	3768.8	90%
4878	H06	128606	435	119748	2260.2	91%
4878	A07	136513	410	69561.2	2332.6	92%
4878	B07	143241	411	118954.3	9473.1	90%
4878	C07	164676	404	195263.3	2694.9	90%
4878	D07	172255	424	184953	2327.3	90%
4878	E07	201631	436	52420.2	2257.4	78%
4878	F07	204232	406	50387.9	2203.3	66%
4878	G07	215718	401	247982.7	1939	70%
4878	H07	234348	421	79675.7	2197.5	91%
4878	A08	280058	430	123591.8	2191.2	91%
4878	B08	290311	421	91434.3	2494.6	91%
4878	C08	295358	408	60757.3	2210.3	62%
4878	D08	305798	404	1247659.5	3476.5	1%
4878	E08	309874	447	78996.8	2383.5	88%
4878	F08	309892	408	101956.5	43451.6	84%
4878	G08	321496	411	43388.1	4283.9	89%
4878	H08	328087	414	87936.3	2745.9	90%

4878	A09	328403	427	68581	3583.2	90%
4878	B09	335506	418	102074.2	4454.5	91%
4878	C09	337832	430	67196.8	2242.4	91%
4878	D09	373600	401	66893.9	2229	90%
4878	E09	376254	447	123952.7	2341.8	90%
4878	F09	378719	404	101903	6022.6	64%
4878	G09	379099	402	140818.5	2649.3	46%
4878	H09	8675	492	3350.2	1991.3	4%
4878	A10	15910	451	41633.1	2025.4	90%
4878	B10	19803	464	46253	2058.6	90%
4878	C10	36508	471	64995.9	2108.9	90%
4878	D10	37553	477	79294.3	2092.8	83%
4878	E10	37641	497	187184	2066.5	88%
4878	F10	41400	493	56971.9	2126.4	91%
4878	G10	55691	493	41783.3	2029.7	85%
4878	H10	60339	487	69389.4	4264.1	75%
4878	A11	64876	495	123085.6	2264.3	89%
4878	B11	70931	451	94243.4	2318.1	77%
4878	C11	73735	485	135877.9	3441.9	87%
4878	D11	80997	473	134326.2	2311.6	77%
4878	E11	103520	462	61425.4	5692.1	9%
4878	F11	107522	499	145497.9	2336.7	89%
4878	G11	116339	459	196242.1	10543.4	1%
4878	H11	146771	476	59861.6	2125.7	60%
4879	A02	166375	464	28717	2591.7	90%
4879	B02	168184	467	26652.1	2794.6	90%
4879	C02	196515	476	28909.6	2840.4	87%
4879	D02	211490	472	21599.9	3073.7	87%
4879	E02	281816	473	1130725	2917.3	56%
4879	F02	292253	464	33286.5	2682.9	88%
4879	G02	317003	456	9156.9	747	1%
4879	H02	319990	475	11061.2	1581.4	80%
4879	A03	322661	475	93954.9	1886.3	75%
4879	B03	335979	452	26490.1	2537.6	89%
4879	C03	342459	469	54207.5	2673.3	89%
4879	D03	343256	478	262421.4	2784.4	1%
4879	E03	371178	500	25073	2506.9	90%
4879	F03	379696	499	46811.1	2471.9	88%
4879	G03	31762	529	28910.7	2399.3	88%
4879	H03	45384	521	18985.9	1897.5	81%
4879	A04	80731	508	15857.9	2311.8	87%
4879	B04	80735	529	47157	2290.4	86%
4879	C04	91529	516	25284.8	2668	89%

4879	D04	133071	512	27021.3	2652	90%
4879	E04	139105	539	25681	2560.7	90%
4879	F04	202386	521	14871	2347.4	26%
4879	G04	345647	547	113134	63904.6	39%
4879	H04	354844	509	1116255.3	1106821.5	47%
4879	A05	654260	550	54767.6	33323.5	86%
4879	B05	679525	533	26931.8	8626.8	83%
4879	C05	727038	542	27465.6	5193.8	86%
4879	D05	143491	579	21562.2	2794.9	81%
4879	E05	177365	566	23040.9	2793.2	58%
4879	F05	268251	576	15000.5	2699.3	80%
4879	G05	330500	561	39483.5	2550.7	88%
4879	H05	122819	657	46384.5	2902.8	89%
4879	A06	227186	697	56313.5	3044	89%
4879	B06	19990	770	45960.8	4889.3	88%
4879	C06	1614	447	55486.8	3054.1	88%
4879	D06	13051	407	53473.9	6037.5	55%
4879	E06	59620	413	48743.4	4330.8	87%
4879	F06	107701	416	20438.4	3080.9	86%
4879	G06	156516	425	11793.8	2195	85%
4879	H06	11667	474	24994.8	3080	42%
4879	A07	159242	463	27249.2	2837.2	73%
4879	B07	277184	454	47108.9	3519.7	38%
4879	C07	310325	502	19687.4	2826.8	85%
4879	D07	30663	405	25362.4	2726.1	88%
4879	E07	158413	430	20900.3	2851.9	87%
4879	F07	222365	435	27655.9	2725.3	89%
4879	G07	341196	410	16723.5	2652.7	82%
4879	H07	19970	499	34954.2	3828.5	76%
4879	A08	3391	554	29761.7	2666	88%
4879	B08	380802	363	17722.6	3183.3	86%
4879	C08	645033	372	31779.4	2665.1	88%
4879	D08	121868	423	362069.4	3041.4	89%
4879	E08	163910	441	15044.4	2557.6	83%
4879	F08	166259	416	76028	2648	90%
4879	G08	168027	424	35111.6	2655.3	88%
4879	H08	203912	410	20462.9	2503.5	87%
4879	A09	311153	434	16277.6	5306.5	49%
4879	B09	638432	407	1948505	1736454.9	52%
4879	C09	5907	463	127741.3	92242.9	78%
4879	D09	67436	487	52218.9	24141.1	51%

4879	E09	96021	456	72254.3	11340	89%
4879	F09	146557	481	26513.2	7886.1	86%
4879	G09	308835	485	26814.4	6507.3	88%
4879	H09	260594	505	22642.4	5423.8	36%

Appendix B

NMR Spectra

^{1}H NMR of Compound 1-(4-chlorophenyl)-3-(7-nitrobenzo[c][1,2,5]oxadiazol-4-yl)urea (GF Urea):

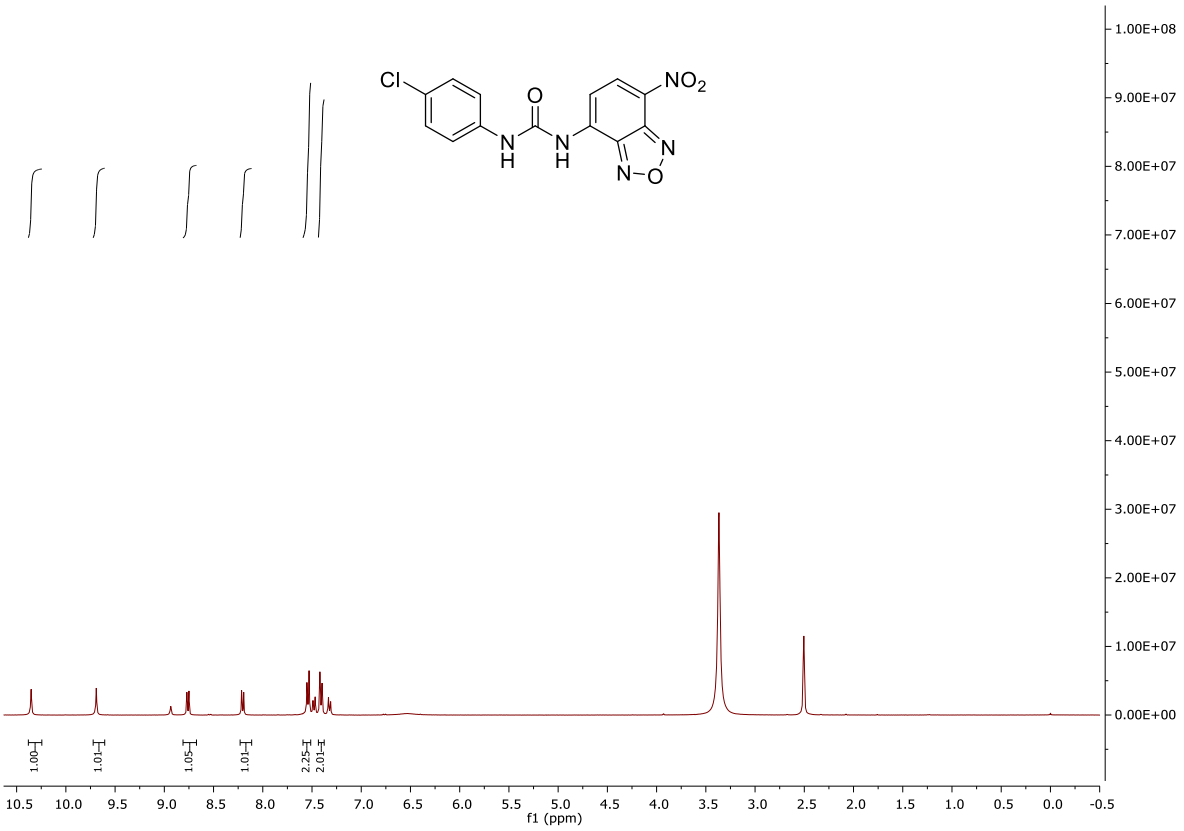

^{13}C NMR of Compound 1-(4-chlorophenyl)-3-(7-nitrobenzo[c][1,2,5]oxadiazol-4-yl)urea (GF Urea):

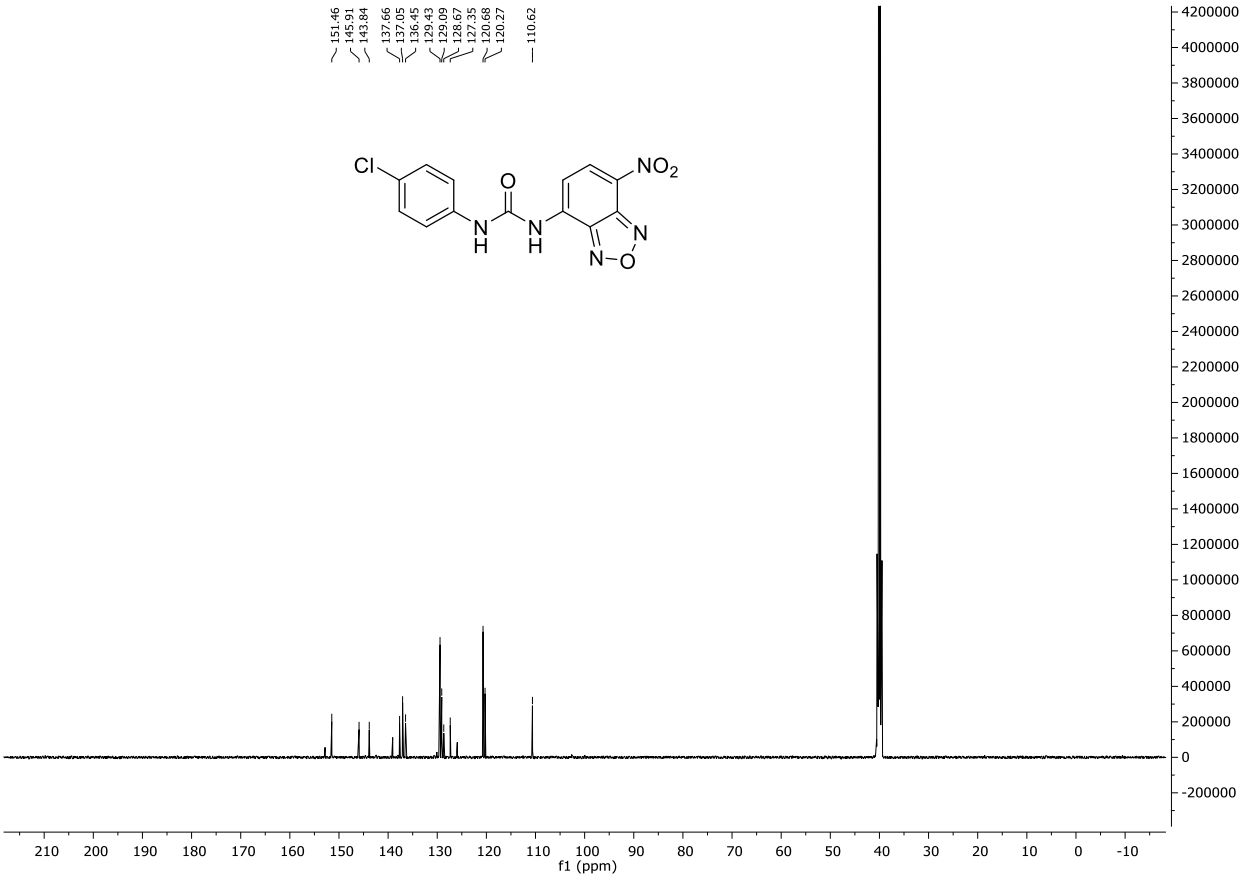

Appendix C

Z-score analysis

$$Z = 1 - \frac{3\text{st.dev}_{Cpos} + 3\text{st.dev}_{Cneg}}{ABS(\text{mean}_{Cpos} - \text{mean}_{Cneg})}$$

-Cpos = values of the positive controls (25 or 100 μM verapamil + 1 μM PBGT)

-Cneg = values of the negative controls (1 μM PBGT)

Plate	Verapamil Conc. (μM)	Cpos mean	Cpos std	Cneg Mean	Cneg StDev	Score
4860	25	78076.85	2942.1313	21907.975	605.63459	0.81
	100	181539	452.23263	21907.975	605.63459	0.98
4861	25	95789.025	4538.6008	19223.675	1147.0671	0.78
	100	181866.35	17893.166	19223.675	1147.0671	0.65

4862	25	116339.9	903.44629	22358.55	1286.3720	0.93
	100	253081.52	21948.537	22358.55	1286.3720	0.7
4863	25	84113.575	6702.2296	18817.85	1482.0786	0.62
	100	169880.8	14370.498	18817.85	1482.0786	0.69
4864	25	127424.52	6544.7259	22887.775	1480.6833	0.77
	100	248094.57	13989.048	22887.775	1480.6833	0.79
4865	25	126060.32	8593.8829	25499.25	490.60859	0.73
	100	275664.67	21133.411	25499.25	490.60859	0.74
4866	25	98025.85	5974.2999	19817.825	2339.3012	0.68
	100	168130.77	3261.4853	19817.825	2339.3012	0.89
4867	25	188826.5	4258.7661	28933.225	352.98937	0.91
	100	372800.65	18294.886	28933.225	352.98937	0.84
4868	25	158539.83	5207.8282	27416.766	780.46893	0.86
	100	367050.73	32091.218	27416.766	780.46893	0.71
4869	25	140178	1684.3958	26107	640.01108	0.94
	100	288040.4	30993.961	26107	640.01108	0.64
4870	25	346633.95	12869.774	70394.1	2876.2539	0.83
	100	596586.55	12082.117	70394.1	2876.2539	0.91
4871	25	79890.15	3145.8568	20502.3	1422.8076	0.77
	100	155310.97	15007.520	20502.3	1422.8076	0.63
4872	25	95830.85	4825.3858	18466.075	1900.9857	0.74
	100	141608.82	7311.6649	18466.075	1900.9857	0.78
4873	25	119502.23	19953.541	9010.2	3597.2473	0.36
	100	267981.55	14053.393	9010.2	3597.2473	0.8
4874	25	57642.125	942.2189	18493.5	335.36095	0.9
	100	119336.2	7500.4482	18493.5	335.36095	0.77
4875	25	101807.55	4334.5771	21747.7	910.27112	0.8
	100	273818.52	12605.656	21747.7	910.27112	0.84
4876	25	73419.075	4317.3601	27869.625	353.85905	0.69
	100	166989.75	16723.523	27869.625	353.85905	0.63
4877	25	172543.92	4298.0784	43931.55	1338.0930	0.87
	100	355302.85	11942.706	43931.55	1338.0930	0.87
4878	25	258041.25	15122.539	72781.7	1087.6716	0.74
	100	415891.45	9683.3323	72781.7	1087.6716	0.91
4879	25	92480.3	3265.4675	28786.8	794.39273	0.81
	100	181500.25	6526.0841	28786.8	794.39273	0.86

Appendix D

List of cell lines

Cell Line	Media	Growth	Organism	Tissue	Source
HeLa	DMEM	Adherent	Human	Cervical cancer	ATCC
PC-3	DMEM/Ham's F-12 medium	Adherent	Human	Prostate cancer	Dr. Matthew Levy
Jurkat	RPMI-1680	Suspension	Human	T-Cell Lymphocyte	ATCC

List of plasmids

Name	Gene Product	Parent Vector	Expression Type	Source
pHaMDR-EGFP	P-GP-EGFP	n/a	Mammalian	M. Gottesman (NCI)